KAUNAS UNIVERSITY OF TECHNOLOGY

IEVGENIIA GOLINKA

RESEARCH AND DEVELOPMENT OF METHODS AND TOOLS FOR MICROPARTICLES SEPARATION FROM BIOLOGICAL ENVIRONMENTS

Doctoral dissertation
Technological Sciences, Mechanical Engineering (09T)

2018, Kaunas

This doctoral dissertation was prepared at Kaunas University of Technology, Institute of Mechatronics during the period of 2014–2018.

Scientific Supervisor:
Prof. Dr. Habil. Vytautas OSTAŠEVIČIUS (Kaunas University of Technology, Technological Sciences, Mechanical Engineering – 09T).

Doctoral dissertation has been published in:
http://ktu.edu

Editor:
Armandas Rumšas (Publishing Office “Technologija”)

ISBN 978-609-02-1478-7

The bibliographic information about the publication is available in the National Bibliographic Data Bank (NBDB) of the Martynas Mažvydas National Library of Lithuania.

KAUNO TECHNOLOGIJOS UNIVERSITETAS

IEVGENIIA GOLINKA

MIKRODALELIŲ ATSKYRIMO METODŲ IR PRIEMONIŲ TYRIMAI IR TAIKYMAI BIOLOGINĖSE TERPĖSE

Daktaro disertacija
Technologijos mokslai, mechanikos inžinerija (09T)

2018, Kaunas

Disertacija rengta 2014–2018 m. Kauno technologijos universiteto Mechatronikos institute.

Mokslinis vadovas:

Prof. habil. dr. Vytautas OSTAŠEVIČIUS (Kauno technologijos universitetas, Technologijos mokslai, mechanikos inžinerija – 09T).

Interneto svetainės, kurioje skelbiama disertacija, adresas:
http://ktu.edu

Redagavo:

Armandas Rumšas (leidykla "Technologija")

ISBN 978-609-02-1478-7

Leidinio bibliografinė informacija pateikiama Lietuvos nacionalinės Martyno Mažvydo bibliotekos Nacionalinės bibliografijos duomenų banke (NBDB).

CONTENTS

INTRODUCTION

Topic Importance

Separation of micro-scale bioparticles is an important issue in the identification and analysis of industrial, biochemical and clinical applications. In order to achieve this goal, microfluidics have been actively adapted since they can accurately manipulate microparticles. Microfluidic microparticle separation techniques are divided into passive and active ones. In active techniques, magnetic or electric fields, optical interaction or acoustic waves are used for optical, magnetic or dialectical interaction of microparticles. Passive methods use distinctive physical properties of the particles, such as their size, density and, in particular, the deformability of cells. However, passive methods tend to suffer from lower selectivity than active methods. The intensification of life and the development of technologies increasingly require the treatment of a larger volume of bioparticles. There is obvious need for low-cost and energy-efficient microparticle separation/purification devices which would be easy to transport and quick to prepare for work in emergency situations (e.g., in a car accident). The research and development of such measures is covered in this work.

Research Aim and Tasks

The aim of this research is to analyze and develop sonic and ultrasonic methods and techniques of microparticle separation in the fluid and in the air. In order to achieve the aim, the following objectives were outlined:

1. To carry out an overview of the research literature on bio/microparticle separation, to formulate the goals and objectives of the dissertation.
2. To develop numerical mathematical models for the separation, handling, and levitation of microparticles by sonic waves in the fluid and in the air.
3. To develop numerical mathematical models for microparticle separation by ultrasonic waves in the fluid.
4. To validate experimentally computational models which combine sonic and ultrasonic microparticle separation in the fluid and in the air.
5. To develop tools for the separation, handling, and levitation of microparticles by sonic waves in the fluid and in the air.
6. To develop tools for the separation of microparticles by ultrasonic waves in the fluid.
7. To create a prototype of the separation of microparticles by ultrasound waves in liquids.

Research Methods

Both theoretical and experimental studies were conducted in the course of the research work presented in this dissertation. Theories of vibrations, fluid mechanics, and acoustic waves physics were applied in numerical modeling which was carried out by means of finite element method within commercial software COMSOL Multiphysics. Methods of sonic and ultrasonic acoustic waves excitation were applied for experimental data processing. For the validation of computational models, several

experiments with different setups were conducted for sonic and ultrasonic microparticle separation, handling, and levitation. The research was carried out at the Institute of Mechatronics, Kaunas University of Technology.

Scientific Novelty

1. Numerical models were developed which combine both sonic and ultrasonic frequency acoustic microparticle separation methods. The developed computational models take into account the complete fluid-cylinder structure dynamical interaction under sonic and ultrasonic frequency excitation.
2. As a result of the numerical analysis, the peculiarities of the acoustic effects on different types of fluids with microparticles were determined. The relations between acoustic and vibrational excitation of the particles in the fluid and in the air were obtained thereby laying the path for the development of microparticle separation devices.

Practical Value

1. Computational models of microparticle separation were used to develop acoustic excitation devices. Their application in different experimental setups is possible by merely changing the model parameters while still using the same acoustic action approach.
2. Microparticle separation/purification device prototypes were developed, designed and manufactured, and one of them was patented. These devices are applicable for microparticle separation from larger volumes of suspension.

Publications and Approbation of Research Results

The results of this dissertation have been published in 6 scientific papers: three in journals listed in WoS Clarivate Analytics, 2 in ISI proceedings, and one as a patent.

The research results have been presented in 9 international conferences.

Statements Presented for Defense

1. Microparticle separation by sonic frequency acoustic waves excitation numerical model and the results of its experimental investigation;
2. Microparticle separation by ultrasonic frequency acoustic waves excitation numerical model and the results of its experimental investigation;
3. Microparticle handling and levitation in the air by sonic frequency acoustic waves excitation numerical model and the results of its experimental investigation;
4. Microparticle sonic and ultrasonic separation by acoustic waves in the fluid and handling-levitation in the air devices;
5. Microparticle separation based on the technology defined in the patent covering an ultrasonic frequency acoustic wave excitation device.

Structure and Volume of Dissertation

The dissertation consists of an introduction, a list of nomenclature, four chapters, conclusions, references, and a list of the author's publications. The total volume of the dissertation is 95 pages including 83 figures and 3 tables.

Chapter One reviews the following positions:

Currently available non-vibrational blood microparticle separation techniques;

Manipulation of microparticles in a suspension while using sonic frequency vibrational excitation;

Manipulation of microparticles in a suspension while using ultrasonic frequency vibrational excitation;

Microparticle handling and levitation in the air.

Chapter Two contains theoretical investigation of biological suspension microparticle separation procedures which were applied throughout the thesis.

Chapter Three discusses the results of the experimental research of biological suspension microparticle separation.

Chapter Four investigates the developed and patented microparticle purification devices.

1. LITERATURE REVIEW

1.1. Currently Available non Vibrational Biological Microparticle Separation Techniques

The separation of microparticles is important in modern biomedical technologies. The currently available erythrocyte separation techniques based on centrifugal sedimentation, magnetic, plasmapheresis or dialysis phenomena require costly medical equipment and involve limitations related to the requirements on the amount of the particles. A centrifugal sedimentation device is composed of different parts and a high-speed rotor [1] in which, for example, the maximum centrifugal force of 112g is applied when erythrocytes are being sedimented at 1000 rpm in a rotor of the maximum sample radius equal to 10 cm. The multisampling analytical centrifuge uses spatial and temporal resolution elimination profiles technology which allows simultaneous measurement of the intensity of the transmitted light as a function of time and position throughout the length of the sample (pic. 1.1). The distance from the center of rotation is taken as a function of the radial position.

The progression of transmission profiles includes information on the kinetics of the separation process and allows for the characterization of particles.

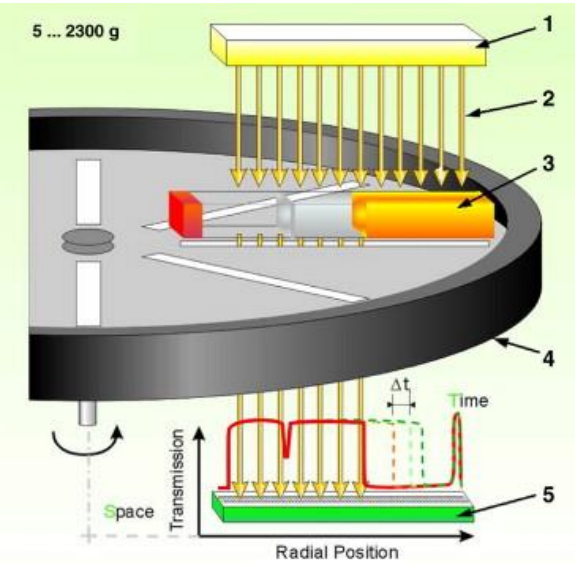

pic. 1.1. The light source (1) sends infrared light (2) which passes through the sample cells (3) and the rotor (4). The distribution of the local transmission over the length of the sample is unregistered by the CCD-Line detector (5). [1].

Up to 12 different samples at constant or variable centrifugal acceleration up to 2300 g can be analyzed. The separation behavior of individual samples can be thoroughly analyzed and compared by determining the movement of any phase boundary or by detecting the variation of the transfer in any part of the sample. With

respect to a particular type of the sample cells, the position corresponds to the defined volume of the sample, the distribution of the particles separation rate can be analyzed by adhering to the 'steady state' method which analyzes the transfer at any point in the sample or by using the 'constant time' method related to the transmission of light along the length of the whole sample (radial positions) at any time during the centrifugation.

According to [2], during the magnetic separation in the microchannel, 1 mL volume of blood ratcheting separation is carried out at 5Hz. The transport of magnetic particles by ratcheting through a wheel using magnetically soft micropillars combined with a directionally cycled rotating magnetic field to dynamically modify the potential energy landscape is presented in pic. 1.2. This creates translating potential wells which trap and manipulate magnetic particles. By applying a magnetic field from a mechatronically controlled magnetic system, the micropillars magnetize in alignment to the bulk field. In the case of a proximal magnetic field, the micro-pillars are magnetized in alignment to the bulk field; the magnetic potential energy is modified, and potential wells in which superparamagnetic particles migrate are introduced. Particles with the increasing magnetic content will have correspondingly higher critical pitches and can, therefore, be separated.

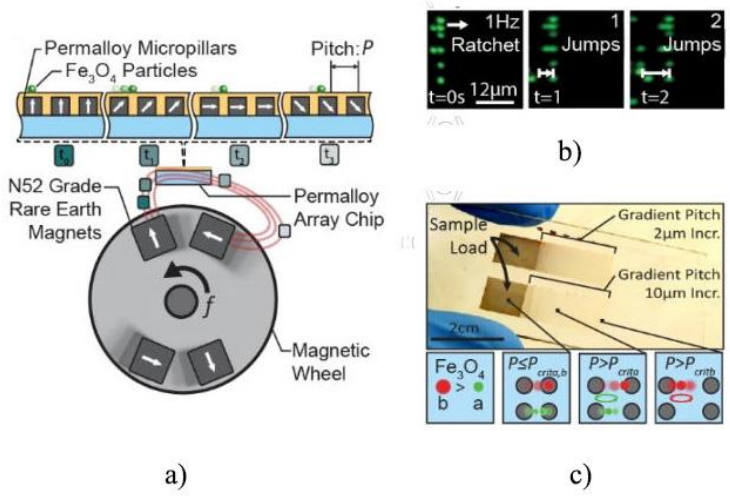

pic. 1.2. Arrays of electroplated permalloy micro-pillars, of pitch *P*, are used for the magnetic ratcheting to create potential energy wells that can be used to capture and manipulate superparamagnetic particles: a) the magnetic ratcheting system consists of a mechatronic device that controls the rotating magnetic circle as well as a microchip consisting of permalloy micro-pillar arrays, each pillar having a 1: 1 ratio; b) since the wheel is cycled at frequency *f*, the particles keep the potential wells and ratchet the pillars according to their size and the iron oxide content. By using a chip consisting of a micro-pillar matrix with a horizontal gradient (c), particles scroll through the array until their critical circular pitch P_{crit} is reached, which is where the particles amass and vibrate [2].

As the magnetic wheel is cycled, particles follow the potential wells and ratchet through the pillars according to their size and magnetic properties (pic. 1.2a, b).

Paper [3] was intended for the development of a six-stage cascade paramagnetic mode magnetophoretic separation (PMMS) system for the separation of suspended blood cells based on their inherent magnetic properties. The blood cell types can continuously be separated by the PMMS system using magnetophoretic forces created from a large magnetic field gradient without fluorescence or magnetic marking. Experimental results showed that the separation of red blood cells (RBCs) in the PMMS system at a volume flow rate was 28.8 μL / h. Therefore, the 5.0 μl blood sample separation time was 10.4 min, with a separation efficiency of 89.5 ± 0.20%. The cross-sectional diagram of the PMMS is shown in pic. 1.3a. Created by an external permanent magnet, the uniform magnetic field is directed around ferromagnetic structures, and a large gradient magnetic field is created in the adjacent ferromagnetic structures. In a large gradient magnetic field, the blood vessels encounter attractive or repulsive magnetophoretic forces depending on their characteristic magnetic properties.

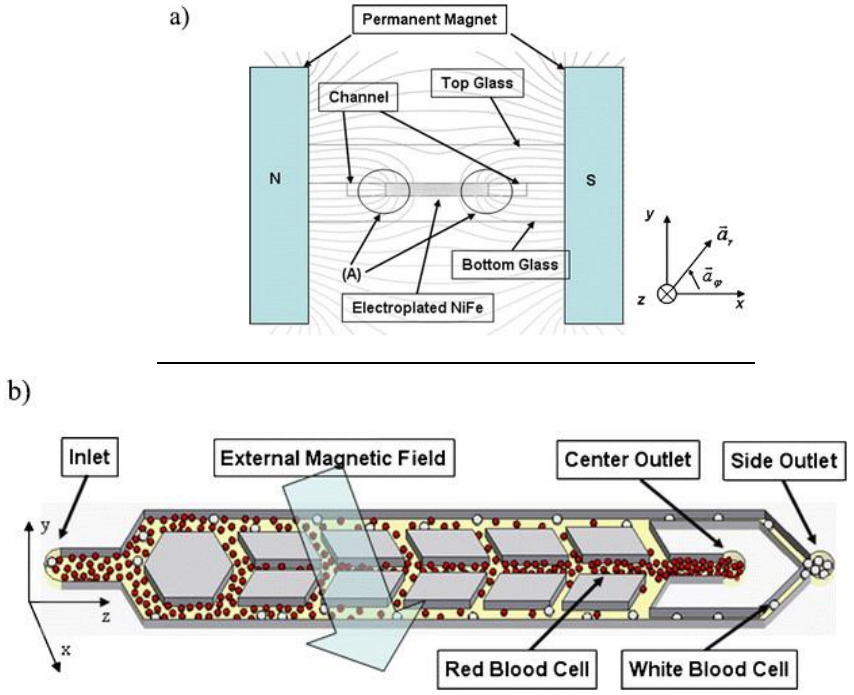

pic. 1.3. (a) In region (A), adjacent to ferromagnetic structures, a high magnetic field gradient is created by using permanent magnets as the field source. RBCs are attracted by the paramagnetic force gradient generated by the ferromagnetic capture structure; (b) PMMS system operation: attracted to the ferromagnetic structure, RBC is forced to the central channel, while the WBCs and other rare cells travel along the outer channel. The remaining RBCs in the outer channel are attracted and re-separated during the subsequent stages [3].

When magnetic particles are placed on the *x* axis or in the microfluidic channel in pic. 1.3a, the magnetic particles whose relative magnetic susceptibility of a blood

cell with respect to the buffer solution is positive (i.e., paramagnetic particles) are attracted toward the ferromagnetic structures, while those particles that have a negative relative magnetic susceptibility of a blood cell with respect to the buffer solution are pushed away from the ferromagnetic structures. Deoxyhemoglobin RBCs have a positive relative magnetic susceptibility of the blood cell in most buffer solutions, and are thus attracted toward the ferromagnetic capture structure by the paramagnetic force.

In the development of the six-stage magnetophoretic separation system, one of the most important factors taken into account was the need for the trapping time for the RBC to move from position (x_1, y) to position (x_2, y), $x_2 \geq x_2$. The already captured RBC will be moved to the central collection channel thus giving more space to other RBCs which would be attracted to the ferromagnetic structures thereby increasing the separation efficiency. If the glass slide containing the microseparation system is limited and if the diagonal collection channels are saturated with a separate RBC, this increases the number of separation stages in the design, which subsequently increases the number of diagonal collection channels and the total volume of the collected RBCs. To transfer the RBC from one point in the outer feed channel to the point of the outer channels in which the cells can be moved to the diagonal collection channels, the RBCs must be exposed to lateral magnetophoretic forces for at least a minimum of the critical amount of time. Reducing the duration of each stage reduces the collection time of the RBCs in the main and outer separation channels. The entire blood sample is transferred to the PMMS system and evenly distributed between two external separation microchannels flowing parallel to the ferromagnetic structures (pic. 1.3b).

The RBC magnetic field is attracted to the ferromagnetic structures and, through the diagonal collection, channels are forced to the central microchannel, while the WBCs and other rare cells are forced outward and moved along two outer channels. The fluid channels network is designed so that only RBCs forced into the edge of the ferromagnetic capture structure are trapped in the diagonal collection channels, while other cells are unlikely to be transferred to the collection channels. The rest of the RBCs in the external channels are attracted and separated by the central flow channel during the later stages of separation. By combining six separation stages in the cascade mode, the RBC level in the external channel is reduced in stages, and, after the six separation stages, RBCs are removed from the flow stream through two external channels (pic. 1.3b).

The separation of micro-scale particles has been an important issue in industrial, biochemical and clinical applications for the identification and analysis of specific particles. Circulating Tumor Cells are likely to originate from clones of the primary tumor, so it can be argued that they can be used for all biological studies applying to the primary cells. ScreenCell devices are single-use and inexpensive innovative devices which employ a filter that isolates tumor cells and sorts them in size [4]. These devices were designed to isolate the Circulating Tumor Cells by size on a microporous membrane filter. They are 19 cm in length and are intended to be isolated from: (i) Fixed cells for cytological studies (ScreenCell Cyto); (ii) live cells for culture (ScreenCell CC) and (iii) molecular biology (ScreenCell MB) (pic.

1.4). Filtration devices contain a filter container; the filter is covered with a removable tip/holder (pic. 1.4a, a and 1.4b, a) which removes the protective membrane (pic. 1.4a, b and 1.4b, b) and allows the insertion and guidance of the collection tube (pic. 1.4a, c and 1.4b, c).

A round track-etched filter consisting of a polycarbonate material is flat, hydrophilic and 18 μm thick. Calibrated round pores (7.5 ± 0.36 μm or 6.5 ± 0.33 μm for isolated fixed or live cells, respectively) are distributed randomly throughout the filter ($1x10^5$ pores/cm^2). Before the filtration of RBCs, 1 ml blood samples should be diluted in 7 or 8 ml of specific dilution buffer for fixed or live cells, respectively. The addition of 1 ml of Phosphate-Buffered Saline after the fixed cells filtration and better cytological studies is filtered by removing RBC debris from the filter. Usually, the filtration is carried out in about 50s. At the end of the filtration, the ScreenCell device nozzle/holder is removed from the filtration tank (pic. 1.4a and 1.4b). ScreenCell Cyto and CC devices (pic. 1.4a) are designed for cytological research and the cell culture. The filter allows for rapid and regular filtering, maintaining morphology and microcluster structures of the Circulating Tumor Cells. With the ScreenCell FC or ScreenCell LC/CC, screen dilution buffers for fixed or live cells, respectively, are diluted. The ScreenCell CC filter is dispensed onto the 24 wells at the end of the filtration of the tissue culture plate by pushing down the red surface at the bottom of the filtration device (pic. 1.4a, e).

The appropriate tissue culture medium and growth factors are added to the well. The multiwell plate is closed and incubated under the specified conditions. Similarly, the ScreenCell Cyto Filter is dispensed to a standard microscope glass slide by pressing the bar at the bottom of the filtration device; on the filter (pic. 1.4a, f), a 7 mm diameter coverslip can be attached with a suitable mounting medium. Then, cytological studies including staining, cell enumeration, immunocytochemistry, or fluorescent *in situ* hybridization probes can be performed directly on the filter. The filtration area for ScreenCell Cyto and CC device filters is limited to a circular ring made from a surgical inbox with a barcode in order to ensure the traceability of the filtered sample. The ScreenCell MB device is non-nucleated for molecular biology studies before or after the cell culture (pic. 1.4b). The Circulating Tumor Cells are isolated over a round filter covered by the lower part of a capsule (pic. 1.4b, a); the blood sample is diluted in a ScreenCell LC dilution buffer before filtration.

At the end of the filtration, the capsule-filter is removed and inserted into the upper inner part of the nuclease-free Eppendorf tube (pic. 1.4b, e) or into a 24-well tissue culture plate (pic. 1.4b, f). The ScreenCell MB filtering device allows any DNA or RNA to be extracted directly from the cells in the filters before or after the cell culture (in this case, the capsule-filter with the cultured cells is directed to the nuclease-free Eppendorf tube) (pic. 1.4b, e and 1.4b, f). A sufficient volume of lysis buffer is added to the capsule-filter, which is then closed with the Eppendorf tube cap (pic. 1.4b, e). After the incubation at an appropriate temperature, the Eppendorf tube containing the capsule-filter is centrifuged for 1 min at 12,000g (pic. 1.4b, e), and the capsule-filter is removed and discarded. The process is

transmitted in a closed Eppendorf tube or used immediately for additional molecular biological procedures.

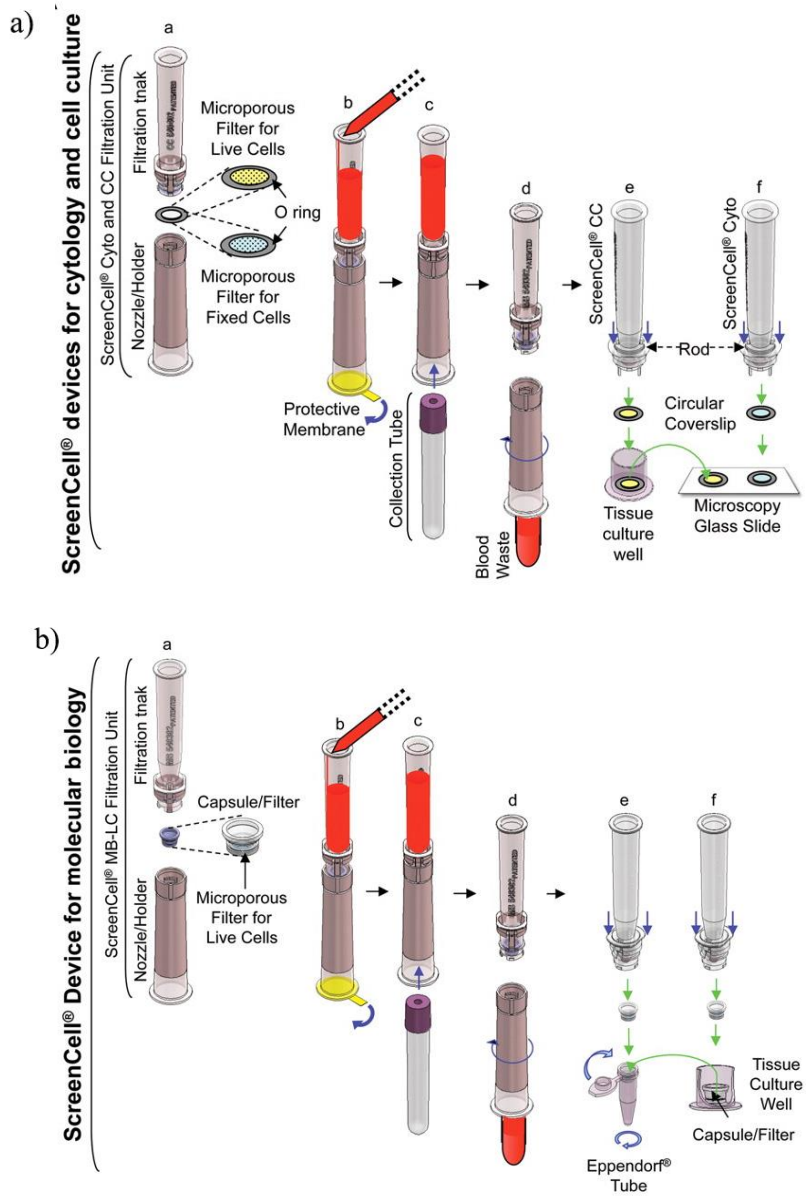

pic. 1.4. ScreenCell device: a) ScreenCell Cyto and CC devices for cytology and cell culture; b) ScreenCell MB for molecular biology [4].

A microfluidic particle separation device using asymmetric laminar flow bifurcation around the barrier is presented in [5]. A particle chooses its path deterministically according to its size. All the particles of a given size follow

equivalent migration paths and therefore have high resolution. 0.8, 0.9 and 1.0-micrometer microspheres, which were used to describe the device, were sorted for 40 seconds with a resolution of ~ 10 nanometers, which was better than the usual flow technique time and resolution methods. Bacterial artificial chromosomes can be separated in 10 minutes with a resolution of ~ 12%. To test these ideas, a device microfabricated in silicon consisting of an obstacle matrix, as shown in pic. 5, was fabricated, in which horizontal obstacle spacing λ was 8 μm, the distance between the rows was 8 μm, and the gap width was d=1.6 μm. Each line was shifted by 0.1λ thus providing 10 lines. The particles were injected from the 10 μm-wide channel at the top of the matrix and passed across the matrix through the flow of the fluid.

In this figure, a separation process that generates equivalent migration paths for each part of the mixture (thus eliminating the multiplanation of the zone) is demonstrated. A laminar flow through a periodic array of micrometer-scale obstacles is used for the separation process. Each row of obstacles is moved horizontally according to the previous row by Δλ, where λ is the intermediate distance between obstacles (pic. 1.5a). For the sake of convenience, let Δλ/λ be 1/3. A fluid that starts with a gap between two obstacles encounters an obstacle on the other line and will bifurcate as it moves around the obstacle. If the fluid is limited and is thus forced to move straight down the array, δ must be equal to Δλ/λ.

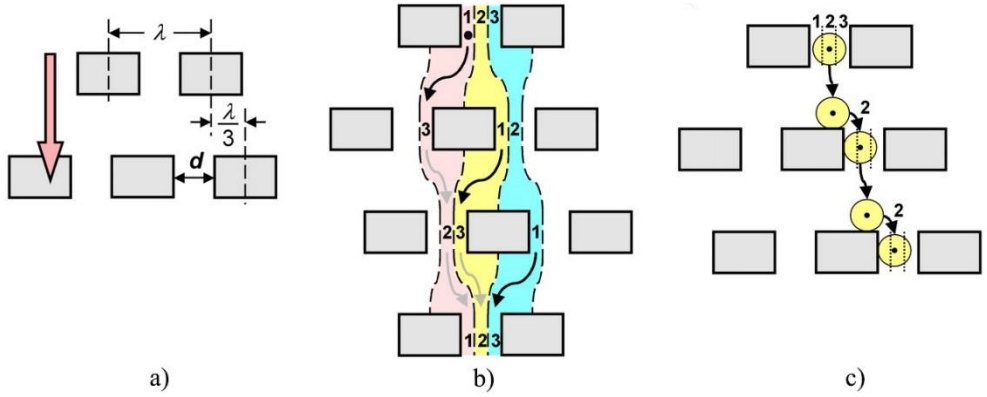

pic. 1.5. Geometric parameters describing an obstacle matrix (**a**). Fluid flow applied vertically (the orange arrow); b) tree fluid streams (red, yellow and blue arrows) do not mix in the gap because they flow through the matrix. Lane 1 of the first obstacle row becomes lane 3 at the second row, and so on. Thus small particles will remain in the same lane; c) the particle whose radius is greater than lane 1 follows a streamline through the center of the particle (the black dot) mowing toward lane 1. The particle moves physically when it enters another gap. The black dotted lines represent lanes [5].

We then realize that the flow through the gap consists of three lanes each of which has a Φ/3 flow by definition. Since the Reynolds number is low (in the range of 10-3 μm) and the flows are laminar, the teams in each lane do not interact (pic. 1.5a, b). It should be noted that the lanes pass through gaps, their positions are changing compared to the gaps. From left to right, gap lanes 1, 2 and 3 are represented. Line 1 becomes lane 3 in the next gap, line 2 becomes line 1, and line

3 becomes line 2 (pic. 1.5a, b). The three lanes rejoin the original configuration after three rows. Particles that are smaller than the lane width will follow the streamlines. The particle starting from line 1 goes through the 3rd lane (the right lane) in the second row, lane 2 (the center line) in the third row and back to the first lane 1 (the left lane) in the fourth row (pic. 1.5a, b).

In fact, particles starting in any of the three lanes will return to the initial lane assignment after three rows, hence the net migration is in the direction of the average flow. This movement is called the *zigzag mode*. In practice, particles can spread to an adjacent lane. However, the microscopic path of all the lanes is equivalent, unlike many particle paths moving through a column of porous beads. Unlike smaller particles, particles with a radius greater than the width of lane 1 will behave differently. This is because the particle center cannot 'fit' to lane 1 in a gap. Since such a particle from lane 2 in one gap moves to a subsequent gap hoping to move through the gap in lane 1, the particle will be 'bumped', so its center will be moved to lane 2 (pic. 1.5a, c). Then the particle will flow in lane 2. This process is repeated every time a large particle approaches a row of obstacles, so the particle remains in lane 2 as it moves down the array. This transport pattern is called the *displacement mode*.

The preparation of monodispersible emulsions is one of the most important methods used in the field of precision chemical or pharmaceutical engineering because the same physical properties are necessary for the precise control of chemical reactions or the physical interaction with outer substrates. A microfluidic system for continuous and droplet separation using microscale hydrodynamics is presented in report [6]. The separation scheme (pic. 1.6a) is based on the focusing and propagation of laminar flow in a pinched microchannel called *pinched flow fractionation* (PFF); continuous separation can be achieved without the use of completed operations or devices. It was examined whether this scheme could be applied to droplets using a pinched microchannel with one outlet and to monitor the behavior of monodispersed droplets that appear to be moving upwards in the suppliers' T-junction.

Analysis using a high-speed image showed that the length of the pinched segment is very important for precise droplet separation. The separation of the polydispersed oil-in-water emulsion was demonstrated while using a microfluidic device with multiple outlets. These results showed that the system was able to sort easily or accurately or to select droplets of a specific size that would be difficult to achieve by using conventional schemes such as centrifugation or filtration. By continuously introducing fluid streams with or without particles from each inlet and adjusting the inlet flow, the position of the particles can be concentrated on one side wall in a pinched segment (pic. 1.6b). Then, with the use of the flow rate profile to the boundary between the pinched segment and the expanded segment, a small difference between the large and small particles may be increased, and then these particles can be separated perpendicularly to the direction of the flow size. By using microchannels with a large number of outlets, the separated particles can be recovered individually.

Since continuous processing can be achieved without complicated structures or operations, this method is useful for particle sorting. In this study, the PFF method is applicable to the separation of emulsion droplets while using microfluidic channels.

If it is possible to sort droplets by using the PFF method without the use of complex devices or schemes, the system will play an important role in sorting droplets into an integrated droplet-base microsystem. In the experiment, the microchannel with three entrances, a T-junction, a pinched segment, an expanded segment and an outlet for the production of uniform-size droplets at the T-junction and the observation of the droplet behavior were developed. Then, a microchannel of six outlets was designed and manufactured for sorting the emulsion droplets that were prepared outside while using a conventional homogenizer.

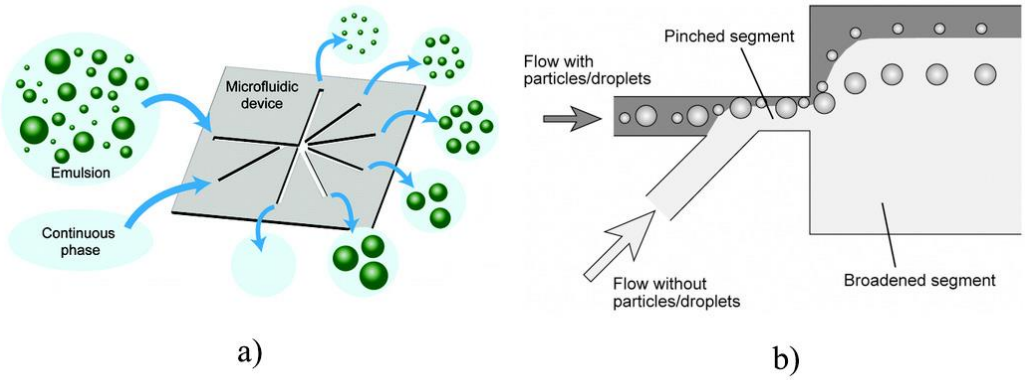

pic. 1.6. The microfluidic system for continuous and droplet separation using microscale hydrodynamics: a) the separation scheme; b) a schematic diagram showing the basic principle of 'pinched flow fractionation' for the size-dependent particles/droplets separation. The initial region of the flow containing particles/droplets is gray-colored [6].

In this study, two types of microdevices were designed and manufactured. A microdevice was developed for the production of monodispersed droplets in the T-junction and facilitation of droplet tracking. In order to substantially change the size of the droplets obtained at the T-junction, several microchannels with different T-junctions geometries were manufactured. To this end, the polydimethylsiloxane (PDMS) plates with a pinched and expanded segment were made with identical master and PDMS plates with a T-junction; they were made from different masters, and then these two types of panels were joined together. The pinched segment is a 12-mm-wide droplet-observing point to help accurately investigate the size of droplets due to the reduced flow rates. The T-junction depth was ~ 20 μm, and the pinched segment's depth was ~ 90 μm. The width of the horizontal channel at the T-junction ranged from 20 to 100 μm. On the other hand, a microdevice was designed to sort pre-filled emulsion droplets. It contains two inlets and six outlets. The microchannel depth was almost uniform, at ~ 50 μm.

Paper [7] provides lateral driven continuous dielectrophoresis (DEP) microseparators for red and white blood cells suspended in highly conductive diluted whole blood. Continuous microseparators make it possible to separate blood cells from the lateral DEP force created by a planar array of interdigitated electrodes

arranged at an angle to the flow direction. A simplified line boot model which was developed for theoretical analysis was confirmed by comparing it with simulated and measured results. It was shown that the lateral-driven continuous DEP microseparator design is practical for the permanent separation of blood cells without the need to control the conductivity of the suspension medium by overcoming the critical deficiencies of the DEP microseparators. Divergent (pic. 1.7a) and convergent (pic. 1.7b) types of lateral-driven continuous DEP microseparators were devised. The divergent type is denoted by the blood cells running down the microchannel length, passing through planar intermediate electrodes at angle θ, as shown in pic. 1.7, a, and driven laterally to the edges of the microchannel.

Conversely, the convergence-type DEP microseparator separates blood cells into the microchannel center when they pass through. In a different type separator, although the WBC and RBC are directed to the edges of the microchannel, the lateral DEP forces acting on the RBC are stronger than the current WBC. Therefore, the WBC propagates towards the microchannel center away from the high density RBC stream at both edges of the microchannel. Consequently, the WBCs and RBCs are continuously separated as WBCs are directed to central outlet #2 whereas RBCs are distributed between the two outermost outlets (#1 and #3) as shown in pic. 1.7a. In the convergent type separator, WBCs diffuse to the edge of the microchannel away from the high-density RBCs stream in the center of the microchannel. Consequently, the WBCs and RBCs are continuously separated into two outermost outlets #1 and #3, and to central outlet #2, respectively, as shown in pic. 1.7b.

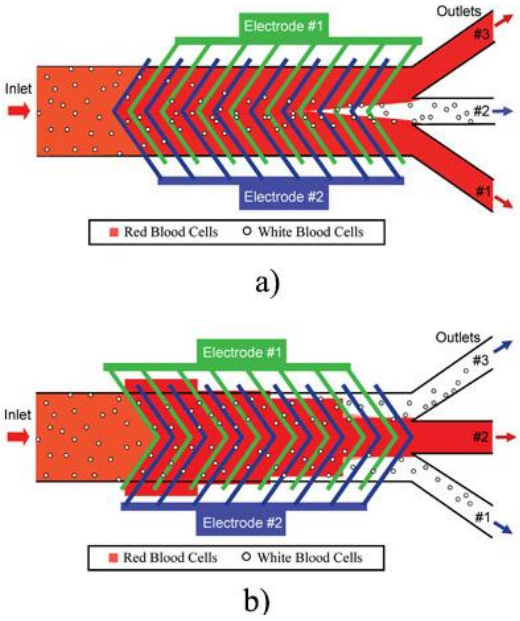

pic. 1.7. Illustrations from: a) divergent and b) convergent type lateral-driven continuous DEP microseparators with an interdigited electrode array [7].

Due to the lateral-drive continuous DEP microseparator, a sinusoidal 2 MHz voltage of 3 Vp-p from the function generator to create a DEP force acting on the blood cells and a syringe pump to ensure a controlled flow of the blood sample through a microchannel were used. A gas-tight glass syringe reduced the variation in the flow velocity. A microscope with a fluorescence sensor to calculate the flow of WBCs to each outlet and to collect the microcurrent passing blood cell images was used. The number of the RBCs extracted from each outlet reservoir were calculated by using a hemocytometer. Polystyrene beads with a diameter of 10 μm were used to monitor the particle movement in an interdigitated electrode array. Bovine serum albumin was used to reduce the nonspecific binding to the surface of the polystyrene beads and the microchannel wall.

Manipulation by microparticles in fluids by sorting and assembling them is applicable in various fields. For these purposes, such methods as dielectrophoresis [8], optical traps [9] and magnetic tweezers [10] were used. Paper [9] deals with the fast scanning laser optical trap with rates greater than 1200 Hz with a single laser beam used to manipulate cells. In [10], a system of magnetic tweezers that allows easy rotary motion is presented (pic. 1.8). The cell containing magnetic particles in the solution are considered to be in the inverted microscope stage.

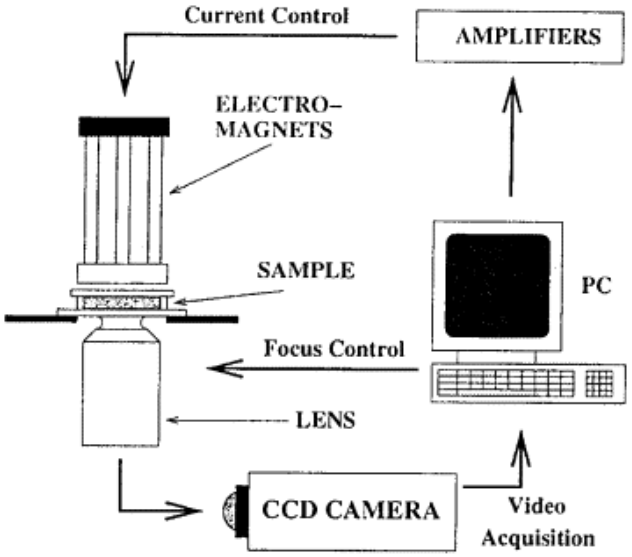

pic. 1.8. A setup of magnetic tweezers. A thin specimen is detectable by an inverted microscope; the CCD image is processed by a computer which drives electromagnets to servo the bead in real time [10].

A system of six vertical electromagnets with their hexagon-shaped columns are directly above the capillary tube. The parallel light illuminates the sample through a 2 mm diameter aperture located in the center of the hexagon. At the *XYZ* translation stage, it is possible to accurately determine the position of electromagnets depending on the optical axis of the objective. The magnetic particle is located with nanometer-accuracy video during micromanipulation. Its position in three spatial dimensions

according to the video rate is determined by the computer program. To eliminate the difference between the desired and the noticeable positions of this bead, the digital feedback loop adjusts the current of each electromagnet. The six-fold symmetry of electromagnets makes it possible to steer the direction of the magnetic field rotation, and hence that of the magnetic particles. The force applied to the bead can be read from the currents driving the coils.

In other articles [11, 12], flow properties have been used for particle sorting and assembling methods while including cascaded shell flows [11] and hydrodynamic filtering [12] for continuous flow in microchannels. The basic concept of the proposed separation method [11] is that microparticles cannot flow in a flow stream whose width is smaller than their diameter. That is why the proposed microchip uses an electrokinetically generated sheath flows to squeeze the flow of sample into a narrow stream, which causes large particles to 'switch' from the initial stream to the sheath flow. The expansion chamber (pic. 1.9) downstream the squeezed area is designed to passively and efficiently increase the distance between two separated particle flows in which smaller particles can be directed to a specific channel for the immediate collection and counting, and larger particles are transported through the sheath flow to a further microchannel region where they are further separated by a second sheath flow and then directed to the appropriate collection channels. However, the minimum flow width that can be generated while using the proposed squeeze method is about 2–3 μm, which limits the size of the particles/cells of this application.

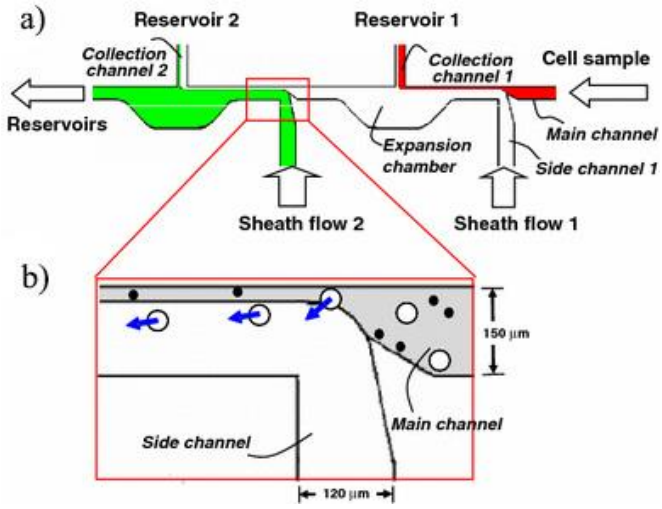

pic. 1.9. a) A scheme of the proposed cell sorting principle; b) an enlarged image for explaining the squeeze effect [11].

A method for continuous concentration and particle classification in microfluidic devices called hydrodynamic filtration is proposed in [12]. The proposed method is based on the fact that the central position of the particle cannot be at a certain distance from the side walls which is equal to the particle radius and is carried out by using a microchannel with a multiple side branch channels (pic.

1.10). By repeatedly taking small amounts of fluids from the mainstream through the side channels, particles are concentrated and directed towards the side walls. Concentrated and aligned particles can then be sized by other side channels (selection channels) downstream of the microchannel.

Consequently, the continuous introduction of a particle suspension into the microchannel simultaneously allows both concentration of particles and their classification. While using this method, the flow profile inside the precisely generated microchannel determines the size of the filtered material. Thus filtration can be performed even when the channel width is much larger than the particle size, without channel blocking. In this study, the concentration of microspheres of polymers of 1–3 μm in diameter was increased by 20–50 times and was collected independently in size. In addition, the selection of leukocytes from blood has been successfully performed.

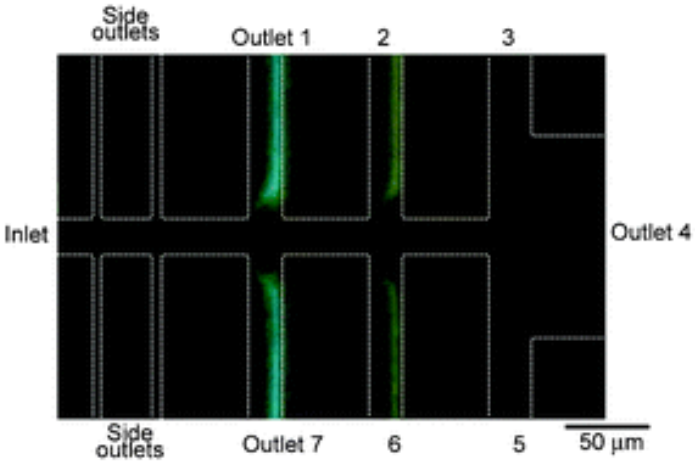

pic. 1.10. A view of a microchannel with multiple side branch channels of different widths [12].

1.2. Manipulation of Microparticles in Fluids by Low-Frequency Vibrations

For the separation of microparticles at the lower (sonic) frequencies, various scenarios were examined, and the first investigations were related to the collection of microparticles in fluids around resonant plaques. In [13], it was shown that the particle clumping in the vibrational capillary tube is the same as that of macroscopic patterns in sand ripples. It was established that the initially equally distributed microparticles inside the capillary tube injected with a syringe pump (pic. 1.11) can be dispersed and accumulated in the formation of regular micron-sized particle clusters. The microcluster wavelength is compared with the data of macroscale sand-ripple patterns and is found to obey the same universal scaling as microparticles do.

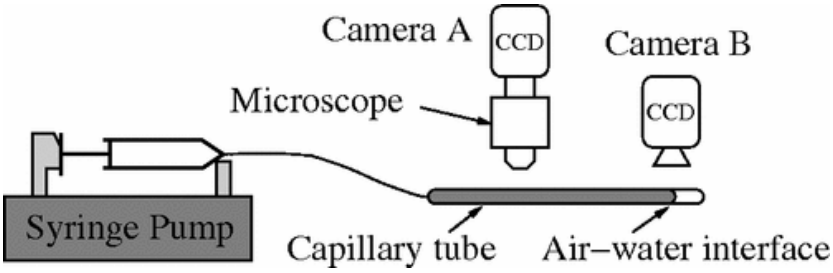

pic. 1.11. A setup for microparticle distribution evaluation [13].

For floating particles, it was shown that they concentrate on the nodes or nozzles (depending on the contact angle) of the vibrating fluid and air interface [14]. The surface tension changes the submersion depth of the particle and makes the particle easier or heavier than the transposed liquid. This means that small floats are sufficiently inert to allow them to move in relation to the fluid. In fact, a small floater on a stationary inclined liquid surface (formed, say, near the walls) drifts along the slope. When the water surface is tilted, the hydrophobic particle (a small piece of plastic) slides down, while the hydrophilic particle (a glass hollow sphere) climbs up. In the presence of a standing wave, the inertia of particles causes a noticeable particle clustering correlated with the wave node model (pic. 1.12).

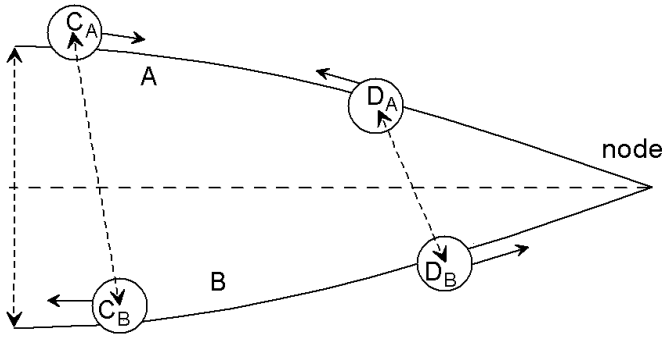

pic. 1.12. Hydrophobic (C_A, C_B) and hydrophilic (D_A, D_B) particle positions and the net forces on the standing wave, half a period [14].

It is necessary to take into account two contributions to the net force averaged over the wave period in order to explain the drift of a single particle in a standing surface wave. The first is due to the fact that the particle between the node's and the anti-node's motion towards the steeper surface is closer to the node, see pic. 1.12. The A and B lines represent the position of the water surface divided by half a period. The dotted arrows indicate the corresponding displacement of the point on the surface of the fluid and the particles between the node and the loops. The particle movements are vertical near the anti-nodes (the maximum height), horizontal at the node and inclined in between.

Therefore, there is the net force that pushes the hydrophobic (heavier) particle to the anti-node and the hydrophilic (lighter) particle towards the node. The second contribution depends on the vertical inertial floating displacement with respect to the

surface. Changes in this displacement have opposite signs of 'heavy' hydrophobic and 'lightweight' hydrophilic particles. Fluid surface accelerations A and B are respectively downwards/upwards – hence the effective form of gravity is smaller at A than at B, so the hydrophilic D_A particle is submerged deeper than D_B and is hydrophobic, or vice versa (compare C_A and C_B). This reflection indicates that the wave frequency is lower than the resonance frequency of the free oscillations of particles with the surface, which is always characteristic of microparticles.

Acoustic streaming still plays a role [15] and is possible in wells that are open in standard laboratories, when using appropriate acoustic frequencies which can be applied with low cost conventional audio components. However, the particle position varies with each cycle [16], where the possibility of manipulating suspended particles in droplets is investigated for their use in microfluidic or 'lab-on-chip' systems using low-frequency actuation and simple measuring instruments. The experimental apparatus (pic. 1.13) consists of a droplet (50 μl) deposited within a shallow (250 μm depth) well on the glass slide. The slide was horizontal and vibrated in the vertical direction by an electromagnetic shaker. Deionized water droplets containing suspensions of 10–30, 42, 60 and 116 μm glass microsphere particles were actuated at two frequencies. Frequencies of 60.59 and 111Hz were chosen in such a way as to give rise to the droplet resonance.

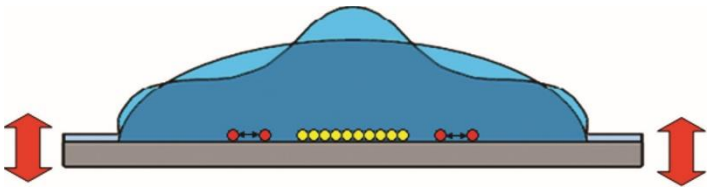

pic. 1.13. Due to the appropriate frequency of vibration, the particles concentrated in a droplet are clustered in axi-symmetric location [16].

The size of the examined particles showed that larger particles (42 μm up) form regular ring patterns in the solid/fluid interface. The location of these rings corresponded with the locations of the resonating droplets' surface anti-nodes. Smaller particles (a mixture of 10–30 μm) do not settle into such rings but rather follow the fluid motion. This indicates that the dominant mechanisms are sensitive to the particle size. In the high-frequency mode (>100 kHz), the relative domination of acoustic streaming and acoustic radiation forces is determined by the particle radius. The acoustic radiation force is proportional to the radius cube (in the resonant sound wave), whereas the acoustic flow (second order) comes from the drag and is proportional to the radius. The radiation force, when it is predominant, collects particles in the nodes and anti-nodes (depending on the fluid and particle parameters).

When switching from high-frequency actuation, when the pressure field is determined by introducing a compressible fluid to a low frequency in which the fluid flow field is found assuming that the fluid is incompressible, the amount of acoustic radiation is irrelevant. However, acoustic streaming can still be significant [17] for two-dimensional viscous channel flow whose walls perform oscillations perpendicular to the channel axis. Focusing is driven by a drifting motion and the

secondary streaming that causes the particles to approach the channel axis. Simultaneously, the streaming together with the imposed flow of Poiseuille drives particles downstream.

At a low frequency (<1kHz), particles have more time to react to the vibrating (first order) fluid. Thus, in each cycle, there is a tendency for particles to be exposed to hydrodynamic focus, so several cycles will result in the collection of particles. In most resonant wave manipulation techniques, such as the optical stationary waves, the amplitude of the oscillations is related to the generated forces, rather than to the patterns formed by the particles. However, when applying low-frequency vibration to a droplet, we see a change in the particle pattern with the increasing amplitude. It can be expected that the free surface of the droplet will move significantly at a higher amplitude thus causing two effects. First, we assume that the movement of the upper fluid and gas interactions from the center of the droplets can be so prominent at high amplitudes that the central disc of the particles is made to be redistributed into the shape of a ring.

Secondly, since the fluid surface of the outer ring is oscillating about a sloping surface, the amplitude tends to increase the radius of the ring that forms as a fluid medium. With a larger amplitude, when the spatial and temporal mode occurs, there is no predicted paternity. It should be noted that the formation of a particle disc in the droplet center at a low amplitude level is not common. This goes in contrast against the expected amount of acoustic radiation directed at the droplet. As a result of experiencing the high-frequency effect, particles accumulate at the pressure node. Since the pressure node does not exist in the center, under the axial symmetric pressure distribution in the droplet, particles will not be segregated there, unless more sophisticated techniques are applied.

Following the trend of the lab-on-chip devices, efforts have been made to reduce the size of such systems by aiming at lower reagent consumption and shorter reaction times [18]. In such a system, while using an open volume fluid, a droplet is examined (pic. 1.14). The test apparatus consists of a 1 mm thick glass plate (10×10 mm), at the bottom of which a square 0.5 mm thick piezoelectric transducer (4×4 mm) is attached with epoxy and coated with silver paint. The structure is mounted on a glass frame as shown in pic. 1.14, a. The pattern of electrodes can be seen in pic. 1.14, in a magnified area as shown below.

The side of the piezoelectric element in contact with the glass is grounded, like all the unused electrodes. By applying a sinusoidal electrical signal to one of the stripe electrodes, the plate is excited to vibration, which couples to the droplet and results in the emission of an acoustic wave into it. By using this peculiar electrode configuration, the generation of heat through losses in the piezoelectric transducer can be reduced. The droplets are visible when using a microscope with a CCD camera and a frame grabber for data acquisition. The illumination is from the top; it is produced by using a pair of swan neck cold light sources, whereas some circles of light spots appear on some experimental images due to the reflection of the surface of the droplet. A typical droplet sticking on the glass plate is shown in pic. 1.15, b from the side to highlight its diameter (about 1–3mm) and the contact angle. To avoid droplet

spreading, the surface was painted with a waterproof pencil that made the surface hydrophobic.

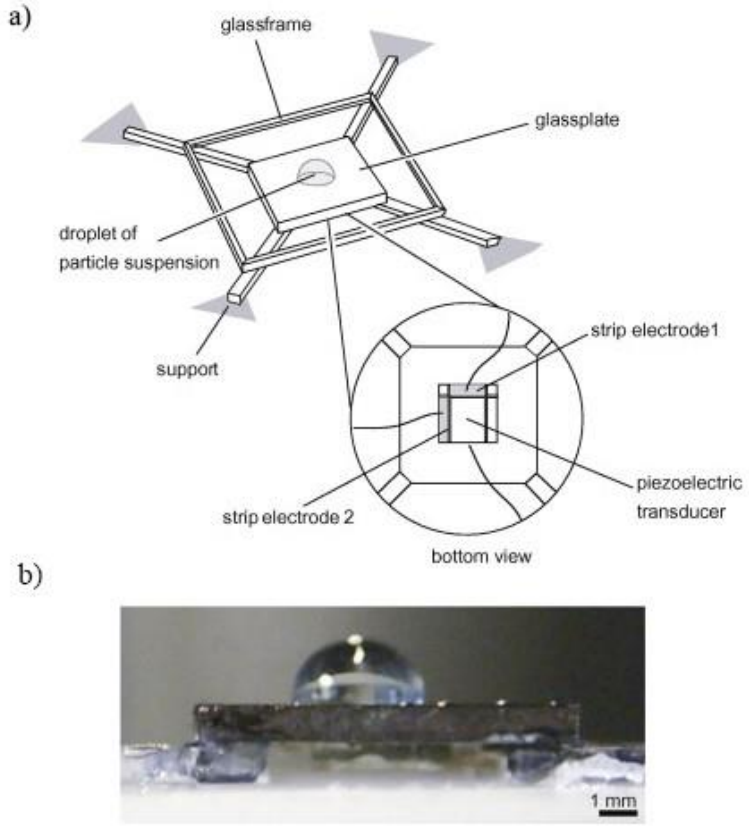

pic. 1.14. a) Schemes of the test apparatus consisting of a 10x10x1 mm glass paneled piezoelectric transducer (4x4x0.5mm) attached to its lower side and used for mechanical excitation. Current signals only to delimited areas (stripe electrodes) defined on the bottom surfaces of the transducer (the rest are earthed). The test device is clamped onto a glass frame and mounted on a microscope for optical observation from above; b) A typical droplet on the glass plate, side view. The piezoelectric transducer and glass frame can also be seen in picture [18].

Study [19] examines a water-air capillary wave pattern which facilitates the collection of suspended particles in the lines, in contrast to the rings previously shown to form in droplets. Hence, a rectangular open chamber (width=4mm and depth=0.25mm) vibrates horizontally at a certain frequency in order to create a harmonious capillary wave in the water-air interface. These capillary waves and the layer of the boundary, which are at the base of the fluid volume, result in the spatial fluctuation of the flow field, which allows the particles to collect at specific locations. The fluid flow generated by this action was simulated by using finite element modeling package COMSOL, and the resulting particle motion was investigated taking into account the viscous drag forces due to this flow. Experiments have been

performed to validate the results of the simulation. The experimental setup consists of a rectangular plastic well that is firmly fixed on a slide and horizontally vibrated by an electromagnetic shaker at a flow field resonance frequency equal to 220 Hz (pic. 1.15).

The electromagnetic shaker is activated via the signal generator through the power amplifier. The particle movement is captured by using a CCD camera connected to a magnifying lens with a light source for better image quality. The research results indicate that the flow field near the base in the vertical direction is very weak compared with the horizontal direction. The particle collection phenomena point to a multiple pass hydrodynamic focusing mechanism because the collection takes place over several cycles.

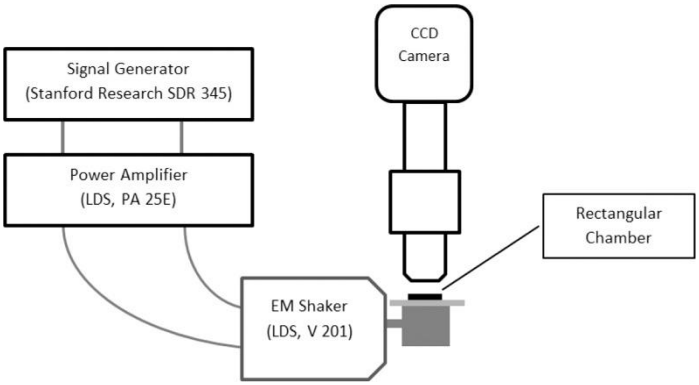

pic. 1.15. A diagrammatic representation of the experimental setup for low-frequency horizontal vibrations [19].

In microfluidic filtration systems, filter clogging is one of the main obstacles to their effective and continuous operation [20]. A low-frequency mechanical oscillation was added to the fluid flow, which allowed the release of aggregated unwanted polystyrene particles trapped between the larger target polystyrene particles in the filters, thus achieving continuous microfluidic sieve operation. Pic. 1.16 visualizes the microfluidic sieving process with laminar flows. As shown in pic. 1.16, a device has an intersection of the fluidic channels with a micro-pillar line arranged diagonally in the direction of the intersection so that particles can be sieved longitudinally (pic. 1.16, b) and retrieved transversely (pic. 1.16, c). To sieve microparticles, the sample solution from the left channel and the buffer solution from the upper and lower channels were injected, leaving the right channel as an outlet (pic. 1.16, a, b).

In the case of microfibrous sieving, a piezoelectric drive was attached to the left channel joint, causing fluctuations that led to the movement of the test solution to the outward direction forward and backward. For microfluidic sieving, a piezoelectric actuator was attached to the left channel. It caused oscillations that led to the movement of the test solution to the outward direction forward and backward. To retrieve the filtered particles, a buffer solution was injected from the upper, left and right channels, which caused the particles to be directed to the lower channel (pic. 1.16, a, c).

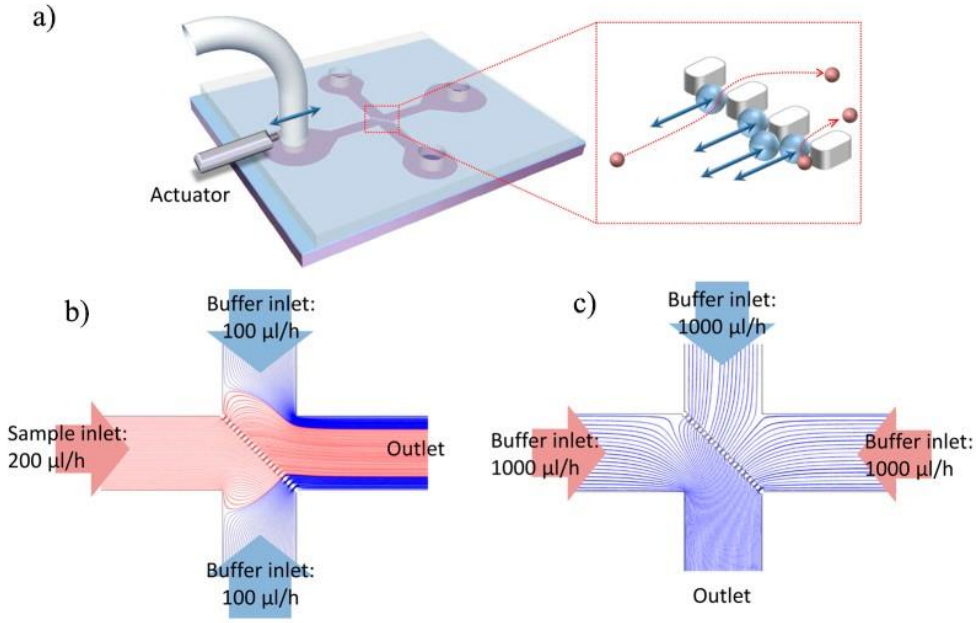

pic. 1.16. Illustration of the microfluidic sieving system: a) Microfluidic chip with four channels and a piezoelectric actuator mounted on the inlet tube. The red box shows an enlarged view of the filter area; b) device flow by entering a filter; (c) retrieval of the sieved particles. The red and the blue colors show the sample and the buffer, respectively [20].

The movement of particles of different sizes in the oscillating fluid was evaluated with a high-speed camera. The oscillation amplitude of a 20µm diameter polystyrene microsphere was monitored for 0.5ml/h and 1ml/h flow speeds with oscillation frequencies ranging from 70Hz to 230Hz in 20Hz steps. This microfluidic sieving method was used for separating cancer cells from the total sample of blood and showed that fluid oscillations prevented filtered cancer cells from blocking filters, which makes continuous microfluidic separation possible to achieve with high efficiency.

1.3. Manipulation of Microparticles in a Fluid Using Ultrasonic Frequency Vibrational Excitation

A subset of particle manipulation methods is the use of vibration, which is highly suitable for microfluidic systems. Many of these methods use high frequency (ultrasound) activation when two mechanisms with dominant particle manipulation are acoustic forces (acting on the particle) and acoustic streaming (acting on the fluid, and thus through the drag on the particle). The acoustic radiation pressure is the integration of the time average into nonlinear pulse conditions with the Navier-Stokes equation over the suspended particle surface. The averaging of time is carried out in one oscillation cycle, which creates a non-zero force acting on particles in the direction of the accumulation of particles in the pressure node or anti-nodes

(depending on the relative compressibility and density compared to the surrounding fluid). Acoustic streaming is a force that is again formed due to the average non-linear momentum terms directly affecting the fluid. The streaming effects are usually visible in the form of rotational flow patterns in the fluid. These ultrasonic mechanisms are well understood, the effect of acoustic radiation has been calculated in the case of one dimensional and arbitrary sound fields [21], and recently the role of viscosity has been investigated [22]. In this paper, a numerical study of the transient acoustophoretic movement of microparticles in the liquid-filled microchannel and powered by acoustic forces resulting from a defined position ultrasonic wave is presented (the force of acoustic radiation emitting sound waves on particles and Stokes drag force from the acoustic streaming flow is concerned). The acoustophoretic particles' velocities are quantified for experimentally appropriate parameters by using a numerical particle-tracking scheme (pic. 1.17). The results show that the transition to the movement of the acoustophoretic particle takes place due to the streaming-induced drag so that the radiation force should dominate over such aspects as the particle size, channel geometry, and the properties of the material.

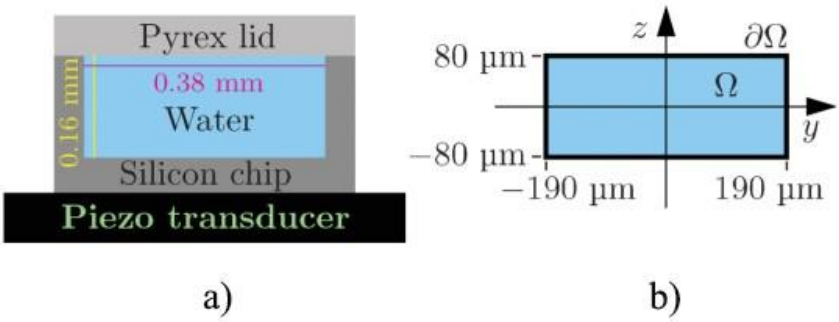

pic. 1.17. (a) End-view sketch of the acoustophoretic microchip with a fluidic channel (width w = 0.38 mm and height h = 0.16 mm) which was used in the experiment. It consists of a silicon microchip (dark gray), a pyrex lid (light gray), water (blue) and a piezo transducer (black); b) The digital model has an appropriate two-dimensional computing area Ω (blue), surrounded by rigid walls ∂Ω (black) [22].

One more system uses the acoustic radiation force to collect particles in nodal planes of the wave excited in the microfluidic ultrasonic separator [23]. When the transducer is operating at ~3 MHz, the half wavelength mode is excited and a standing wave is generated in the fluid channel, i.e., the fluid microchannel height is about half the acoustic wavelength, h=λ/2. As the R-ray particle passes through a standing wave, they are forced into the plane of the node and extracted through the second of the two outlets, respectively, with the flow Q1 and Q2, and Q2> Q1 (pic/ 1.18).

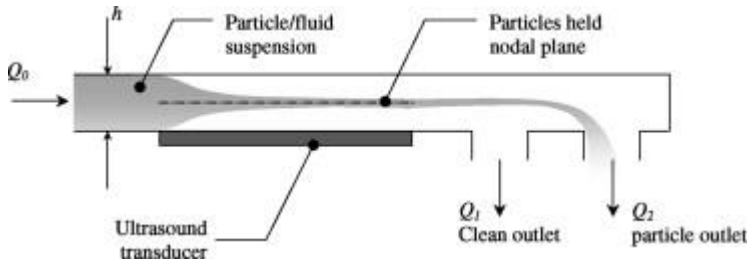

pic. 1.18. A schematic view of the separation device operating in the half wavelength mode [23].

To investigate the acoustic and fluid forces of such a system, a particle model was developed. To simulate the fluid drag force, the CFD software was used to determine the speed profile of a mixture of the fluid/particle mix passing through an acoustic field. Then, the profile is included in the MATLAB model. A numerical method based on the particle force components was used to determine particle paths. By using particle coordinates, both the particle concentration over the fluid channel and the concentration over several outlets are calculated.

In study [24], enrichment, controlled aggregation and manipulation of microparticles and cells with an ultrasound cage integrated into a microfluidic chip compatible with a high-resolution optical microscope were performed. The cage is designed as a dual-frequency resonant filleted square box integrated into the fluid channel (pic. 1.19). The chip-transducer system (pic. 1.19, a) is made from a 14.75 × 50 mm^2 glass-silicon stack with a layer thickness of 0.20, 0.11 and 1.0 mm, a dry etched microchannel in a silicon layer. The cage dimension is 0.30 × 0.30 × 0.11 mm^3. The inlet channel has a cross-section of 0.11 × 0,11 mm^2 (pic. 1.19, c and 1.19, d).

The cage was excited by two wedges transducers whose nominal resonance frequencies were 2.50 and 6.89 MHz, respectively, which were mounted on the top of the chip (pic. 1.19, a) by glue gel. All the driving voltages were no more than 10 V. pic. 1.19, b shows a simulated normalized *x* and *z* force components for the actuation frequency of 2.51 MHz. In pic. 1.19, c, 10 μm beads are trapped, arranged and stored near the center of the cage (slightly moved downstream due to viscous fluid drag). Pic. 1.19, d, shows a final aggregate containing ~ 104 beads. Here, we see that such a large aggregate cannot be fully caged in 3D. The beads in the lower right corner are driving to the cage wall with a dotted line, pic. 1.19, d. This effect is also provided for the simulations (see the corresponding area, pic. 1.19, b). However, for smaller aggregates (up to several hundred particles), this effect can be completely avoided when the ‘funneling’ of the incoming particles takes place in the field of levitation (see pic. 1.19, c).

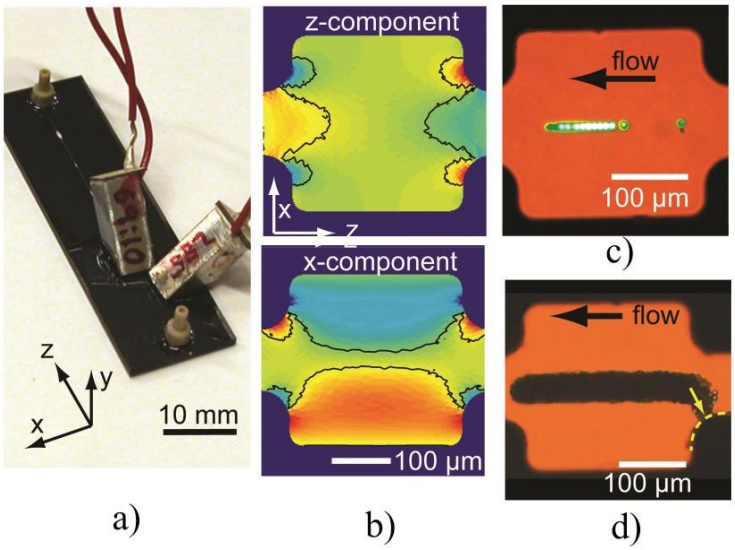

pic. 1.19. a) Chip-transducer system photography; b) Simulation of the 2.51 MHz normalized acoustic power *z* (retention) and *x* (focusing) components. On a color scale, the red is positive, the blue is negative, and the green is zero. 3D caging of (c) 10 µm beads and (d) 5µm beads with 2.57 and 6.81 MHz actuation (10 Vp.p. in both cases) [25].

It means that individual particles can be trapped in three dimensions and can be controlled from one-dimensional to three-dimensional aggregates. The shape and position of the caged aggregate of 10 µm beads were characterized in 3D with confocal microscopy.

The methods that can dexterously manipulate single particles, cells and organisms are invaluable for many areas of biology, chemistry, engineering, and physics. In [25], a stationary acoustic wave 'acoustic tweezers' that can trap and manipulate single microparticles, cells and entire organisms in a single-layered microfluidic chip is presented. The operation mechanism of acoustic tweezers and the device structure are shown in pic. 1.20. The 2.5 × 2.5 mm^2 polydimethylsiloxane (PDMS) channel was associated with a piezoelectric substrate of lithium niobate ($LiNbO_3$) asymmetrically between two orthogonal pairs of chirped interdigital transducers located on the surface of the piezoelectric substrate. Chirped interdigital transducers have a linear gradient in their finger period (pic. 1.20, a), which allows them to resonate at different frequencies. In this experiment, the chirped interdigital transducers use 26 electrode pairs with various electrode widths and spacing, which increases linearly from 25 to 50 µm in 1 µm increments. The aperture of the chirped interdigital transducers is 3.5 mm in width, more than a 2.5 × 2.5 mm^2 square channel width to ensure the full coverage of the standing field.

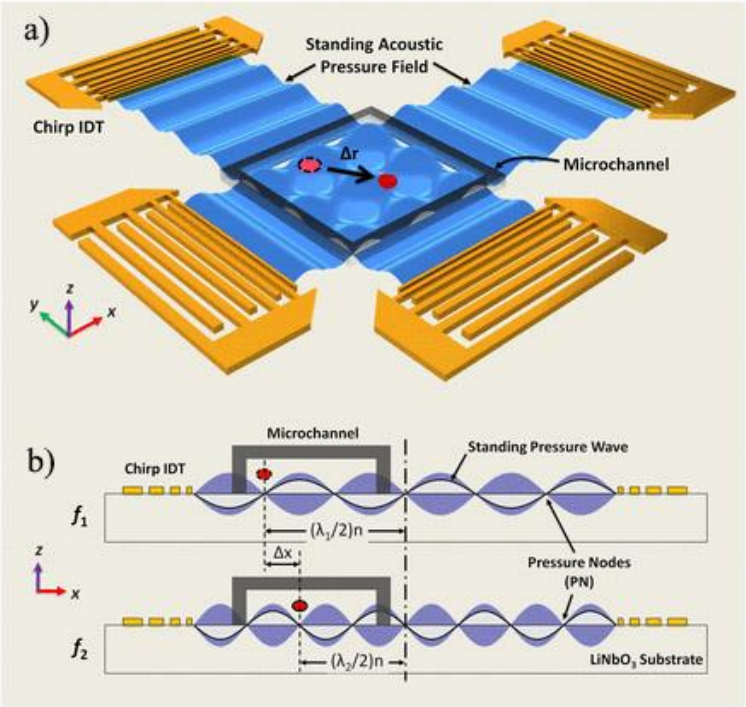

pic. 1.20. The structure of acoustic tweezers and its operational mechanism: a) A schematic illustration of the microfluidic device with orthogonal pairs of chirped interdigital transducers for continuous standing acoustic wave generation; b) A standing field of the surface acoustic wave generated when driving on chirped interdigital transducers at frequencies f_1 and f_2. When the particles are trapped in the nth pressure node, they can be translated across distance $(\Delta\lambda / 2)$ n by switching from f_1 to f_2. This ratio indicates that the particle displacement can be adjusted by varying the pressure node in which the particle is trapped [26].

Each chirped pair of interdigital transducers was independently tied with the radio frequency signal to generate surface acoustic waves, and the interference among them forms a standing surface acoustic wave field on the substrate. The surface acoustic wave leaks into the adjacent fluid medium and determines the fluid pressure; in this area, the acoustic radiation produced by suspended particles is generated. Acoustic radiation forces, depending on their elastic properties, emit particles into nodes or anti-nodes in the acoustic field. Most objects, including *C. elegans*, cells, and polystyrene beads, are pressurized into pressure nodes due to their density and/or compressibility changes compared to the background media. A large bandwidth of the chirped interdigital transducers translated into the system means a wide range of the possible operational surface of standing acoustic waves, which defines the broad range of operation of the device. By using a chirped interdigital transducer with different input radio frequencies, it is possible to move the pressure nodes generated from the standing surface acoustic wave interference. As a result, a single *C.*

elegans/cell/particle, which is trapped in the pressure node, can be freely manipulated in two dimensions.

Bessel-function acoustic pressure fields can be used to capture and control microparticles [26]. A circular 16-element ultrasound array generates and manipulates the acoustic field in a chamber trapping microparticles and agglomerates (pic. 1.21).

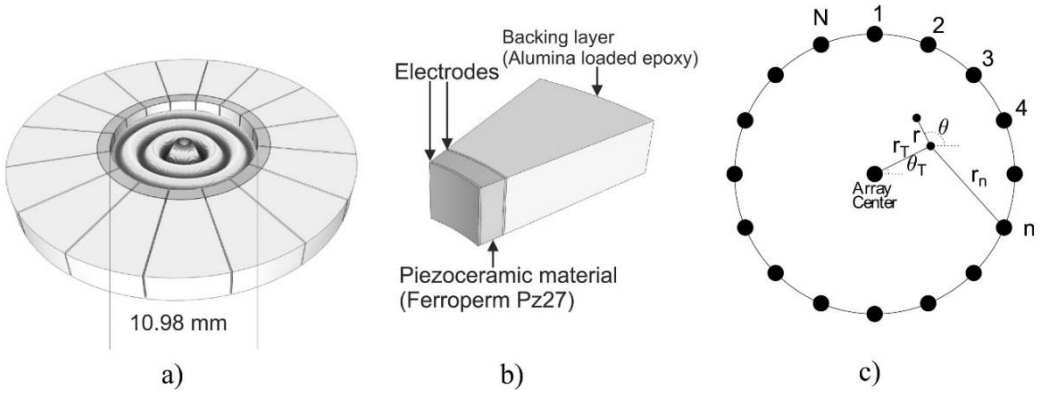

pic. 1.21. Experimental device diagrams showing a) a device for a circular array of 16 elements and a predicted Bessel functional acoustic pressure field; (b) a piezoelectric element construction of one element; and (c) a schematic view of the device showing the coordinates of the system [27].

This device is made of a piezoceramic ring of internal radius R = 5.49 mm, wall thickness t = 0.87 mm, height h = 1.60 mm. The ring was coated with an absorbent substrate layer (an epoxy with 60% added aluminum oxide) and cut into a 16-cell inner circumference of 2.16 mm. The array was controlled at f = 2.35 MHz for the first-thickness extensional resonance frequency of the elements. This corresponds to the wavelength in water, $\lambda = 622$ μm, and the central control radius $r_T = 560$ μm. The pressure field generated by an array does not form a force perpendicular to the ring plane, i.e., in the vertical direction when the ring is horizontal. Therefore, in order to prevent settling due to gravity, a resonant stage of levitation, consisting of a piezoelectric plate below the chamber and a glass-coverslip reflector above, was added. The operating frequency of 2.45 MHz and 14 Vpp was taken by trapped particles in a horizontal plane, one above the other, on which the circular array would manipulate.

In [27], the sorting of microparticles was achieved while using only acoustic radiation forces based on their size. Pic. 1.22 depicts a standing surface acoustic wave based microfluidic equipment scheme. A pair of interdigital transducers (IDT) was arranged in a transparent piezoelectric substrate ($LiNbO_3$), and the PDMS channel was placed and coupled to the substrate between the pairs of the interdigital transducer couple. The three input channels are aligned into one linear channel and the main test section, followed by five dividing outlets.

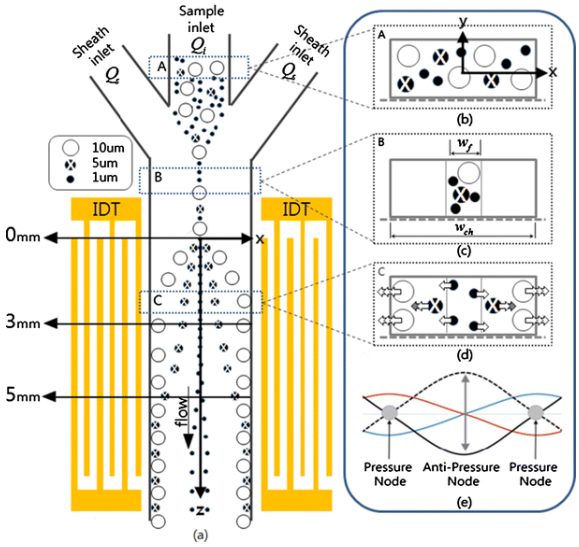

pic. 1.22. Graphs of the microfluidic device and working principles: a) The samples and the sheath flow containing particles of three different diameters (1, 5 and 10 μm) are shown. The sample and the sheath flow containing particles of three different diameter sizes (1, 5, and 10 μm) are illustrated; b–d) The image of the cross-sectional particle image in the sample flow, before and after focusing by the sheath-flow, and under the standing surface acoustic wave field, respectively; e) The position of the pressure nodes along the channel (illustrated by the channel dimensions (d)); the pressure node(s) was/were located at the walls, and the pressure anti-node(s) was/were near the middle of the channel [28].

The inlet channels allowed the particle flow through the middle channel to be inserted with the sheath-flow through the outer channels. The particles were concentrated in the hydrodynamic direction towards the central part of the channel downstream. Then the particles were subjected to the side acoustic forces of the standing surface acoustic wave. By adjusting the flow rate ratio between the sample and the sheath fluids, the width of the focused sample stream was kept constant and ranged between 10 and 14 μm. The introduction of the alternating current signals into IDT created a pair of surface acoustic waves that propagated in the opposing directions towards the main test-section channel.

The interference between these two surface acoustic waves generated their cancellation and superposition, which resulted in the formation of a structural standing surface acoustic wave. Since the two surface acoustic waves are of the opposite signs but of the same magnitude, the minimum pressure nodes are created along the longitudinal direction and vice versa. These pressure oscillations generate lateral acoustic radiation forces acting on the parallel *y*-*z* plane (see pic. 1.22) against the microchannel particles by pressing them either in the pressure nodes (minimum pressure amplitude) or pressure anti-nodes (maximum pressure amplitude) depending on the relative density and compressibility of the particles and the medium.

The use of the acoustic radiation force based on the compressibility installation described in [28] for better particle separation efficiency which is defined as the

fraction of the particles collected in the center outlet is demonstrated in pic. 1.23. The technology presented in this paper allows solving the problem of embolization by using the possibility of separating the red blood cells or erythrocytes from lipid particles (pic. 1.23, a). Since the particles are red blood cells and lipid drops in the plasma, erythrocytes accumulate in the pressure node (in the center of the channel), and the lipid particles accumulate in the pressure anti-node (near the side walls). At the end of the channel, the red blood cells pass through the central outlet (pic. 1.23, b), and the lipid particles exit through the side outlets thus separating the two particle types.

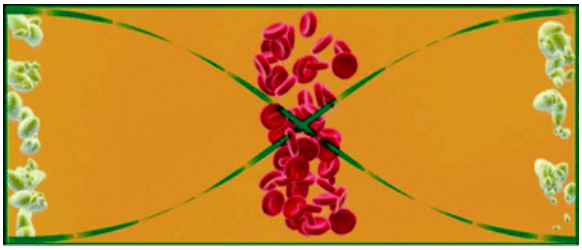

a)

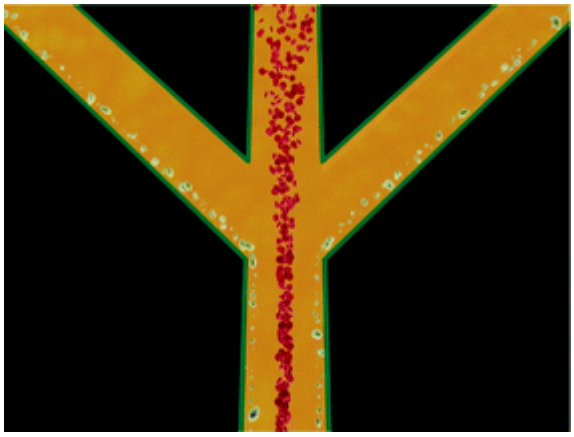

b)

pic. 1.23. a) The cross-section of the channel with red blood cells and lipid particles: when activated by ultrasound, the two particle types are separated; b) When the main channel is divided into three outlet channels, the laminar flow properties of the laminar flow allow separating red blood cells and lipid particles through the side outlets thus separating the two particle types [29].

In paper [29], the particle and cell clustering in distinct free surface patterns of microfluidic volumes are investigated. By using ultrasound, diffuse microparticles are forced into two basic positions: nodal lines (the pressure minima) of a standing wave within the fluid bulk, and different locations in the air/liquid interface a (free surface); the latter has not been previously demonstrated by ultrasound waves. The test device in use is shown in pic. 1.24. It consists of a 0.5 mm thick piezoelectric element with a 0.5 mm thick silicon wafer and a stainless steel fluid chamber sized 0.5 × 3 × 4 mm.

By the injection of 6 μL of the particle/cell suspension, the device was actuated while using an AC signal at frequencies that cause a standing wave (e.g., f~1.53 MHz). The time between filling the chamber with the suspension and actuation was reduced to limit sedimentation. It is worth noting that, during the experiment, evaporation was not pronounced.

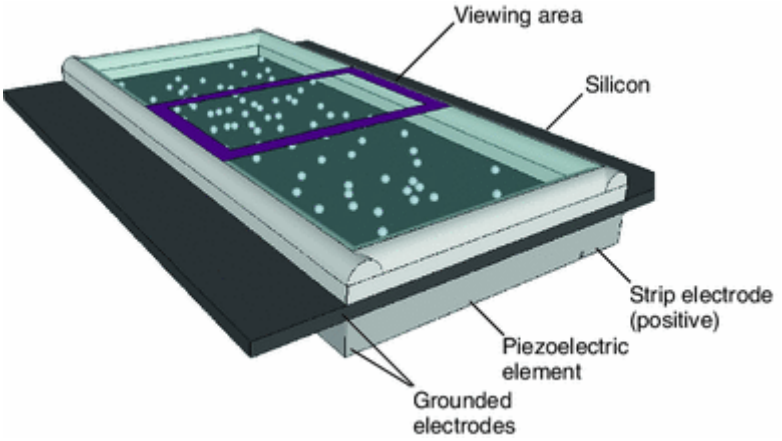

pic. 1.24. The device consists of an open microfluidic chamber near the silicon substrate bonded to a piezoelectric element. In order to experiment with the alternative amount of open fluid, the chamber has been replaced by a sessile droplet [30].

Due to any evaporation, it will be necessary to shift the resonant frequency of the device in order to satisfy the decrease in the fluid volume, and hence in the mass as well. Some experiments were also performed on a 2.1 μL droplet on a silicon substrate identical to the device, as shown in pic. 1.16, although without the chamber. This device was actuated at frequencies that contained multiple nodes (for example, F ~ 1.296 and 1.490 MHz) to monitor the effects of complex nodal patterns on the free surface particle group. The particle behavior was investigated and recorded by using an upright microscope with an additional illumination source attached to the camera.

In [30], two-dimensional particles separation was created by a simple experimental installation based on acoustic radiation and Stokes' drag. Pic. 1.25 shows a fused silica cell (30 mm in length, 8 mm in width, and 12.62 mm in height) with a transition channel of l_y = 3,0 mm wide and featuring a l_z = 1,5 mm high cross-section. The cell was sealed with a 2 cm × 2 cm thick lead zirconate titanate transducer with a 500 kHz resonance frequency. The cell wall thickness (5.56 mm) and the channel height (1.50 mm) were equal to 500 kHz ultrasound half-wavelength in silica glass and water. Thus a standing wave node should be formed in the center of the channel and get filled with water. One end of the cell was connected to a syringe pump with a polytetrafluoroethylene tube, which generated laminar flow in the cell.

A solution containing particles was introduced from the other end of the cell with a syringe. The transducer was driven by sinusoidal signals generated by the function generator and amplified by a bipolar high-speed amplifier. The transducer was set on the three-dimensional stage to control the vertical and lateral positions. The

particle behavior was directly observed on the *x*-*z* plane while using a CCD camera with a zoom lens. The digital data was stored and processed with a personal computer.

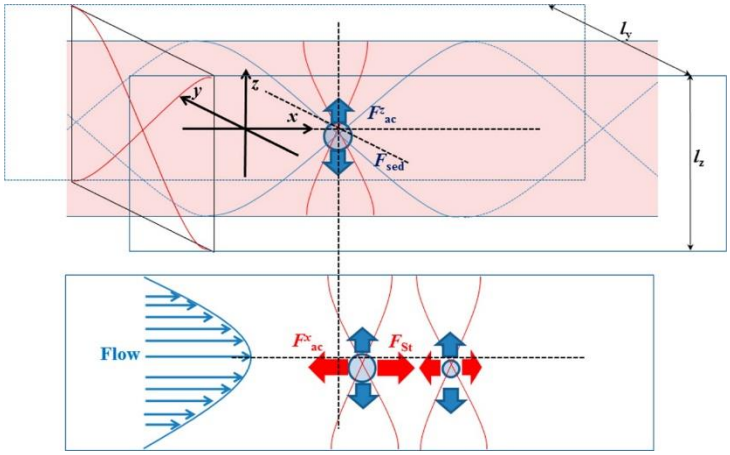

pic. 1.25. A schematic diagram of the two-dimensional separation. The red and blue curves are respectively vertical and horizontal ultrasonic standing waves. The broken lines are nodal lines. The particle is entrapped at the intersection of the nodal lines because there is no other force, but it levitates slightly below the vertical node due to the sedimentation force (F_{sed}) when the ultrasonic standing wave is vertically formed (see the upper figure). The flow allows the separation of particles of different sizes due to the different Stokes' drag levels (F_{st}), as shown in the bottom figure [30].

The particle size and its relative coordinates were determined by digital imaging. The pixel size on the image was calibrated with a vertical *z*-stage shift with one pixel corresponding to 0.46 μm, so the accuracy of the coordinates was less than ~ 1 μm. Several lateral nodes were detected along the separation channel (x-direction), but since the strongest trapping occurred at the midpoint along the channel, the particle behavior was observed near this node. As a sample, polystyrene latex was used. Therefore, the use of vertical and lateral acoustic forces allowed the simultaneous recognition of the size and composition of particles along the different axes of separation. However, this method has a limitation in the applicability to particles of dimensions smaller than micrometers.

1.4. Microparticle Handling and Levitation in the Air.

The non-contact transportation of small particles around the circular trajectory was investigated [31]. A circular aluminum plate with a piezoelectric ring was used for the vibrating plate. According to FEA calculations, the piezoelectric ring electrodes were divided into 24 units to generate a bending vibration mode with one nodal circle and four nodal lines with a 47.8 kHz resonance frequency. After switching the position of the divided electrodes in the direction of the circle, the vibration plate nodal lines can rotate, and the trapped particles can be manipulated by air with a circular trajectory.

[32] presents the acoustophoretic concept for the contactless transportation and handling of materials in the air (pic. 1.26). Spatiotemporal modulation of the levitation of the acoustic field allows continuous processing and transport of several objects from a the spherical to the wired type, but it is not limited to acoustic wavelengths.

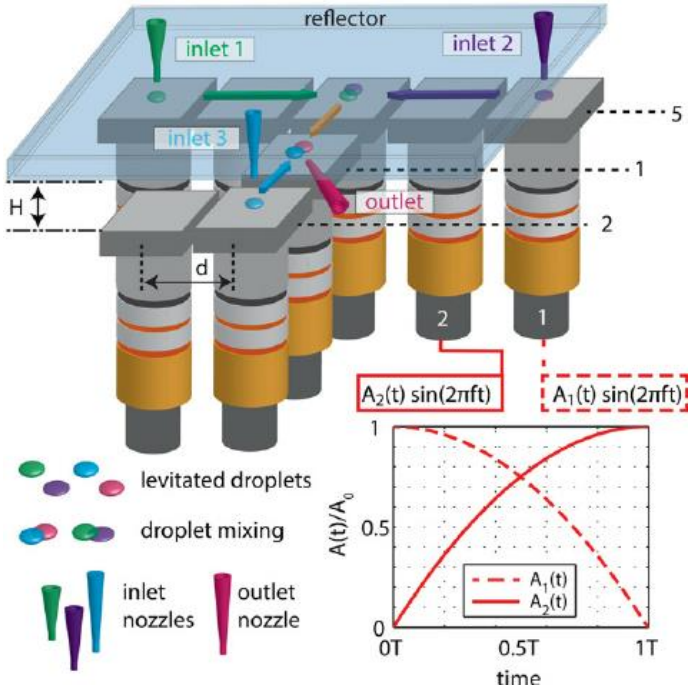

pic. 1.26. Non-contact multidrop manipulator and its actuator schematics. In this example, droplets are introduced in three locations (inlets 1, 2, and 3) into five systems for one or two LPT levitators. Their number corresponds to the number of LPTs for certain rows. All the rows are in the same plane parallel to the reflector plane. The droplets transfer and mix, and the final sample enters the outlet. Drops can be introduced manually with a micropipette, or with an automatic syringe pump and a glass capillary. Reflector height H is adjustable with a linear micrometer stage [32].

The independence of the working principle from the properties of special materials (electrical, magnetic or optical) is illustrated by the extensive application experiment palette. Noncontact manipulation methods are useful for biotechnology, micromachinery technology, and the processing of new materials.

Document [33] describes advanced manipulation techniques for the transport of small objects in the air. The standing wave was created by two sound beams that cross each other and were created by bolted Langevin transducers. The expanded polystyrene particles were trapped in the sound pressure nodes of the standing wave field. The position of the trapped particles was shifted by changing the phase difference between the two sound beams. When the trapped particles are transported, it spatially varies in a direction perpendicular to the transport of particles.

In the field of life sciences, ultrasonic particle manipulation tools have many promising applications developing the capabilities of current manipulation

technologies. Work [34] shows ultrasound manipulation of a particle and cell by microfluidic channel with a piezoelectric array. An array integrated into a flat, multilayer resonator structure directs the particles to the plane of the pressure node along the midline of the channel, and then go toward the acoustic velocity maximum centered above the subset of the elements that are active.

Sound can levitate objects of various materials and sizes through water, air, and tissues. This allows us to manipulate fluids, cells, compounds or live materials without contamination or without touching. However, acoustic levitation requires that targets be loaded with acoustic elements or face limited maneuverability. The phase that is used to drive ultrasound phase arrays and to show that acoustic levitation can be used to rotate, translate, and manipulate particles while using even a one-sided emitter is optimized [35]. This optimization method can be applied to the scenarios with reflectors and any spatial arrangement of acoustic elements. A holographic structure of acoustic elements that allows rapid trapping and bridges between optical and acoustic traps is presented (pic. 1.27).

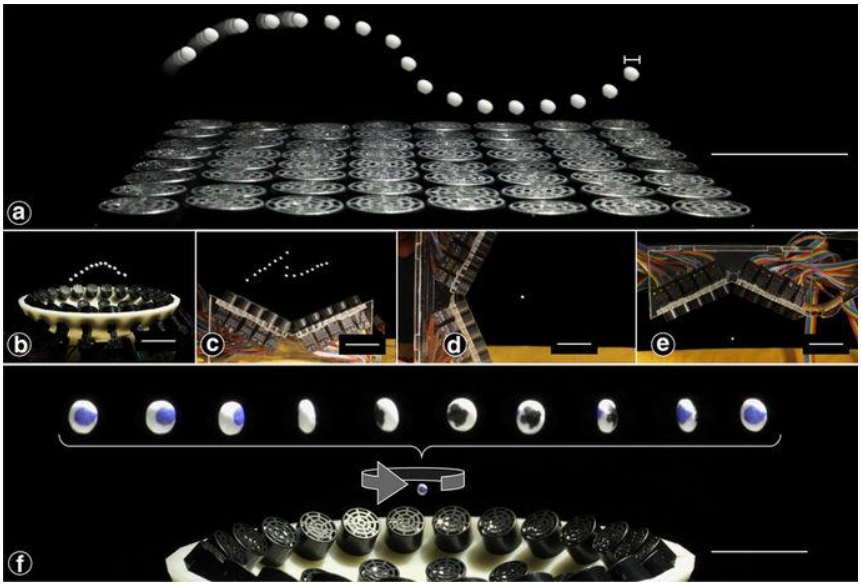

pic. 1.27. Mid-air photos of one-sided levitation. Polystyrene particles having a diameter of 0.6 to 3.1 mm are levitated above one-sided arrays. Acoustic transducers (10 mm in diameter) are powered by 16 Vpp and 40 kHz. (a-c) Particles can be transported together with 3D paths up to 25 cm s^{-1} while using different arrangements and without moving the arrays. (c–e) Traps are strong enough to be able to hold the spheres and neutralize the gravity from any direction. (f) Asymmetric objects, such as ellipsoidal particles, can be rotated up to 128 r.p.m. The scale bars represent 2 mm for the particle in **a** and 20 mm for the other cases [35].

In general, aerosols mixed in the air medium can be regularly manipulated by means of the interactions between the aerosols and the acoustic field. The manipulable properties of aerosols can be engineered through a geometric parameter and the acoustic resonance condition of the underlying device. Aerosols manipulated by

modulated multiple acoustic wavepackets (MAWP) in the acoustic resonance condition are proposed and demonstrated in the paper [36] whose application make part of an efficient aerosol removal technique. The experimental results indicate that the removal efficiency of aerosols was mainly influenced by the different harmonic order. The technique and the process proposed in this paper were feasible for the industrial application (pic. 1.28). This device consists of two opposite Helmholtz resonator sources (HRS) and one cylinder resonant waveguide used as an aerosol container. HRS is made up of a speaker and a Helmholtz resonator and emits an acoustic wave with a single resonant frequency.

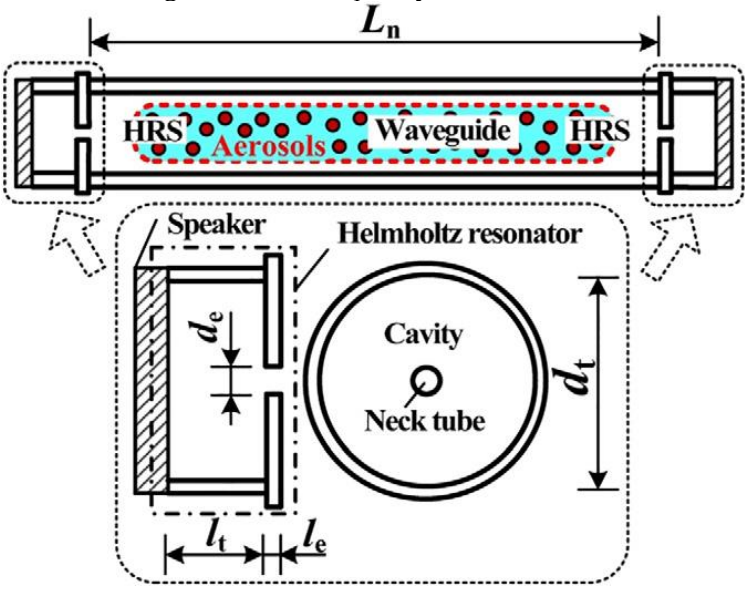

pic. 1.28. A schematic diagram of the experimental device [36].

Two Helmholtz resonator sources (HRS) at both ends of the waveguide are equipped with two identical HRSs as a parity-time operator to achieve the symmetry of time and space of the synthetic standing wave in the waveguide. The synchronous acoustic waves are pumped into an aerosol container to allow the energy to be manipulated by aerosols and to compensate for the loss from the waveguide. As far as HRS is concerned, several important advantages of this device can be found in comparison with important comparative studies. In the device, all the component natural frequencies and geometric parameters should correspond to the resonance similarity condition. The MAWP is modulated by means of the synthetic standing wave field at the resonant frequency 1.268 kHz.

The aerosol manipulation processes through MAWP consist of the aerosol shift, collision aggregation and deposition between the dot and the antineck of a single wave packet. As a visual inspection confirming the standing wave, the processes may also be applied in modulating the MAWP simultaneously. The manipulation efficiency can be increased due to the increase of the wavepacket amount under the same operating conditions. The acoustic radiation force causes the shift and accumulation of aerosol

in the waveguide, whereas the secondary radiation force enhances the collision aggregation and deposition thereof.

In [37], the acoustophoretic separation of spherical solid particles in the air by using an acoustic Fresnel lens is demonstrated. In addition to the gravitational and drag forces, freely falling millimeter particles face large acoustic radiation forces around the lens focus, where the interaction of forces determines the particle trajectory differentiation in terms of size or material properties. Depending on the concentration of a strong acoustic field, the radiation force can direct particles whose source intensity is significantly lower than that required for acoustic levitation in a standing field. When the lens is designed to have a focal length of 100 mm at a frequency of 25 kHz, the finite element method simulates sharp focusing with a full-width at half-maximum of 0.5 wavelengths and a field amplification of 18 dB (pic. 1.29).

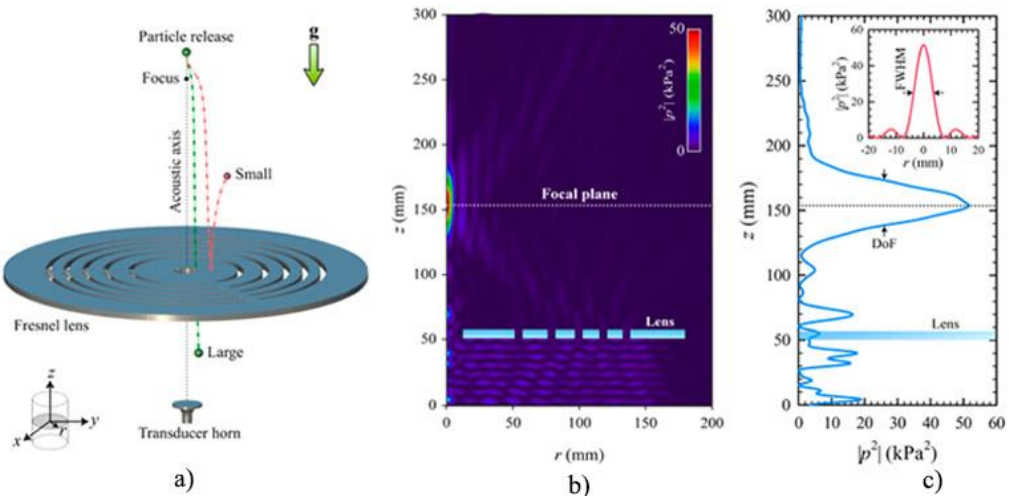

pic. 1.29. Fresnel lens and its acoustic characteristics: a) A Fresnel lens sketch and the particle size separation scheme; b) Acoustic intensity distribution in 2D over the computational domain at f_0 and SPL = 153.0 dB, and (**c**) Change in intensity through the acoustic axis and the focal plane [37].

The Fresnel lens depicted in pic. 1.29 a is a steel cylindrical disc in the air with concentric openings – focal length $f_L = 100$ mm at $f_0 = 25.0$ kHz, the resonance frequency of an available Langevin transducer used in levitation experiments. In order to obtain sharp focus, the components of the diffracted acoustic fields emanating from the adjacent openings must have differences $\Delta l_{i,i+1} = n\lambda_0$, where i = 1, 2, 3, 4, n is an integer and $\lambda_0 = c_a/f_0$ is the wavelength in the air, where the sound speed is denoted by c_a. Thus the radii of the concentric holes r_i are measured from $r = 0$ to the center of the ith opening in the radial direction. The lens is capable of being sharp-focusing, as shown in pic. 1.29, b. The maximum sound pressure level (SPL) at focus is 171.1 dB, thus introducing a significant enhancement of 18.1 dB. For comparison, in order to trap an acrylic particle with diameter d = 1.0 mm against gravity in a levitation experiment with standing acoustic fields, the source sound pressure level is at least 165 dB. Thus particle manipulation by the lens not only requires reduced acoustic

intensity in excess of the magnitude but also offers tunability by adjusting the source sound pressure level to allow that the possibility of adjustment of particles of the same type with diameters larger than a critical value d_c.

The focal spot setting parameters are Depth of Focus (DoF), which is defined as the distance between two points on the acoustic axis, at which the acoustic intensity halves measured from the focus are equal, and the full-width at half maximum (FWHM) along the radial direction. These parameters are presented in pic. 1.29, c, which includes the acoustic intensity plot on the acoustic axis and the dotted line, as shown in pic. 1.29, b. Correspondingly, DoF and FWHM are 53.0 mm (3.9 λ_0) and 7.0 mm (0.5 λ_0), as calculated from Pic. 1.29, c, which indicates that sub-wavelength focusing of the acoustic field is achieved by using the Fresnel lens.

From the literature review, we see that ultrasonic vibrations are commonly used for transporting microparticles and are distributed by using ultrasound waves. Most scientific works are intended only for the transport of microparticles or their levitation. We propose the use of non-ultrasonic acoustic waves that multiply in cylinders and which in their shape are excited by acoustic waves of the same piezoelectric transducer.

1.5. Motivation for Research

It has been shown that up to now there are no fast and inexpensive mods for the separation of larger volumes of fluid in the technology market. This is especially important in cases of blood spilled in various accidents or surgical interventions. An overview of this topic research shows that ultrasound techniques are most commonly used for the separation of microparticles in microchannels, so blood samples can only be prepared for laboratory testing. A larger volume of blood is cleaned by using stationary equipment that cannot be transported. Given that, within a few hours, the suitability of such blood for further use is limited, the proposed methods and equipment are timely and very important. The aim of this work is to create the tools that will be used to overcome this gap.

1.6. Chapter Conclusions and the Objectives of the Thesis

This chapter presents a comprehensive review of recent publications, technological means and descriptions of the existing microparticle separation in fluids and handling/levitation in air methods. Based on this, the following conclusions were drawn:

- Currently available non-vibrational blood particle separation techniques based on centrifugal sedimentation, magnetic, plasmapheresis or dialysis phenomena require costly medical equipment and exhibit limitations related to the requirements on the amount of the particles.
- The separation of microparticles at the lower (sonic) frequencies is associated with the small number of particles in microchannels.
- The use of high frequency (ultrasonic) activation, when two mechanisms of the dominant particle manipulation are acoustic radiation forces

(acting on a particle) and acoustic streaming (acting on the fluid, and thus on the drag in relation to the particle) has so far been related to the single type of or several microparticles only.

- No previous research works have been found related to the handling and levitation of microparticles flow in the air while using the same low-frequency oscillator.

2. THEORETICAL INVESTIGATION OF MICROPARTICLE SEPARATION IN FLUID AND HANDLING/LEVITATION IN AIR.

Based on the findings of the literature review and the formulated objectives, the possibilities of microparticle separation from the larger volumes have to be theoretically investigated before proceeding to the subsequent steps. This chapter presents the information regarding the design and operation principles of the object under consideration. Numerically, it is demonstrated that the low-level pressure field nodal circles of acoustic radiation waves, separate microparticles at different velocities. We use the *Comsol Multiphysics* software to confirm that the distribution of microparticles in the biological suspension or water in the acoustic pressure field is the same, but the rate of convergence of particles in the low-pressure field excited in the piezoelectric cylinder is several times different.

2.1. Modeling the Microparticle Separation Process

The aim is to investigate the presence of a steady-state ultrasonic wave for fluids and particles for levitation in an acoustic field. For this segment, the *Comsol Multiphysics* software (*Comsol, Inc*., Burlington, Mass., USA) was used to model the effects of acoustic pressure on sonic and ultrasonic frequencies. The forces acting on the particles while they are in the acoustic field, which allows the particles to separate or concentrate are related to:

1. Radiation power – one of the most important forces which affect the body in an acoustic field. Its action force leads to the particle movement in the acoustic standing wave field.
2. Stokes' forces act on the moving particles in the field of an acoustic standing wave [38] thus applying the resistance or frictional force on a particle.
3. The force of Bjerknes [39]. When particles reach the pressure node, they are subjected to the force of interaction called the Bjerknes force. The strength of the interaction is a radiation force experienced by the particle due to the acoustic wave from another particle.
4. The force of gravity. Against any particle in the earth's gravitational field, the force of gravity, or the force of attraction of the earth's surface, applies. The particles that are already in the field of the acoustic pressure node experience the force of gravity which causes the particles to settle if they are located in a stationary state, or deviates them from a straight course to the nearest node of pressure.
5. The force of Bernoulli [40]. When particles are in the field of acoustic pressure node in the fluid which moves at velocity *v*, the Bernoulli force of attraction arises due to the reduced pressure between the particles.

The aim is to investigate the effect of acoustic standing waves on the levitation of fluid and microparticles in the acoustic field. The standing acoustic wave generates a force of acoustic radiation which acts on the particles. This force arises from the pressure and the acoustic field interaction with the particles. At the initial time moment, the elastic particles are evenly distributed in a constant acoustic field, and then, due to the emerged acoustic radiation force, they begin their movement.

The acoustic radiation force is an important nonlinear force exerted by acoustic fields on particles. The acoustic radiation force F_{rad} on the particle can be calculated as the time-averaged second-order forces acting on a fixed surface $\partial\Omega$ in the inviscid bulk encompassing the particle. For inviscid fluids, vector F_{rad} is the sum of the time-averaged second-order nonlinear acoustic pressure field $\langle p_2 \rangle$ and momentum flux tensor $\rho_0 \langle v_1 v_1 \rangle$ [41],

$$\begin{aligned} F_{rad} &= -\int_{\partial\Omega} \mathrm{d}\mathbf{r} \left\{ \langle \mathrm{p}_2 \rangle n + \rho_0 \langle (n \cdot v_1) v_1 \rangle \right\} \\ &= -\int_{\partial\Omega} \mathrm{d}\mathbf{r} \left\{ \left[\frac{\kappa_0}{2} \langle \mathrm{p}_1^2 \rangle - \frac{\rho_0}{2} \langle \mathrm{v}_1^2 \rangle \right] n + \rho_0 \langle (n \cdot v_1) v_1 \rangle \right\} \end{aligned} \tag{1}$$

here: ρ_0 is the fluid density, $\boldsymbol{v}_1$ is the the first-order acoustic velocity field, $\langle p_1 \rangle$ is the the first order linear pressure field, κ_0 is the explicit expression for the compressibility, n is the normal vector.

The radiation force acting on a small particle placed in a standing wave is a gradient force of the potential function U_{rad} [21]:

$$F_{rad} = -\nabla U_{rad}, \tag{2}$$

$$U_{rad} = V_p \left[f_1 \frac{1}{2\rho_0 c^2} \langle p^2 \rangle - f_2 \frac{3}{4} \rho_0 \langle v_1^2 \rangle \right], \tag{3}$$

$$f_1 = 1 - \frac{K}{K_p}, \quad f_2 = \frac{2(\rho_p - \rho_0)}{2\rho_p + \rho_0}. \tag{4}$$

here ρ_p is the particle density, c is the the speed of sound, f_1 is real-valued and depends only on the compressibility ratio between the particle and the fluid.

The dipole scattering coefficient f_2 is related to the translational motion of the microparticles and depends on the viscosity of the fluid, K is the bulk modulus of the fluid, K_p is the bulk modulus of the particle, and V_p is the volume of the particle. The acoustic radiation force on a compressible, spherical, micrometer-sized particle of radius $r = 5 \cdot 10^{-6}$ m, suspended in a viscous fluid in an acoustic field of wavelength λ = 0.11 m at room temperature was analyzed. The numerical model contained a circular fluid container with a rigid bottomed disc-shaped piezo transducer-bimorph of radius of $R = 20 \cdot 10^{-3}$ m, which was electrically excited by harmonic law at frequency f_0 = 13.8 kHz. The modeling procedure was accomplished with the microparticles in artificial blood suspension. The model uses the following physical quantities: c = $1.48 \cdot 10^3$ m/s is the speed of sound in blood; ρ_p = $1.12 \cdot 10^3$ kg/m^3 is the particle density; K_p = 2.2 GPa is a bulk modulus of the particle and the amplitude of the normal acceleration of the transducer is $a_0 = 7.5 \cdot 10^3$ m/s^2.

2.2. Microparticles Manipulation in Fluids with Sonic Frequency Acoustic Waves

The aim is to investigate the possibility of separating microparticles by using acoustic frequency in liquids and the particle/levitation treatment in the air. For this purpose, a conical plastic container with a rigid bottom which is a discrete piezoelectric transducer was chosen (pic. 2.1).

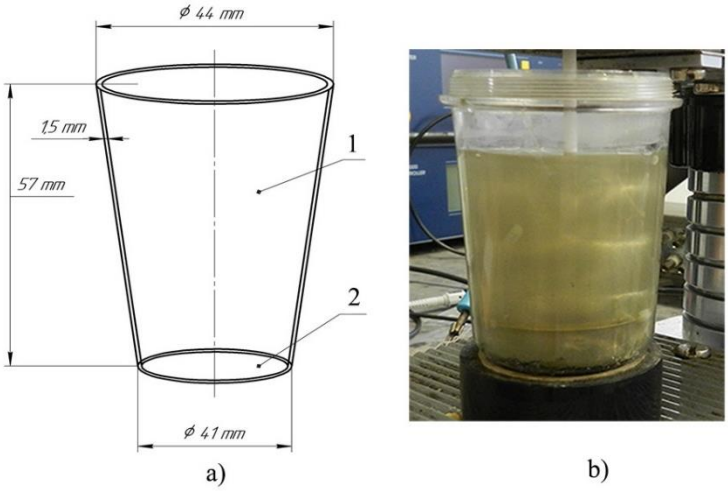

pic. 2.1. a) A scheme of the conical plastic container with a rigid bottom which is a discrete piezoelectric transducer: 1is a container, 2 is a disc-shaped piezo transducer-bimorph; b) A practical model of the conical plastic container with a rigid bottom.

Boundary conditions:

- The bottom 2-piezo normal acceleration;
- The top is open;
- The lateral surface-acoustic pressure (container 1).

Comsol Multiphysics for simulating physics-based pressure acoustics problem in the frequency domain was used. The acoustic fluid pressure was applied in the frequency domain.

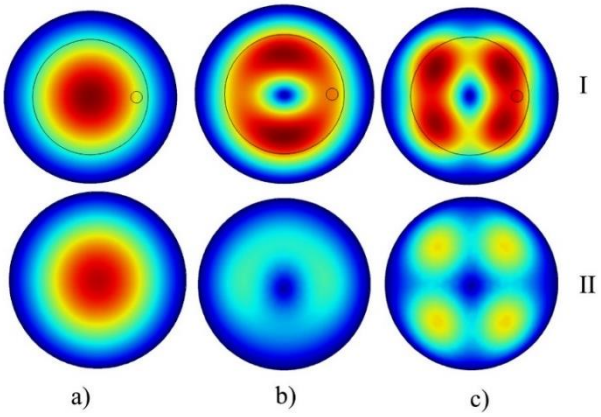

pic. 2.2. Results of a disc-shaped piezo transducer-bimorph modeling in interaction with a fluid column. I is the line which shows the oscillations modes from the side of piezoceramics; II is the line which shows the oscillation modes from the side of viscoelastic fluid: a is the first mode at 1.40 kHz, b is the second mode at 5.39 kHz and c is the third mode at 13.0 kHz

Among all the types of free elastic vibrations, it is possible to identify modes of oscillations whose frequency spectrum corresponds well to the experimental results of micro/nanoparticles separation theoretical calculations in the approximation of the plane motion. Such modes of oscillations are capable to excite acoustic standing waves in fluids under consideration.

After carrying out the modeling of a water-column and a piezo transducer, the following results were obtained. Oscillations in the first mode were at 1.40 kHz (pic. 2.2, a), the second mode was 5.39 kHz (pic. 2.2, b), the third at 13.0 kHz (pic. 2.2, c). The simulation results are presented from two positions – from the type of deformation from the side of piezoceramics in the upper line (I) and from the side of the liquid column surface in the lower line (II) of pic. 2.2.

Based on the results of the simulation, it is evident how the oscillations of the piezo transducer change upon contact with the fluid. The value of the displacement decreases, and, after passing through the fluid, it significantly weakens. Another interesting fact is that the force of pressure drops when the resonance mode increases. The strength F_z of the radiation pressure in the direction of the acoustic axis of the piezo transducer bimorph is determined by the flux of the pulse through the surface of the object [42]:

$$F_z = -\int_s \Pi_{zi} n_i ds \quad (5)$$

here $\Pi_{zi} = \bar{p}\delta_{zi} + \rho v_z v_i$ is the acoustic impulse density tensor, n_i is the projection of the normal to the surface of the object in the direction *í*, $\bar{p} = \frac{\rho}{2c^2}(\frac{\partial \Phi}{\partial t})^2 - \frac{\rho v^2}{2}$ is the time-averaged overpressure in the acoustic wave, v = grad Φ is the vibrational velocity, Φ is the potential, ρ is the density of the fluid, c is the velocity of sound in the fluid, and v_z and v_i are the components of the vibrational velocity.

Since the piezo transducer is rigidly mounted onto the bottom of the conical container, it also excites the walls of that container. As shown in pic. 2.3, the mechanical vibration of the piezo transducer activates a deformable container body, triggers the corresponding field of the acoustic pressure level, the minimum of which coincides with the minimum point of the amplitude of the radial oscillation of the deformable container body.

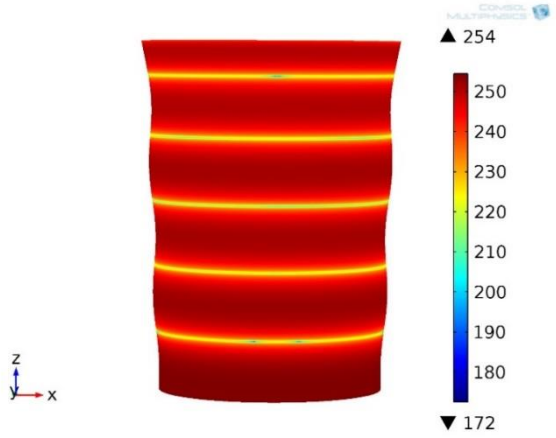

pic. 2.3. A vibrating container and acoustic pressure level (in the expression through the sound pressure level, dB_{SPL}) on its surface where the excitation frequency measures 13.8 kHz.

On the surface of the container, five pressure level bands are formed at 13.8 kHz. It is known that, during the separation of particles in the field of the acoustic wave, they propagate precisely to a low acoustic pressure level zone.

This physical phenomenon can be applied to the separation of microparticles while using low sonic frequency mechanical vibrations. At the initial time t = 0 s, the microparticles are evenly distributed in volume, i.e., contaminated or shaken fluid (pic. 2.4). The axial section of the container below shows the distribution of the acoustic pressure level field in the fluid volume: the three upper zones of the low sound pressure level are located in the perpendicular fluid flow across the longitudinal axis, whereas the two low levels are not.

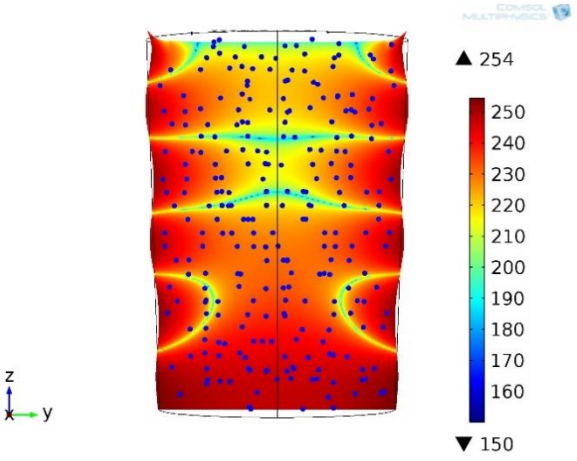

pic. 2.4. The axial section in the *yz* plane of the vibrating container and the acoustic pressure level (in the expression through the sound pressure level, dB_{SPL}) with distributed microparticles in the suspension at time t = 0s of the disc-shaped piezo transducer-bimorph excitation at 13.8 kHz frequency.

In pic. 2.5, microparticle positions in the field of the sound pressure level at t = 12s and their trajectories are provided. As we can see, the microparticles ‘cling’ to the vessel wall in low acoustic pressure level zones.

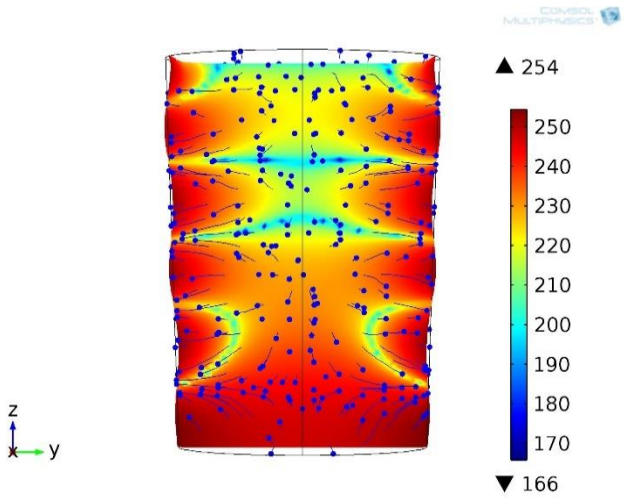

pic. 2.5. The axial section in the *yz* plane of a vibrating vessel and the acoustic pressure level (in the expression through the sound pressure level, dB_{SPL}), and the positions of the particles at time t = 12s as well as their motion trajectories. The excitation frequency is 13.8 kHz.

When analyzing the effect of acoustic waves on the volume of fluid with microparticles, we notice that microparticles accumulate in certain areas of this volume where the zones of acoustic wave nodes or anti-nodes settle down. The microparticle movement is vertical near the anti-node, horizontal at the node and inclined in between. Therefore, there is a net force pushing the hydrophobic (heavier) particle to the anti-node, and a hydrophilic (lighter) particle towards the node. When acoustic waves are applied to each other, a resonating liquid can be seen, which leads to the distribution of microparticles in the volume.

Pic. 2.6 shows the microparticles’ trajectories in the other plane, if observing from the top of the container, which corresponds to the *XY* plane in pic. 2.5. At the initial time point, the particle positions are shown in pic. 2.6, a, and pic. 2.6, b after 12 s.

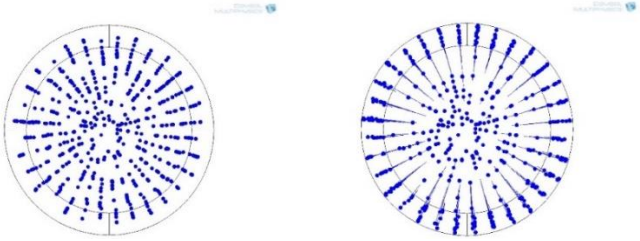

a) b)

pic. 2.6. Microparticles’ positions from the top of the vessel: a – at the initial time t = 0s, b – after 12 s.

As we can see, the microparticles ‘drift’ towards the surface of the container. This is due to Eigenvibrations of the wall of the container, which deforms one of its mods depending on the frequency of the excitation. A traveling acoustic wave generates a stream of fluid with microparticles, and when these microparticles run off, they fall into the lower pressure nodal sections of the vibrating wall.

2.3. Manipulation of Microparticles in a Fluid Using Ultrasonic Frequency Acoustic Excitation

The aim is to investigate the microparticles’ separation possibility by using ultrasonic frequency acoustic waves in the fluid. For this purpose, a tube-shaped piezoceramic transducer was chosen (pic. 2.7).

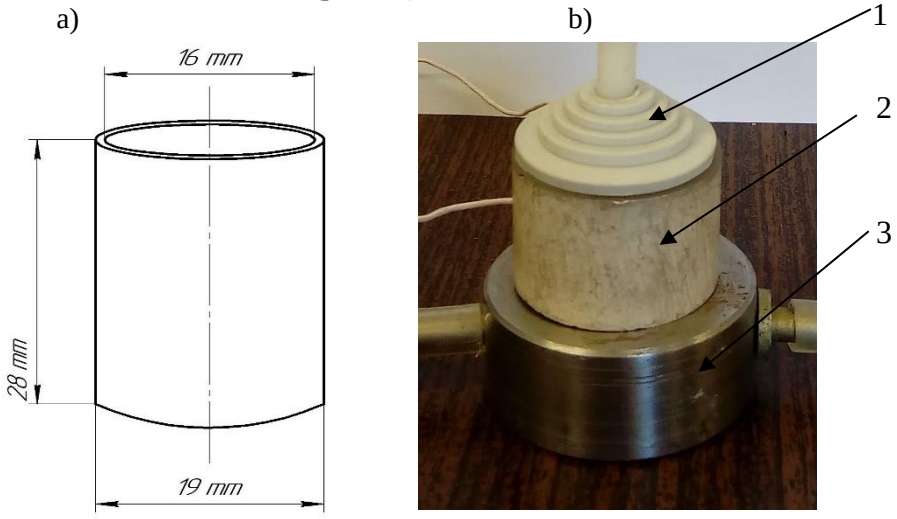

pic. 2.7. a) A scheme for the modeling of a tube-shaped piezoceramic transducer for microparticle separation; b) A photo of the piezoceramic transducer: 1 is the cover for the device; 2 is the piezotransducer; 3 is the collector for the sedimentation of microparticles.

For this modeling, a piezo-driven tube-shaped piezoceramic transducer for fluid sonication has been used. A piezoceramic transducer (of dimensions of Ø19xØ16x28mm) was made of piezoceramic material type PZT-4 [43] (*Morgan Advanced Materials Inc*., Windsor, UK). This material is ideally suited for ultrasonic, high-power acoustic radiation applications and is capable of producing large mechanically drive amplitudes while maintaining low mechanical and dielectric losses. PZT-4 material properties are given in Tab. 2.1.

Table 2.1. Physical properties of PZT-4

Density (10^3 kg/m^3)	7.7
Young’s modulus (10^{10} N/m)	7.3

Curie point (°C)	350
Mechanical Q	1000
Relative dielectric constant $\varepsilon_{33}^{T}/\varepsilon_0$	1725
Dielectric loss (1 kHz)	0.4
k_{31}	0.32
k_p	0.54
d_{31} (10^{-12} m/V)	-130

The boundary of the domain was excited by the normal displacement of a tube-shaped piezoceramic transducer cylinder element. The pressure field of the acoustic standing wave is shown in pic. 2.8. whereas the acoustic pressure level is shown in pic. 2.9.

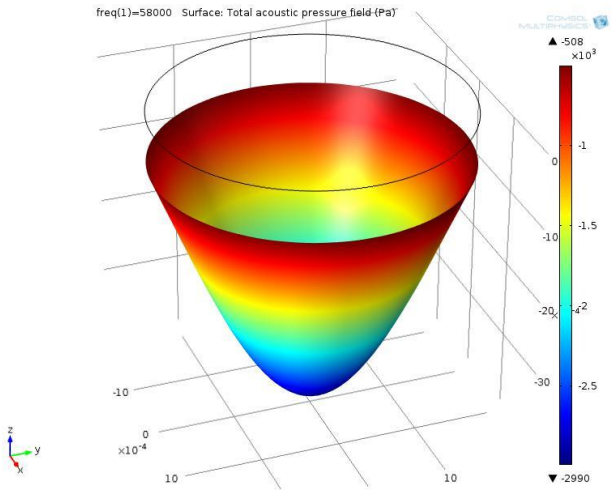

pic. 2.8. The sound pressure field of the acoustic standing wave

The acoustic radiation force on a compressible, spherical, micrometer-sized particle of radius $r = 5 \cdot 10^{-6}$ m suspended in a viscous fluid in an ultrasound field of wavelength $\lambda = 4.5 \cdot 10^{-3}$ m at room temperature was analyzed, thus $r << \lambda$. The numerical model contained a piezoelectric transducer cylinder with an internal radius of $R = 5.5\ 10^{-3}$ m and an inverse piezoelectric effect which was electrically excited by the harmonic law at frequencies $f_0 = 350$ kHz. The cylinder was filled with a fluid,

and by exciting the piezoelectric cylinder at a certain frequency, the standing waves were exposed in it. The modeling procedure was composed of two stages: in the first stage, the particles in a water suspension were simulated; in the second stage, blood properties were attributed to the biological suspension. Particle parameters were the same in both cases. A 2D model of the system was studied. The model uses the following physical quantities: the speed of sound in water: $c = 1.57 \cdot 10^3$ m/s; the speed of sound in a biological suspension: $c = 1.48 \cdot 10^3$ m/s; $\rho_p = 4 \cdot 10^3$ kg/m^3 is the particle density; $K_p = 2.2$ GPa is the bulk modulus of the particle, and the amplitude of the normal acceleration of the transducer is $a_0 = 7.5 \cdot 10^6$ m/s^2.

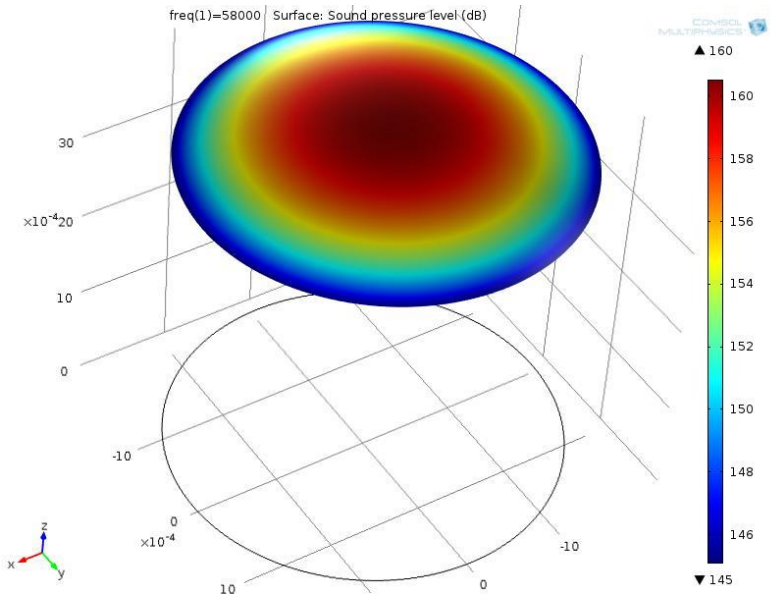

pic. 2.9. The sound pressure level of the acoustic standing wave.

For the effective separation of microparticles, the frequency of excitation of the acoustic waves was chosen that concentrates microparticles in two rings and equals to 350 kHz. The pressure fields of the standing waves in a biological suspension and in water suspension are shown in pic. 2.10.

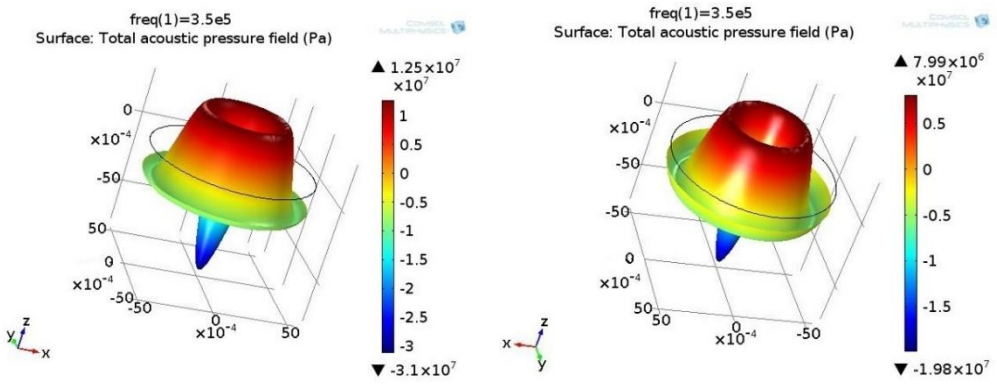

a) b)

pic. 2.10. The pressure field (Pa) of the standing wave in **a** biological and **b** water suspension. The excitation frequency equals 350 kHz. The high-pressure area is represented in the red and blue area of low pressure. The values of the high and low pressure reach several kPa but in the opposite directions.

The acoustic pressure levels for these two substances are presented in pic. 2.11.

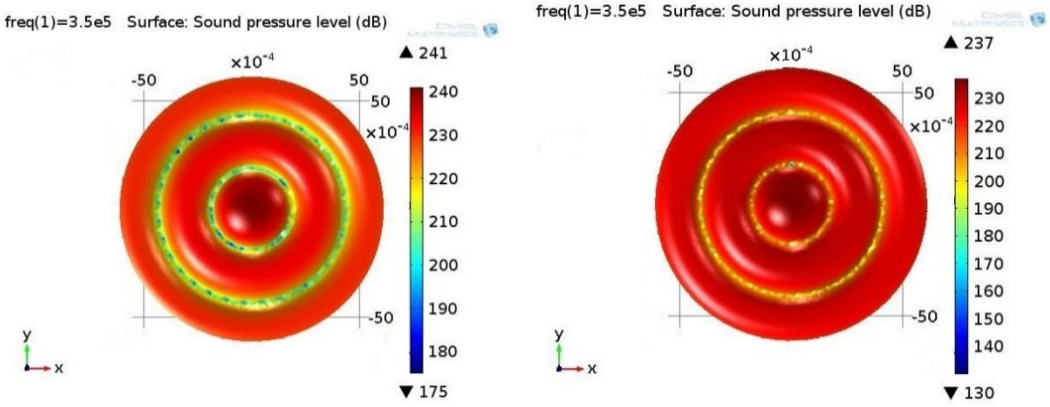

a) b)

pic. 2.11. The acoustic pressure level (in the expression through the sound pressure level, dB) in **a** biological and **b** water suspension. The excitation frequency equals 350 kHz.

The acoustic pressure field is analogous in both fluids, i.e., there are three high-pressure areas and two low-pressure areas in between. However, the low-pressure areas differ in different fluids: in the case of the biological suspension, they are wider in comparison to those of the water suspension. Consequently, this is caused by different parameter values of the fluids (biological and water suspensions in this case). Due to the standing acoustic waves, the acoustic radiation force develops and acts on microparticles. This force occurs due to the pressure and the acoustic field interaction

with the microparticles. At the initial moment of time t_0, the microparticles are uniformly distributed in the acoustic field (pic. 2.12), and later, due to the acoustic radiation forces and the drag force that are generated, their movement begins.

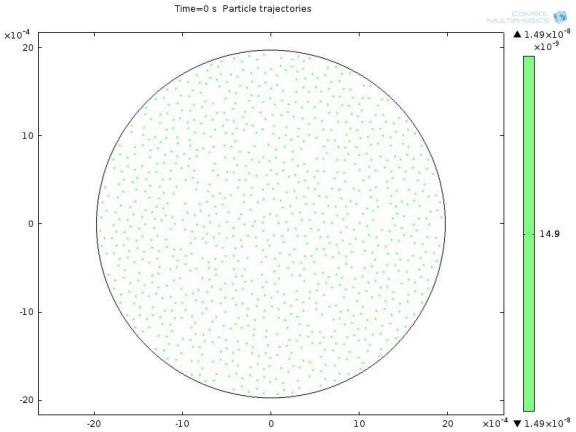

pic. 2.12. The distribution of microparticles in the acoustic pressure field in the biological suspension at the initial moment of time t_0.

The distribution of the microparticles in the acoustic field at different points in time are shown in pic. 2.13 for the biological suspension. The color of the microparticles represents the speed at the moment of time t_i which is calculated by integrating the equations of motion.

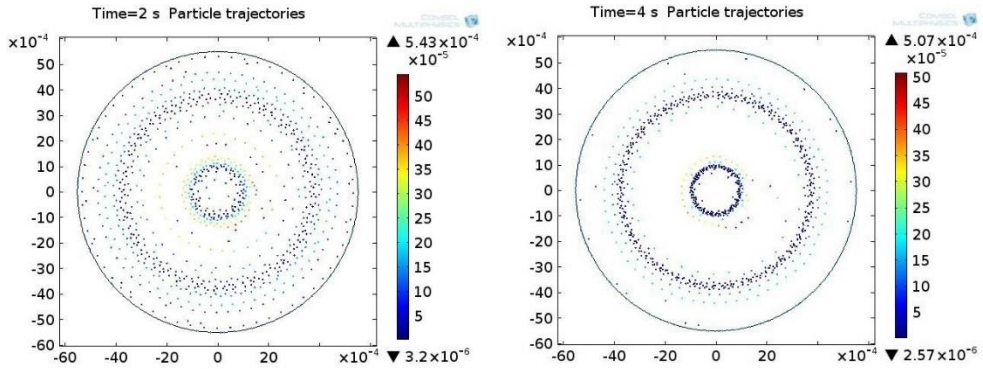

a) b)

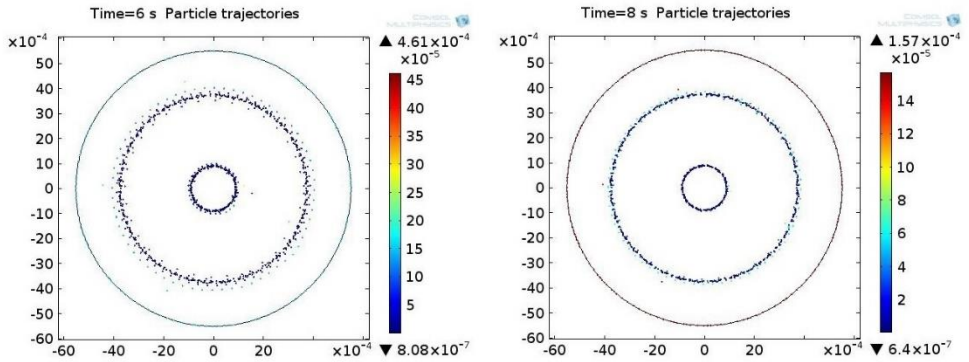

pic. 2.13. The distribution of microparticles in the acoustic pressure field in the biological suspension at different times t_i: a) 2s; b) 4s; c) 6s; d) 8s.

The distribution of the microparticles in the acoustic field at different points in time are shown in pic. 2.14 for the water suspension.

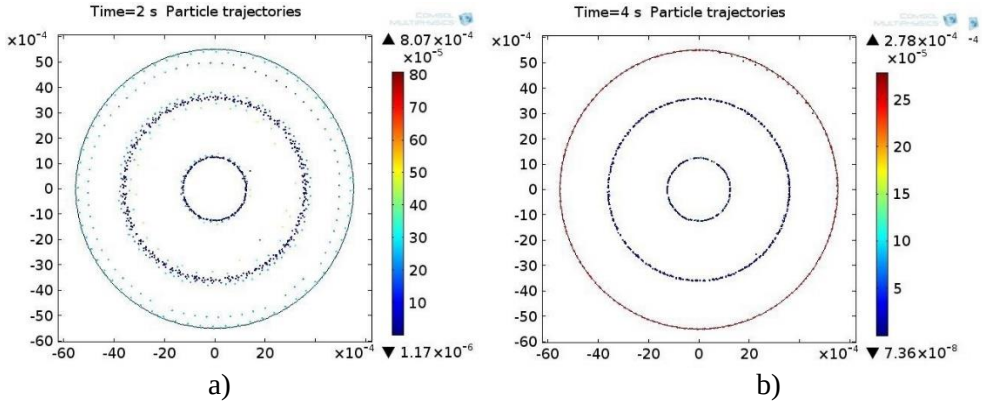

pic. 2.14. The distribution of microparticles in the acoustic pressure field for the water suspension at different times t_i: a) 2s; b) 4s.

It was found that the distribution of both biological and water suspension microparticles in the acoustic pressure field is the same, yet the velocity of microparticle convergence to the low-level pressure field is different. When the fluid is water, the microparticles get into the low acoustic pressure field in 4 s, whereas in the case of the biological suspension, it takes twice the time, i.e., 8 s. Another difference between the fluids under investigation is the microparticle distribution in low acoustic pressure fields. The concentration areas of the biological suspension microparticles at the end of the process, i.e., when the fluid becomes stationary, are broader in comparison to the areas obtained while using water as a fluid (see pic. 2.14).

Both peculiarities may be explained by different values of the analyzed fluid properties. Finally, the third difference lies in the geometrical discrepancy of the small

radius low acoustic pressure level areas: in the case of the biological suspension as a fluid, the area radius is smaller by 30% in comparison to that of the water suspension. This fact should be taken into consideration when separating biological suspensions of differing viscosity. The consideration of this effect enables us to control the microparticle distribution in the desired areas of the acoustic field. This entails a quick and reliable microparticle concentration in the desired acoustic field areas (by changing the characteristics of vibrations generated by the transducer). This is a technological approach towards the removal of microparticles from suspensions.

The simulation results have shown that the microparticle density does not affect the acoustic pressure because it is created by an external effect, in this case, it is the reverse piezo effect. However, the density of the microparticles influences the separation time interval. This time interval particularly increases when the fluid and the microparticle density ratio are approaching unity. As the fluid and the microparticle density ratio is very important, from the engineering point of view, this ratio directly affects the tube-shaped piezoceramic transducer length. In our case, the length of the tube-shaped piezoceramic transducer and the flow rate of the fluid were sufficient for the microparticle separation time interval equal to 8 s. In theory, if the fluid and the microparticle density are close, the time of the process of purification increases considerably, thus requiring a larger length of the separator operation.

2.4. Vibroacoustic Handling and Levitation of Microparticles in Air

The sound can levitate objects of various sizes and materials through the air, water, and tissue. It allows manipulating cells, liquids, compounds or living things without touching or without contamination. However, acoustic levitation requires the targets to be enclosed with acoustic elements, or else it is denoted by limited maneuverability. From the literature review, we see that ultrasound vibrations are commonly used for the transport of microparticles, and they are levitated by using ultrasound waves. Most of the research works are devoted only to the transport of microparticles, or to their levitation. We propose the use of non-ultrasonic acoustic waves propagating in a cylinder, which, in its own form, is excited from the same disc-shaped piezoelectric transducer-bimorph for acoustic waves excitation.

The concept of acoustic levitation and handling is based on the wave equation theory, and the solution as a sum of forward and backward propagating acoustic waves is expressed as the following [44]:

$$p(x) = P_m/2\ sin(n\pi x/\lambda_n - 2\pi ft) + P_m/2\ sin(n\pi x/\lambda_n + 2\pi ft) \qquad (6)$$

where $p(x)$ is the sound pressure; $P_m=2A$ is the amplitude of the sound pressure peak of the waveguide; A is the disc amplitude of the piezoelectric converter-bimorph vibration; λ_n is the length of the waveguide; f is the acoustic field frequency; n is the harmonic number; x is a spatial variable; t is a time variable.

Formula (6) shows that the superposition of the forward and reflected sinusoidal acoustic waves is a localized wave packet showing the development of sound pressure over time and space. Obviously, the sum of the two sinus functions depends on a new

type of solution, and not simply on the sinus function. As the size of microparticles is much smaller than the acoustic standing wavelength (30mm – 300mm), the microparticles exposed in the acoustic field are subjected to the action of the acoustic radiation force.

The organic glass cylindrical container with a lid whose bottom is a disc-shaped piezoelectric transducer-bimorph is filled with air. The cylindrical container is a deformable body in which disc-shaped piezoelectric transducer-bimorph oscillations cause mechanical vibrations and acoustic pressure fields. This physical phenomenon describes the physics of a deformable body and the acoustic field, and explains why it is necessary to examine the coupled physical system and simulate the corresponding task. This task connecting the deformable body and the acoustic field physics was implemented in COMSOL Multiphysics by using the digital finite element method. The experimental study found that the system's resonant frequency is 14.2 kHz. After conducting modal analysis, from the obtained results (pic. 2.15), it can be noted that in the acoustic field there are three clearly defined high and low-pressure zones that are repeated successively.

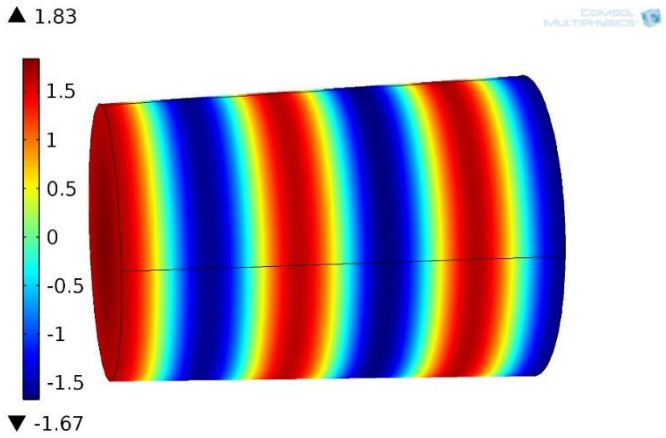

pic. 2.15. Acoustic pressure (Pa) field on the cylindrical container surface, excitation frequency 14.8 kHz.

The dependence of this pressure on the cylindrical container is given in pic. 2.16, which shows that we have two and a half waves. In this dependence of the pressure on the cylindrical container, the zero-length corresponds to the bottom of the container.

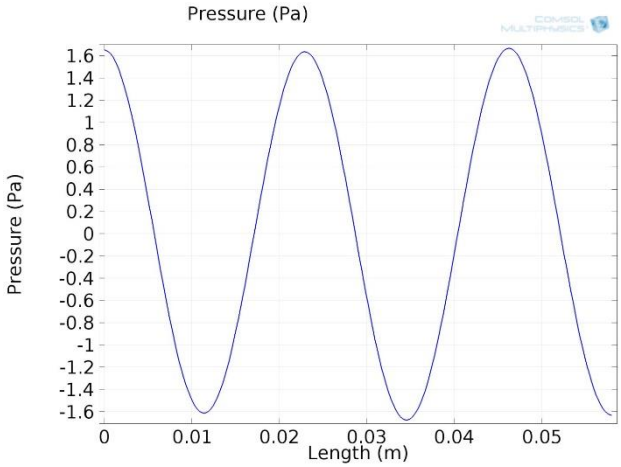

pic. 2.16. Acoustic pressure dependence along the cylindrical container generatrix.

The distribution of the sound pressure level is presented in pic. 2.17, pic. 2.18 and pic. 2.19, respectively.

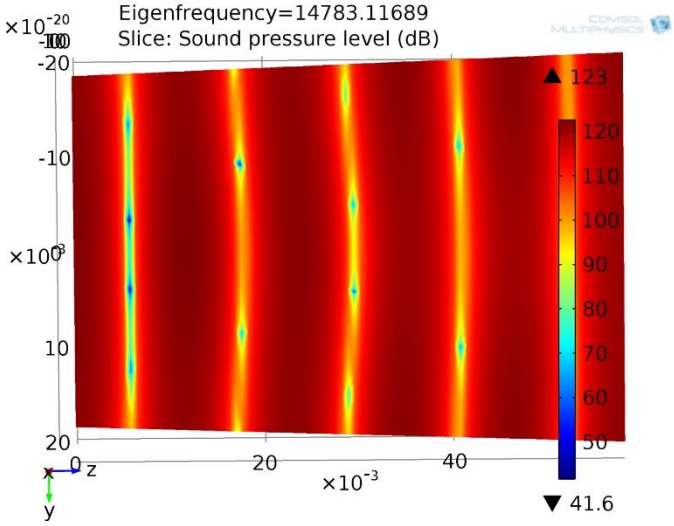

pic. 2.17. The acoustic pressure level in the cylindrical container section.

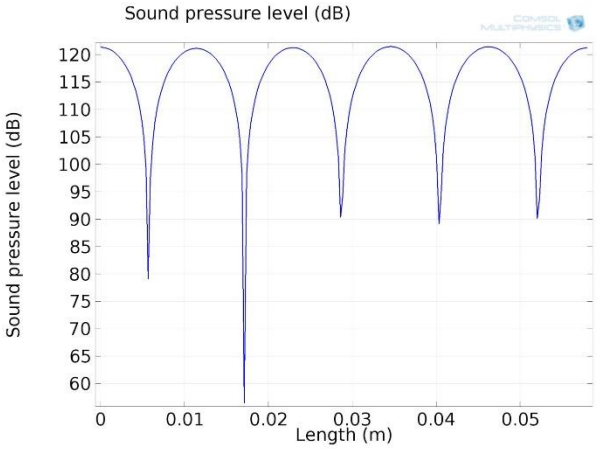

pic. 2.18. The acoustic pressure level distribution on the cylindrical container surface.

We see that the lowest level of the acoustic pressure matches the value of the zero acoustic field. Pic. 2.17 and pic. 2.18 show that there are five low-level acoustic pressure levels, sharply defined, narrow areas. The acoustic pressure level field on the cylindrical container body is shown in pic. 2.19, which shows the low-pressure zones that have been parted in parallel.

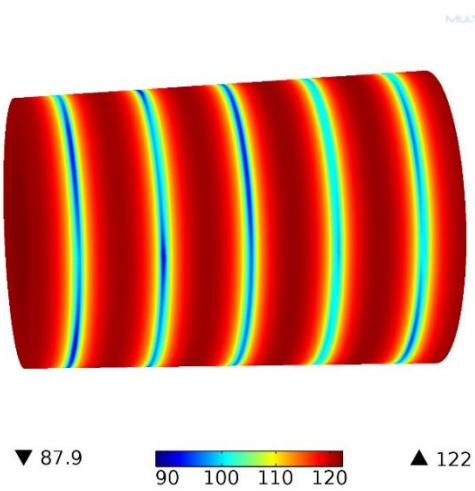

pic. 2.19. The acoustic pressure level field on the cylindrical container surface.

2.5 Chapter Conclusions

1. Multi-physics computational models of separation, handling and levitation of microparticles by sonic frequency acoustic excitation waves were developed. Vibrational modes of the suspensions of the separation microparticles were obtained. The most effective was the third selected mode, and the microparticle separation

process was simulated at 13.8 kHz excitation frequency. The conical cylinder-shaped, fluid-filled container with the bottom-mounted piezo transducer-bimorph works for both the wall of the container and the microparticles in fluid and separates microparticles in 12 s.

2. The multi-physics computational model of microparticle separation by ultrasonic frequency acoustic excitation waves in the tube-shaped piezoceramic transducer was developed. The most effective frequency was found to be the 345 kHz excitation frequency. The microparticle separation rate has been found to be influenced by the suspension viscosity, in which it is submerged. When the fluid is water, microparticles get into the low acoustic pressure field in 4 s, whereas in the case of a biological suspension, it takes twice the time, i.e., 8 s. The concentration areas of the biological suspension microparticles at the end of the process, i.e., when the fluid becomes stationary, are broader in comparison to the areas obtained while using water as a fluid. The third difference lies in the geometrical discrepancy of the small radius low acoustic pressure level areas: in the case of the biological suspension as a fluid, the area radius is smaller by 30% in comparison to that of water. This fact should be taken into consideration when separating biological suspensions of various viscosity.

3. EXPERIMENTAL RESEARCH OF BIOLOGICAL SUSPENSIONS MICROPARTICLE SEPARATION

3.1. Separation of Microparticles by Sonic Frequency Acoustic Excitation

To study the proposed theory, a piezo transducer with a range of operation from 1.3 kHz to 25 kHz was used. For the validation of the simulation results, the holographic interferometry setup was used.

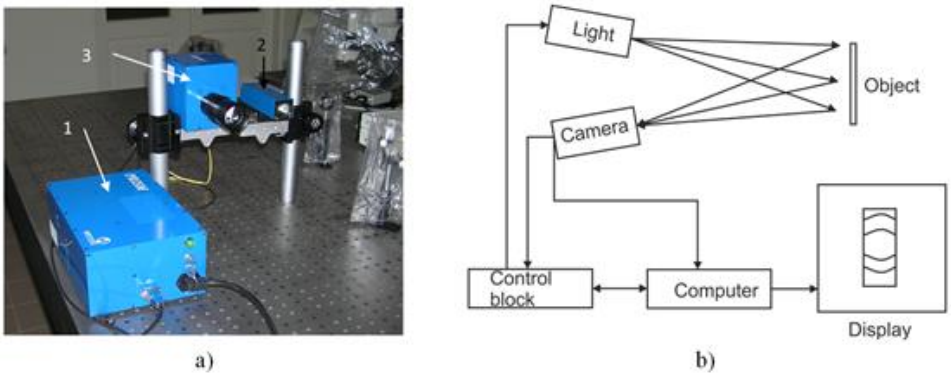

pic. 3.1 Holography System PRISM: (**a**) is the set-up picture; (**b**) is the operation scheme.

The main characteristics of the PRISM system are presented in Tab. 3.1.

Table 3.1. The main characteristics of the PRISM system.

Measurement Sensitivity	**< 20 nm**
Dynamic measurement boundary	100 μm
Measurement boundary	> 100 μm
Greatest measurement area	1 m diameter
Distance to the object	> ¼ m
Data registration frequency	30 Hz

The block-scheme of the experimental setup with the laser holographic interferometry system is presented in pic. 3.2.

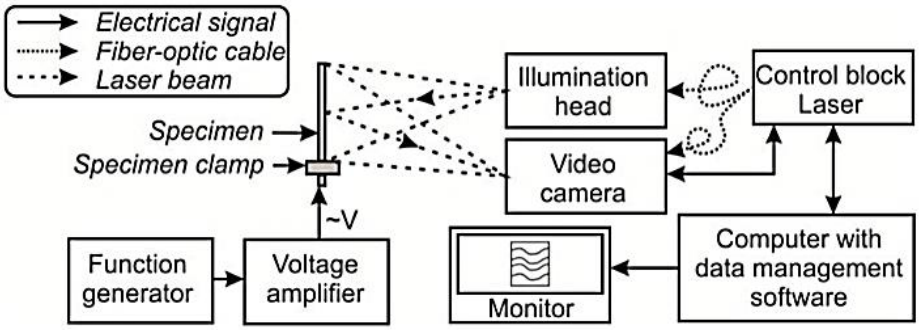

pic.3.2. A block-scheme of the experimental setup with a laser holographic interferometry system.

For a visual comparison of the experiments, it was necessary to check whether the results were obtained by means of laser triangulation displacement transducer for the sake of further experiments. Therefore, the holographic method was used to analyze displacements in the piezoceramic transducer. In the tests, the PRISM system was used (pic. 3.3).

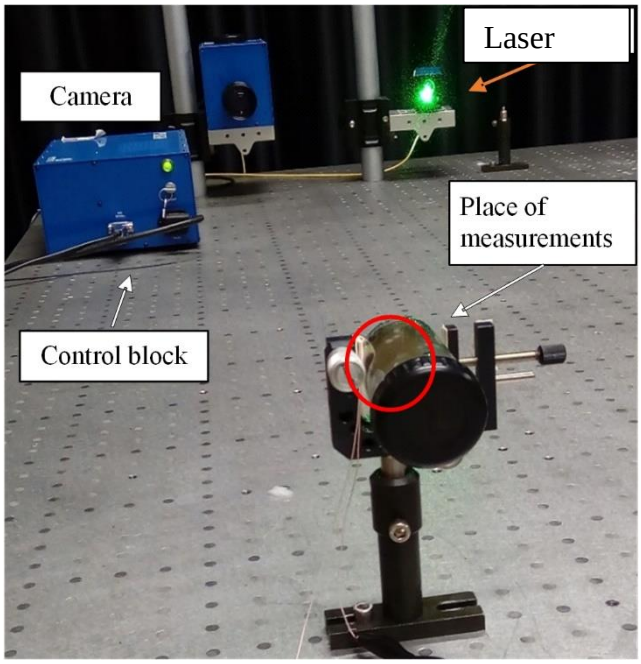

pic.3.3. The holographic interferometry setup used in the experiment.

To determine the working and resonant frequencies of the piezo transducer, a study of a loaded actuator on a holographic installation was initially carried out (pic. 3.4). The results showed that the first mode of the piezo transducer is 4.4 kHz at a voltage

of 200 mV (pic. 3.4, a), the second is 9.4 kHz (pic. 3.4, b), and third is 13.9 kHz (pic.3.4, c).

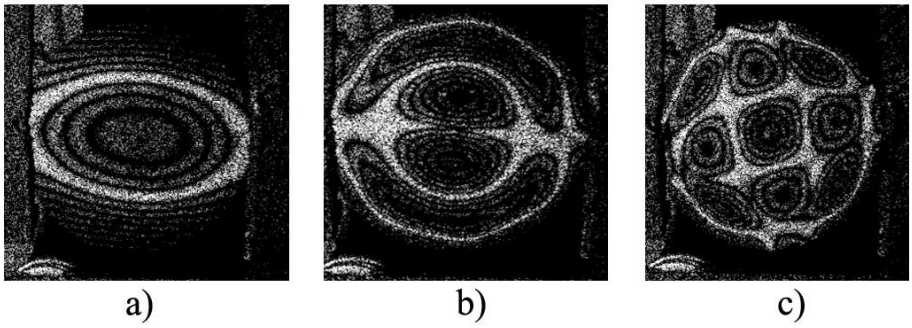

pic. 3.4. The holographic pattern of displacement of the surface of the piezo transducer bimorph, depending on the resonance mode: a at 1.4 kHz, b at 5.4 kHz, c at 13.9 kHz.

The next step in the study of the piezo transducer was the identification of its displacement by using the *Polytec PSV-500-D-HV* device. The studies were carried out in the static load mode with different input signal frequencies. Each of the forms of deformation was determined from the peak values of the deformation.

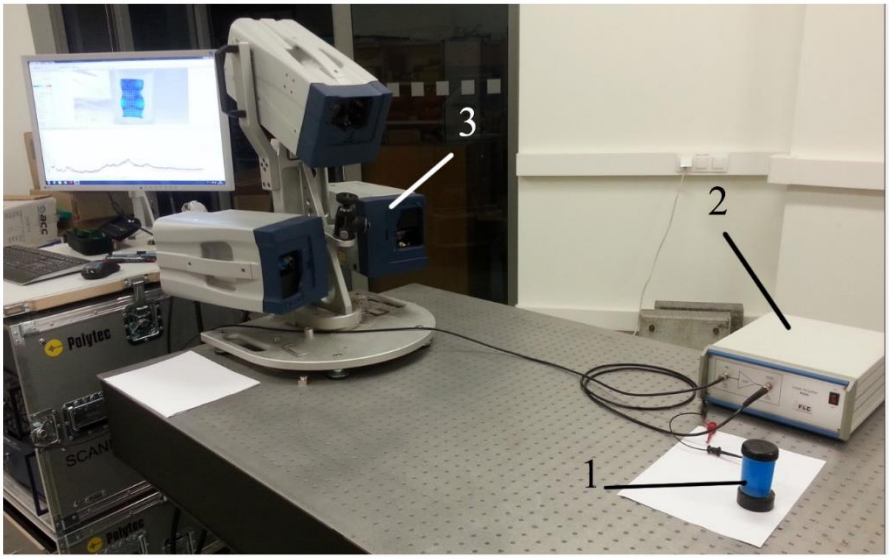

pic. 3.5. The experimental setup: 1 – an experimental object; 2 – a liner amplifier *P200* (*FLC Electronics* AB, Sweden), 3 a 3D scanning vibrometer *PSV-500-3D-HV* (*Polytec GmbH*, Germany).

Each of the following forms of deformation has its own peculiarities in the zonal distribution. The higher is the disc-shaped piezo transducer-bimorph mode, the

smaller is the deformation region each of the peak points has, but the number of points increases (pic. 3.6).

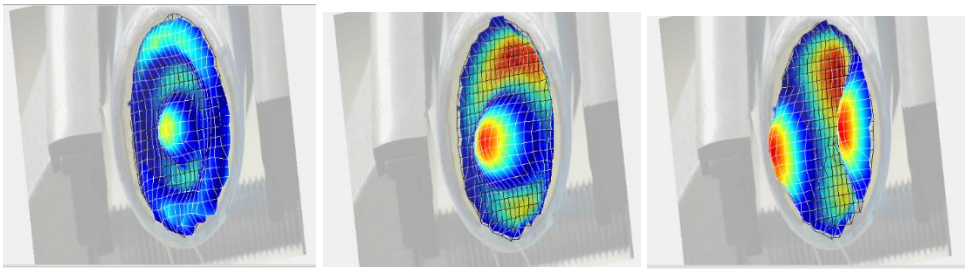

a) b) c)

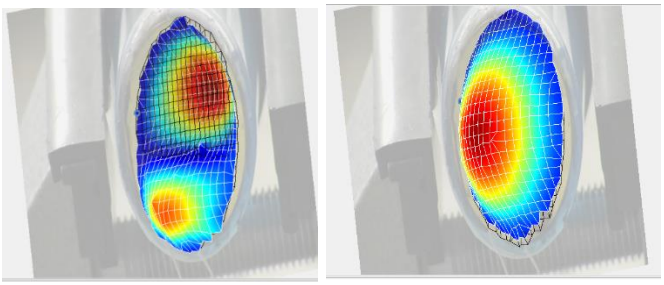

d) e)

pic. 3.6. The displacement of the disc-shaped piezo transducer-bimorph and the search for modes at different frequencies: a) 13.81 kHz; b) 5.01 kHz; c) 3.95 kHz; d) 2.48 kHz; e) 1.03 kHz.

Since the piezo transducer is rigidly mounted on the bottom of the conical container, it also excites the wall of that container (pic. 3.7).

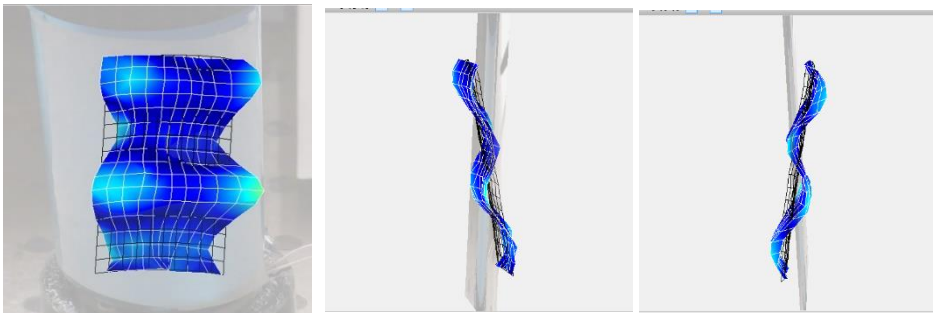

a) b) c)

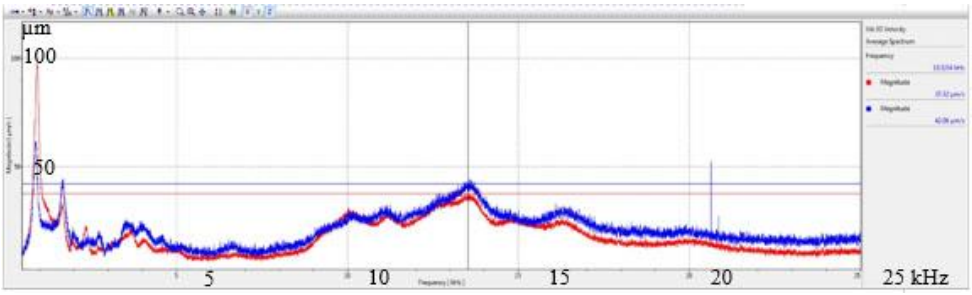

d)

pic. 3.7. Displacement of the wall (a–c) of the conical container at 13.52 kHz and its peak displacement plot (d).

The numerical values of displacement of the piezotransducer are shown in the strain diagrams of each mode (pic. 3.8). The axial displacement for the fourth mode is 75.86 µm (pic. 3.8, a) at five peak points; for the third mode 89.22 µm at three peak points with the largest at the center of the disc (pic. 3.8, b), for the pre-peak value of the third mode, it is 53.86 µm, and we see four deformation points, which leads to the decrease in the numerical value (pic. 3.8, c), for the second mode, we detect 94.55 µm and two poles of displacement of the disc-shaped piezo transducer-bimorph surface (pic. 3.8, d) whereas the first mode with the greatest deformation has an axial value of 205.54 µm and a single bending point (pic. 3.8, e).

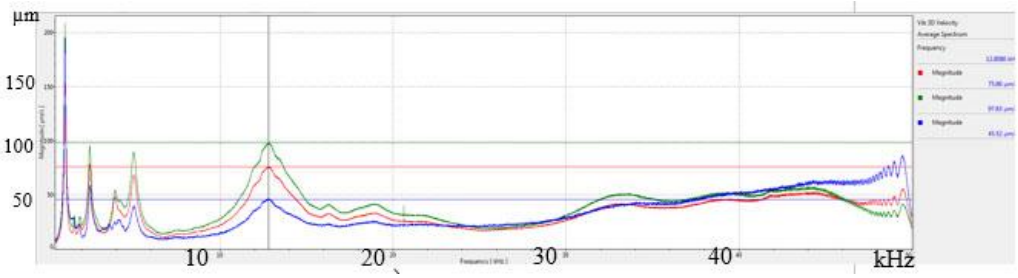

a)

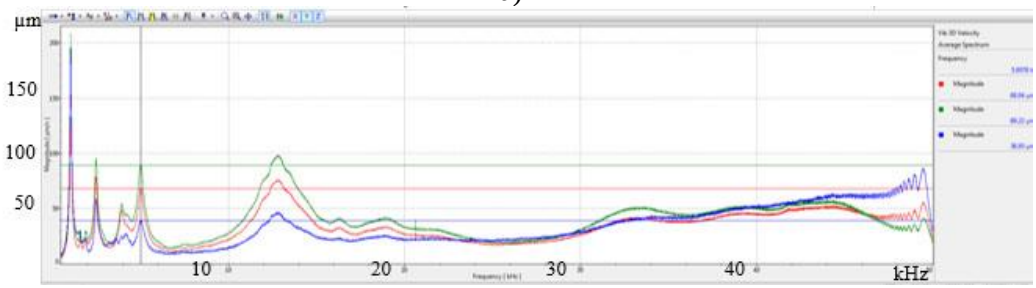

b)

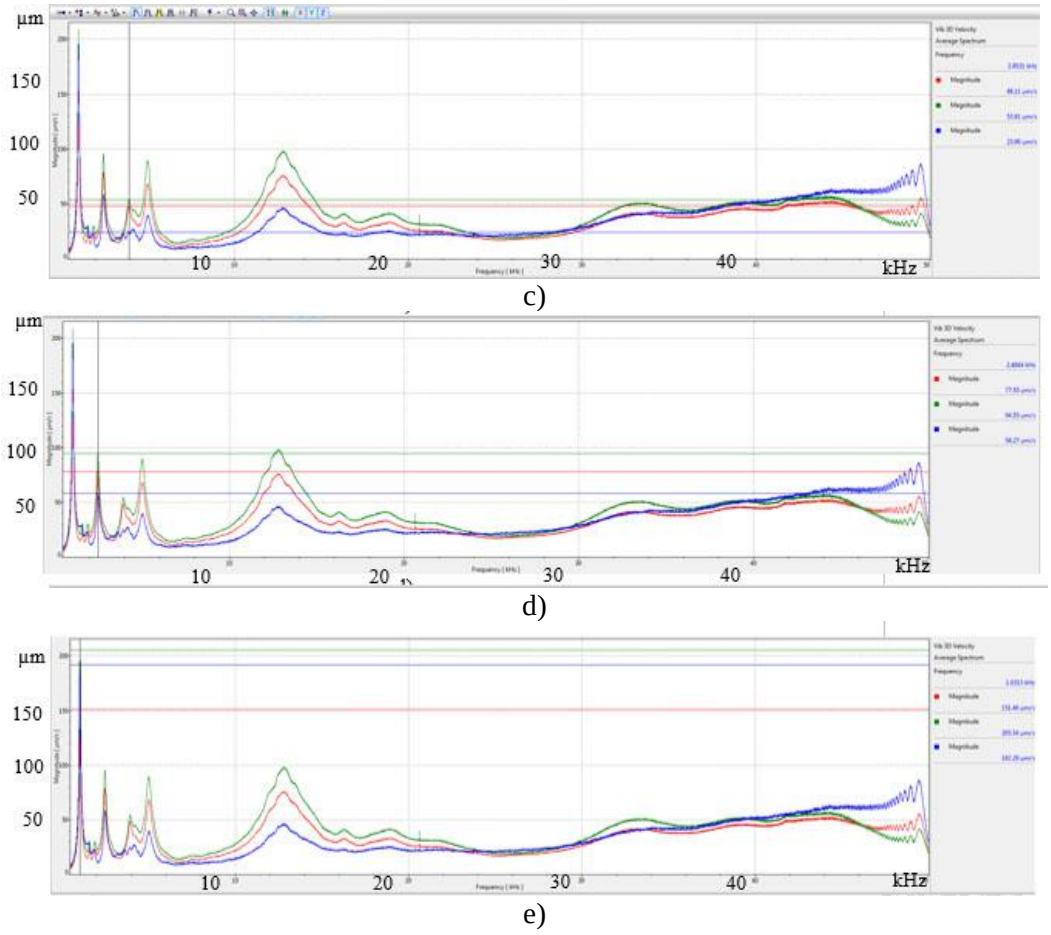

pic. 3.8. The displacement of the disc-shaped piezo transducer-bimorph: a) 13.81 kHz; b) 5.01 kHz; c) 3.95 kHz; d) 2.48 kHz; e) 1.03 kHz.

Also, it was investigated how the deformation of the piezo transducer changes when the conical container is filled with water. For the experiment, the third mode was selected. The results have shown that for an empty conical container, the resonating frequency at a given mode is higher by 2.3 kHz, while the displacement and inertia increase significantly when the conical container is filled with a fluid. Since water acts as a waveguide and since the sound dispersion in the water is lower, the deformation parameters also increase (pic. 3.9).

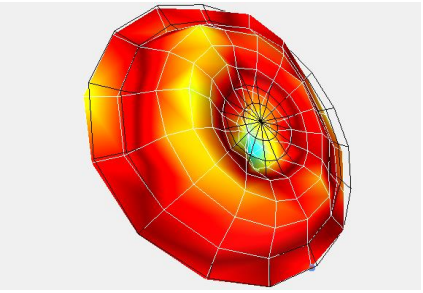

pic. 3.9. Investigation of deformation of the disc-shaped piezo transducer-bimorph with a water column: excitation 5 V, III mode at 12.594 kHz.

When analyzing the results of the displacement magnitude change, we can clearly see that the water filling of the container increases the value of the peak displacement of its wall (pic. 3.10). However, at the same time, the level of the noise of the signal increases. This is due to the fact that when the energy is stored, the inertial motion of the piezo transducer increases. So the effect of increasing the displacement of the piezo transducer was discovered during the examination of the disc under a load of the water column.

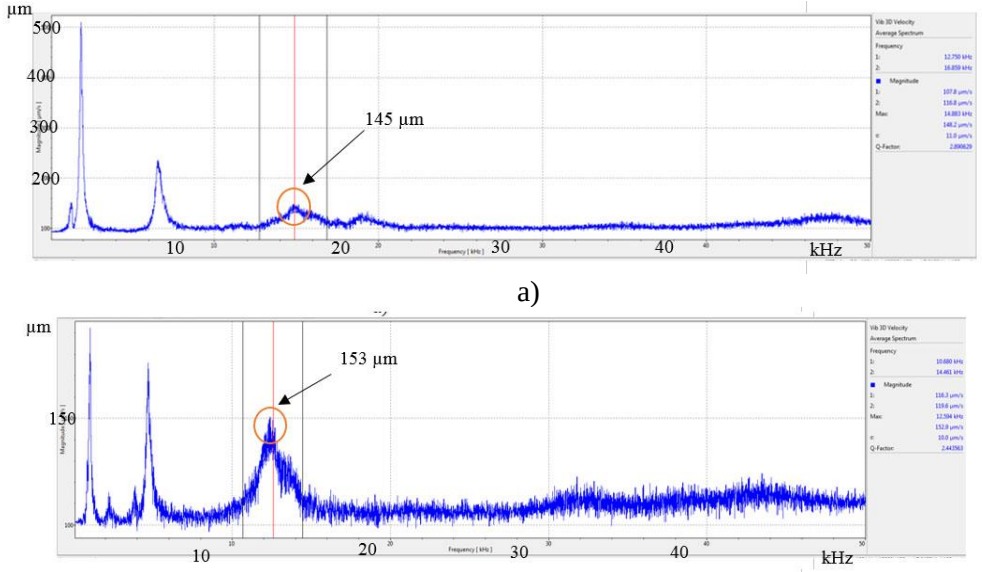

pic. 3.10. Investigation of the deformation of the disc-shaped piezo transducer-bimorph: a) without fluid 5V, III mode at 14.883 kHz; b) with fluid 5 V, III mode at 12.594 kHz.

Interesting results were obtained by doubling the excitation signal amplitude. First of all, it affected the resonance frequencies of the piezo transducer. Resonance frequencies for a rigidly fixed perimeter of the piezo transducer are presented in Tab. 3.1.

Table 3.1. Dependence of the peak values of the resonance on the applied voltage and of the conical container with and without fluid.

Type of measurement / Mode	I	II	III	IV
Piezo transducer without fluid at 5 V	1.867 kHz	6.563 kHz	14.883 kHz	18.961 kHz
Piezo transducer without fluid at 10 V	1.852 kHz	6.641 kHz	14.805 kHz	18.898 kHz
Piezo transducer with fluid at 5 V	1.023 kHz	4.695 kHz	12.594 kHz	-
Piezo transducer with fluid at 10 V	1.023 kHz	4.602 kHz	12.469 kHz	-

Pic. 3.11 shows graphical representations of the resonant vibrations of the disc-shaped piezo transducer-bimorph with a fluid column at 10 V excitation signal.

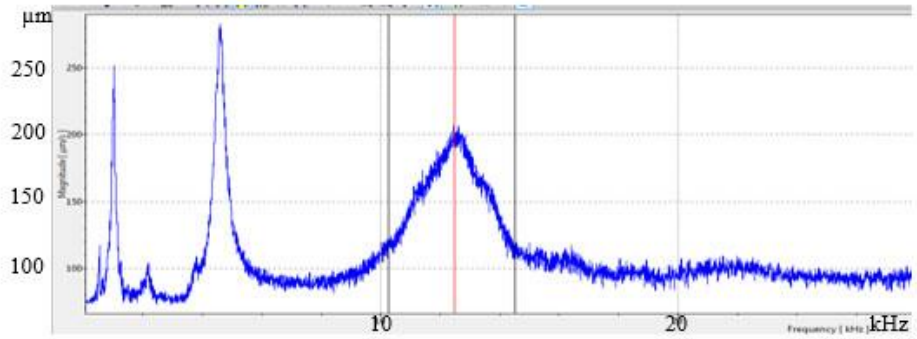

pic.3.11 A graphical representation of the resonance modes for a disc-shaped piezo transducer-bimorph fixed on a container bottom: b) The input signal voltage is 10 V, and the container is filled with a fluid.

The Eigenmodes of the disc-shaped piezo transducer-bimorph under fluid column are shown in pic. 3.12.

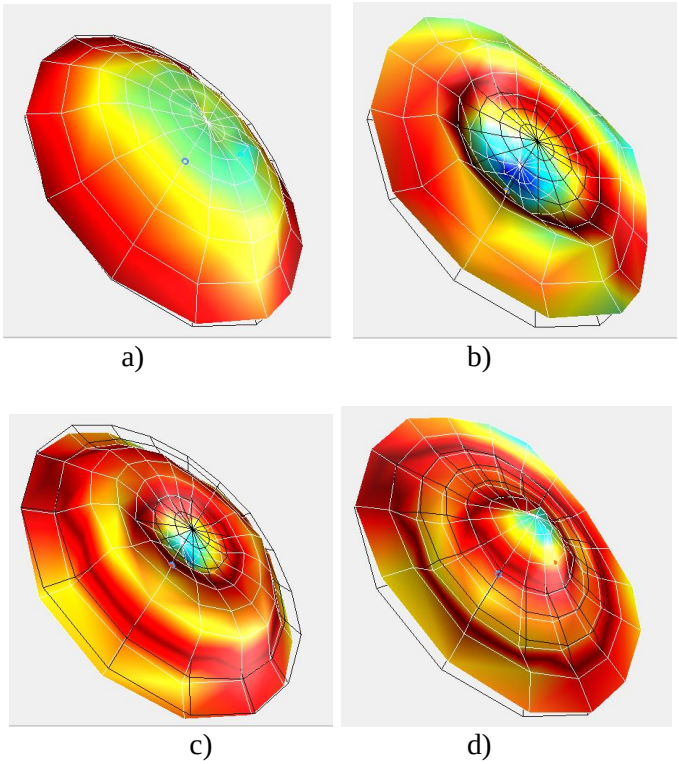

pic. 3.12. Eigenmodes of the disc-shaped piezo transducer-bimorph under the fluid; excitation signal amplitude 10 V; frequency: a) 1.023 kHz, b) 4.602 kHz, c) 12.469 kHz, d) 17.588 kHz

The displacement of the piezotransducer vibrating at the third and the fourth resonance modes does not differ prominently. Taking into account the amplitude-frequency characteristic given in pic. 3.12, b, we see that the third mode has the widest frequency band, at which it is possible to obtain stable results with some movement in this range.

The experimental setup of microparticles separation in suspensions is presented in pic. 3.13, a. During the experiment, it was found that after 5–8 seconds from the excitation signal applied to the resonator microparticles begin to accumulate around the acoustic nodal circles of the conical container wall thus stratifying in the test container sections disposed at same distances from each other. The third and the most stable resonance result was at 12.2 kHz. For the clarity of the experiment, observations were made regarding the effect of the amount of fluid in the test container on the obtained result. As a result, a proportional number of concentrated clusters of particle fractions of the suspension was obtained depending on the height of the fluid column (pic. 3.13, b, and c).

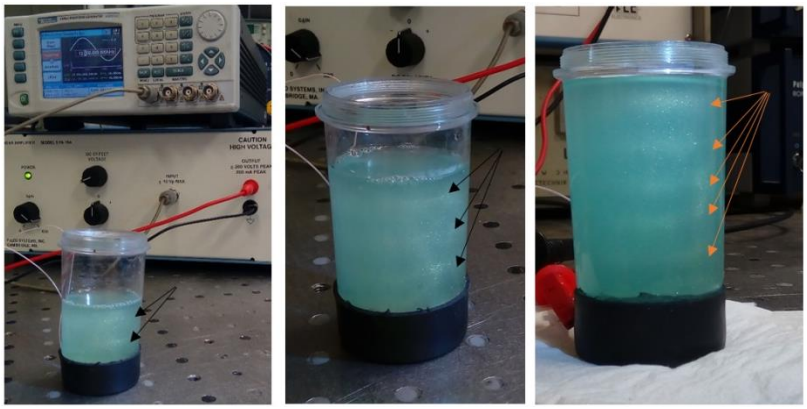

a) b) c)

pic. 3.13. Experimental setup (a) and microparticle concentration circles (b, c), depending on the height of the fluid column at a frequency of 12.2 kHz.

3.2. Experimental Validation Procedure of Ultrasonic Separation of Biological Suspension Microparticles

To validate the results of modeling, experiments with a piezo-driven ultrasonic tube-shaped piezoceramic actuator for fluid sonication were conducted. To assess the separation process of microparticles suspended in a suspension while using ultrasonication and to determine the vibrating deflection shapes and the Eigenmodes of the piezoceramic tube-shaped actuator, an experimental setup with a *Polytec* 3D scanning vibrometer (*Type PSV-500-3D-HV*, *Polytec GmbH*, Waldbronn, Germany) was developed and is shown in Pic. 3.14, a.

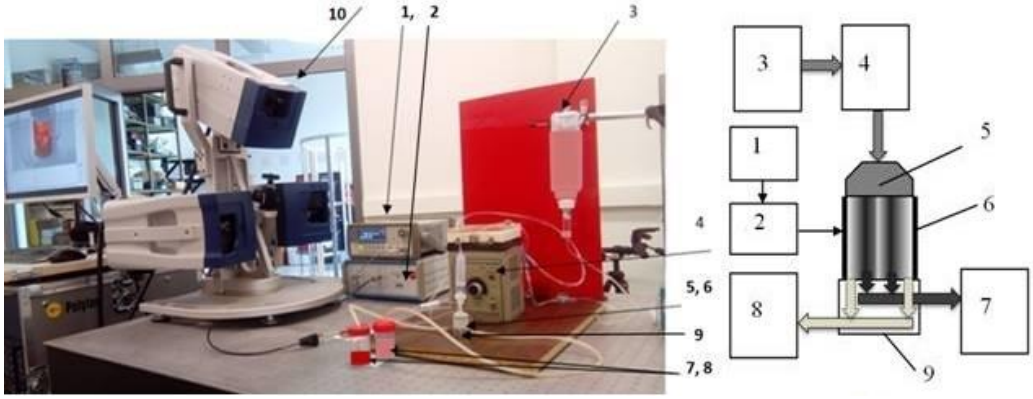

a) b)

pic. 3.14. Photo of the experimental setup a) and the block diagram b) for the separation of microparticles suspended in a fluid: an ultrasonic frequency signal generator (*Agilent 33220A*) – 1, a voltage amplifier *P200* (*FLC Electronics*) – 2, a container of the suspension – 3, a peristaltic pump (model *NP-1M*) – 4, the inlet of the actuator – 5, a piezoelectric tube-shaped actuator – 6, containers for the microparticles phase and the fluid phase – 7 and 8, a collector of the fluid – 9, and *Polytec* 3D scanner-vibrometer – 10.

The experimental setup consists of the scanning vibrometer 10, the piezoelectric tube-shaped actuator 6 driven by an ultrasonic frequency signal generator 1 (*Agilent Technologies, Inc*., Loveland, Colorado 80537, USA) and a voltage amplifier 2 (*P200 – FLC Electronics AB*, Sippedalsvagen, Sweden). For the fluid flow rate control and transfer to the actuator, a peristaltic pump 4 (*model NP-1M*, *LOIP Ltd*., Saint-Petersburg, Russia) is used. Container 3 with the fluid is connected to the inlet tubing of the peristaltic pump, and the outlet tubing of the pump is connected to inlet 5 of tube-shaped actuator 6. The bottom end surface of a tube-shaped piezo actuator (dimensions Ø19x Ø16x28mm) is glued with elastic silicone to the ring-shaped surface of outer diameter Ø17mm of the manufactured collector (pic. 4.8). The sonication of the fluid is carried out by the use of a tube-shaped actuator; an ultrasound standing wave is applied to separate/distribute microparticles in the researched fluid. The separated particles and the liquid phase through fluid collector 9 are collected in containers 7 and 8. The displacement of the piezoelectric tube-shaped actuator and its frequency response are measured by using *Polytec* 3D scanning vibrometer 10.

A block diagram of the experimental setup is presented in pic. 3.12, b. It explains the direction of the fluid movement in the system for the separation of microparticles suspended in a fluid. In suspension container 3, the fluid with microparticles is stirred and transferred to peristaltic pump 4 which regulates the flow rate of the fluid before entering actuator inlet 5 and the separation chamber of piezoelectric tube-shaped actuator 6. An ultrasonic standing wave sonication of the fluid in the flow was established by the piezoelectric actuator driven by signal generator 1 and voltage amplifier 2. After sonication, the suspended microparticles were separated into the enriched and the cleared phases by collector 9, and then they were transported into separate containers 7 and 8. The duration of the sonication process in the separation chamber of the tube-shaped actuator was controlled by the flow rate of peristaltic pump 4. The stable separation pattern of the microparticles was formed after 5–10 s and was monitored by the *Nikon* microscope *Eclipse LV100* (*Nikon Corp*., Tokyo, Japan) with a *CMOS* camera *INFINITY1-1C* (*Lumenera Corporation*, Capella Court, Ottawa, ON, Canada).

In the experiments, microparticle suspensions of water and artificial blood which correspond to the human blood in terms of their viscosity, density, and acoustic velocity parameters, were used. As a microparticle phase in the suspension, the material of zeolite with color pigments was used (made by *SIGMA-ALDRICH*, 3050 Spruce Street, Saint Louis, MO 63103, USA). The microparticle dimensions were 0.5–15 μm.

To assess the separation process of the microparticles suspended in a liquid using ultrasonic sonication and to determine the vibrating deflection shapes and the Eigenmodes of the piezoceramic tube-shaped actuator, an experimental setup with a *Polytec* 3D scanning vibrometer (*Type PSV-500-3D-HV*) was developed and is shown in pic. 3.15.

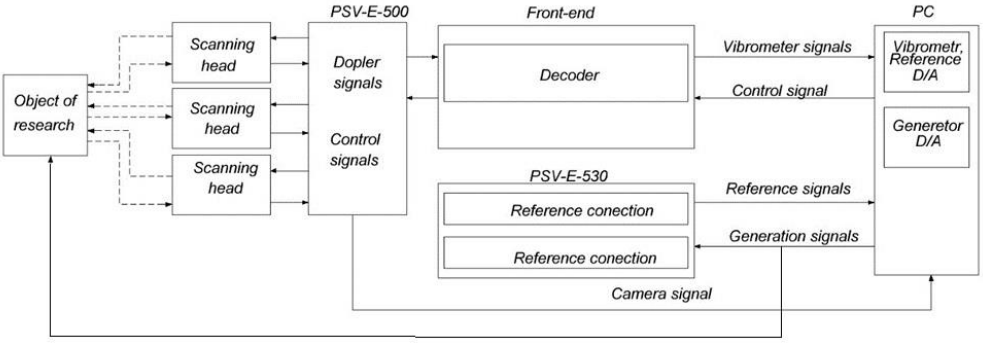

pic. 3.15. A block-scheme of the experimental setup with a *Polytec* 3D scanning vibrometer.

The operational deflection shapes (ODS) and the Eigenmodes of the tube-shaped piezoelectric actuator were determined with a *Polytec* 3D scanning vibrometer. An outer surface of the tubular actuator was virtually segmented, and each segment was 3D-scanned. pic. 3.16, a, shows the scanned segment and the grid of the measurement points. To minimize the gravity influence on the microparticle separation process, the tubular actuator was positioned vertically. To determine the resonance frequency of the researched actuator suitable for the microparticle separation, the frequency spectrum was obtained in the operational frequency range from 100 to 650 kHz.

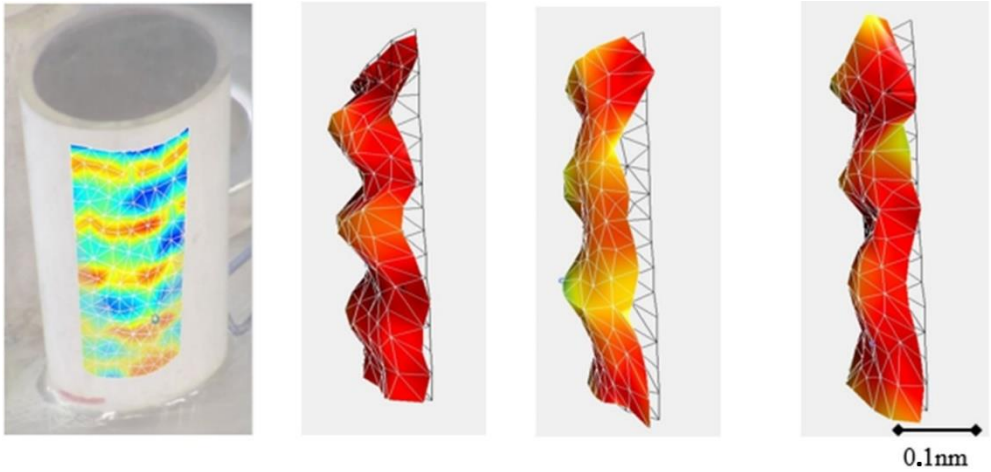

a) b) c) d)

pic. 3.16. A photo of the tube-shaped prototype actuator and a segment of its surface a) which is 3D-scanned to determine the vibrating deflection shapes and the Eigenmodes of the actuator b), c) and d).

Pic. 3.16, b, c, d shows the displacement of the scanned surface of the actuator (a segment of the outer surface) at an operational frequency of 345 kHz with different

fluids. Measurements were taken for the actuator without a suspension (pic. 3.16, b), with a water-based suspension (pic. 3.16, c) and with a biological suspension-synthetic viscous fluid (pic. 3.16, d). As it can be seen from the results, the displacement of the actuator without and with the viscous fluid are similar. This is due to viscous damping and fluid inertia.

The frequency spectra of the actuator with the fluid was measured with a 3D vibrometer (pic. 3.17), and the obtained values confirm the simulation results.

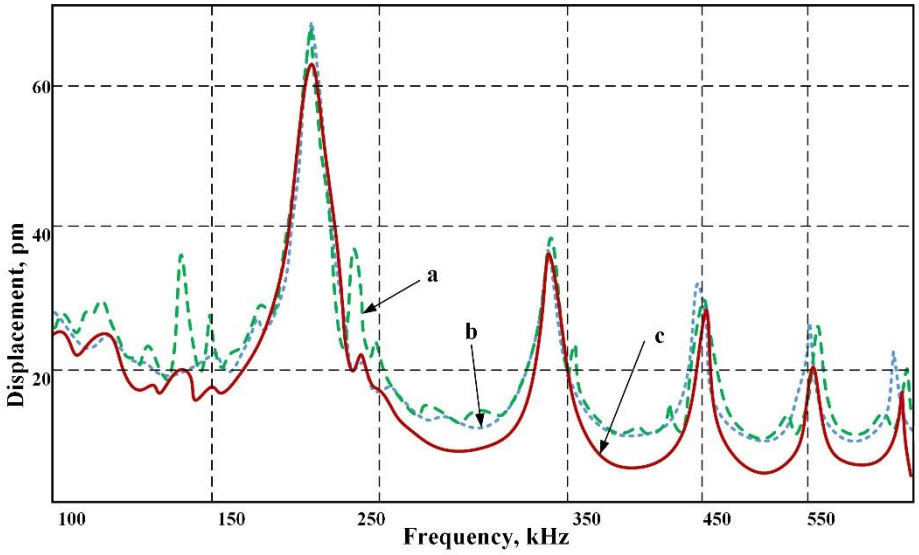

pic. 3.17. Frequency average spectrum of the actuator scanned surface obtained by measurement via a 3D scanner: a – without fluid; b – with water; c – with a biological suspension – a viscous fluid.

A stable resonance frequency of 345 kHz allows us to obtain a constant fluid flow separation into fractions. At a frequency of 202 kHz, the amplitude of deformation is the greatest, but the practical study showed flow instability that led to suspension mixing rather than its separation. So, we had to give up the greater amplitude to continually collect microparticles and move them to the desired trajectory of the acoustic signal. Here, (a) denotes the deformation in the fluid without suspension, (b) stands for the signal for a water suspension and (c) describes the operation when using a biological suspension – a viscous fluid. As can be seen from the graph, in the viscous flow, there is a certain attenuation at the non-resonance frequencies.

The separation of the particles from the suspension in the piezo cylinder under the influence of the standing ultrasonic wave is shown in pic. 3.18. For a comparison, the data is given for a frequency of 202 kHz (pic. 3.18, a) and for a frequency of 345 kHz (pic. 3.18, b). The time spent on the separation of the suspension flow into

fractions was 4 seconds for a water-based fluid and 8 seconds for a biological suspension – a viscous fluid.

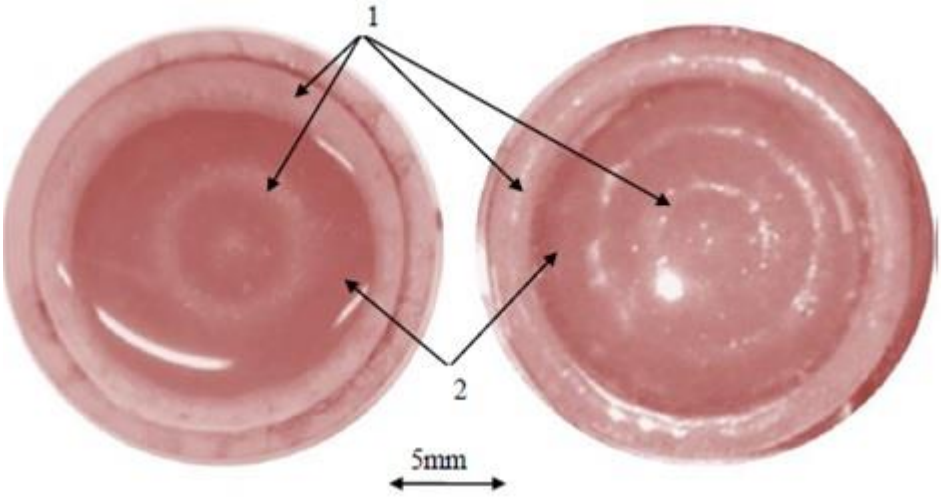

a) b)

Pic. 3.18. The distribution of the particles in the cylinder with the suspension under the influence of a standing ultrasonic wave: a) excitation frequency of 202 kHz; b) excitation frequency of 345 kHz.

3.3. Vibroacoustic Handling and Levitation of Microparticles in Air

What regards acoustic levitation, there is a steady wave between the emitting surface and the reflector. Radiation pressure and non-linear acoustic field properties determine the potential for acoustic levitation. It differs nonmonotonically between the radiating surface and the reflector. If it is strong enough to overcome the gravitational force, a small amount of material can be levitated and trapped. The acoustic potential node may correspond to an acoustic pressure node or anti-node depending on the density and compression of the levitating material and the surrounding medium. The concept of acoustic levitation and handling is realized by using a vibrating cylinder whose vibration is excited by a disc-shaped piezo actuator-bimorph placed at the bottom, which at the same time causes an acoustic wave that reflects from the reflector at the other end of the cylinder (pic. 3.19). The sound of the generated acoustic wave determines the levitation of microparticles concentrated on the nodal points of the vibrating cylinder surface. In this way, it is sufficient to excite the sonic rather than ultrasonic frequency signal so that the microparticles could be levitated from the cylinder surface.

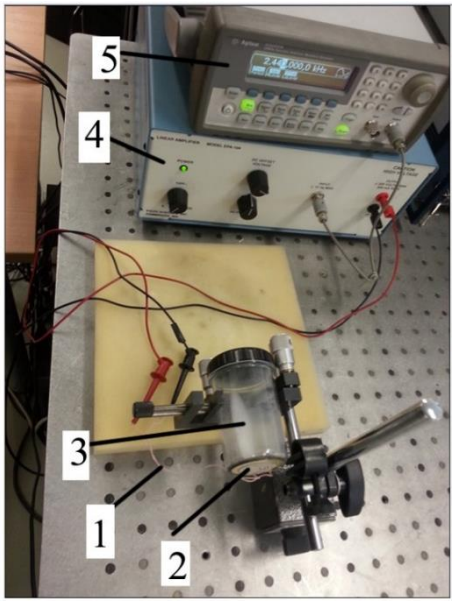

pic. 3.19. The experimental setup: 1 is the cylinder resonant waveguide; 2 is the disc-shaped piezo transducer-bimorph; 3 are microparticles; 4 is the signal generator (*Agilent 33220A*); 5 is a linear amplifier *EPA-104*.

The Eigenmodes of the disc-shaped transducer in the air are shown in pic. 3.20.

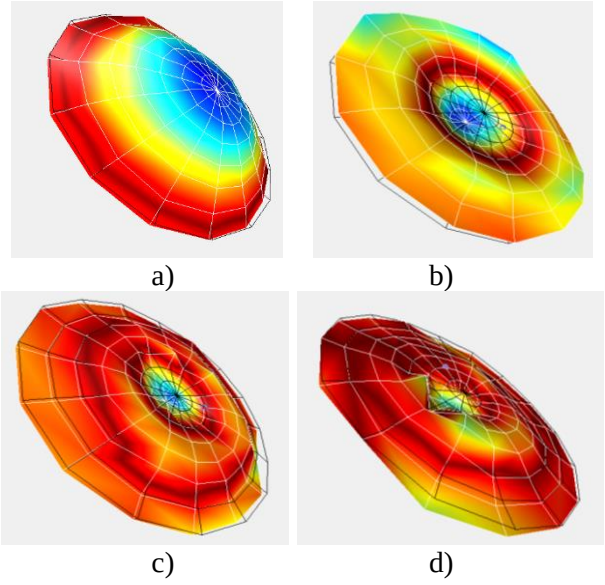

pic. 3.20. Eigenmodes of the disc-shaped transducer in the air, load 10 V, frequency: a) 1.852 kHz, b) 6.641 kHz, c) 14.805 kHz, d) 18.898 kHz.

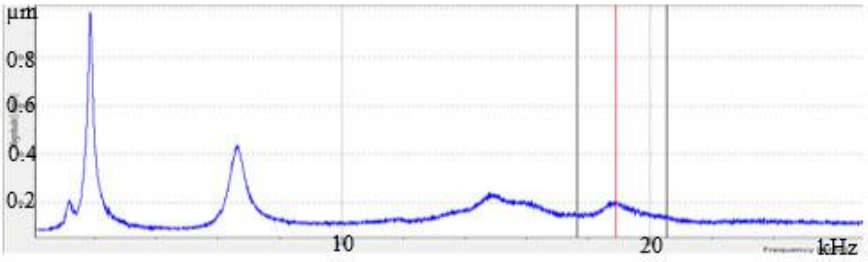

pic. 3.21. Graphical representations of the resonant vibrations of the disc-shaped piezo transducer-bimorph in the air at the input signal of 5 V.

The third piezo transducer vibration mode in the air is presented in pic. 3.22.

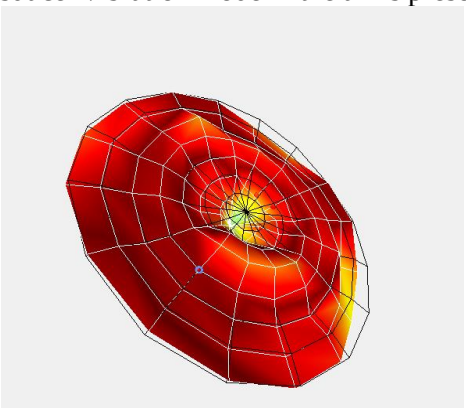

pic. 3.22. The third piezo transducer vibration mode in the air at 5V and 14.883 kHz.

During the experiment, the motion of microparticles was observed, which proves that the formation of ribs is a result of the vortex air flow caused by acoustic stationary waves. The microparticles are joined by ribs in the acoustic wave at the pressure nodes in the waveguide. As a result, the circular air movement on both sides of the microparticles ribs is observed. The vortex formation generates regular levitating microparticle structures (pic. 3.23).

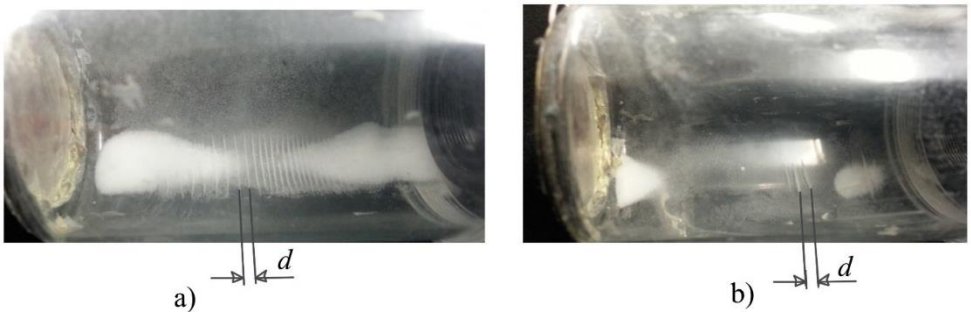

pic. 3.23. Photos of levitating microparticles on the wall nodes of a vibrating cylindrical container with different excitation frequencies: a – at 2.44 kHz; b – at 14.2 kHz.

The experiment results show that, in cases of frequencies exceeding 2 kHz, distance *d* between the microparticles ribs is stable and equals ~ 3 – 5 mm. The vortex intensity is proportional to the air flow rate. Thus the highest ribs are formed by the acoustic pressure in the areas with the highest speed. There are no ribs in the sound speed nodes because there the air does not move. The distance between the ribs depends on the frequency due to the simple energy and angular momentum conversion. With the increasing frequency, the air velocity also increases, which means that the vortices of the air spin faster. The conservation of the angular momentum can be expressed as:

$$\omega_0 r_0^2 = \omega r^2, \tag{7}$$

where ω_0 is the initial angular velocity; r_0 is the initial vortex radius; ω is the angular velocity at a higher frequency; r is the wavelength at a higher frequency. If vortex angular velocity ω is proportional to the frequency of acoustic wave f, formula (7) can be expressed as

$$r \sim r_0 (f_0/f)^{0,5} \tag{8}$$

A comparison with the experimental data yields function $r = a f^b$ graphically presented in pic. 3.24, where a = 740 and b = -0.5 are experimentally determined parameters, and $r << \lambda$, where λ is the acoustic wavelength.

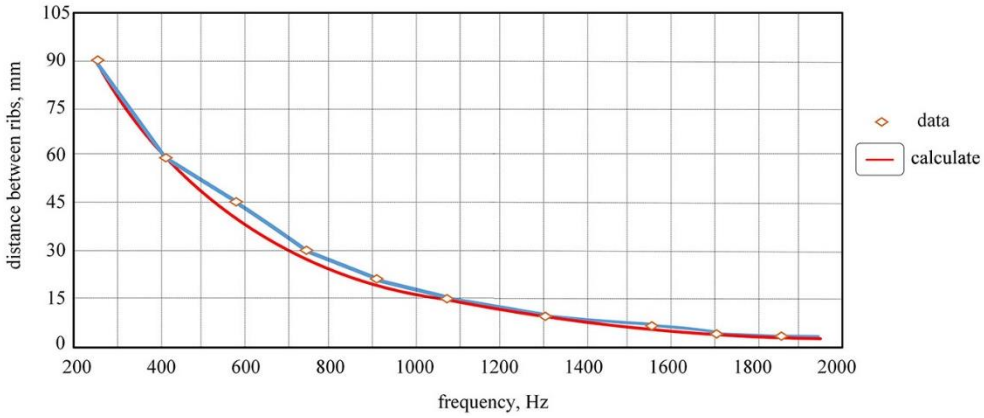

pic. 3.24. The dependence of the distance between the microparticles ribs and the sound frequency according to the calculation data and the experiment results, fit.

The possibility of controlling microparticles by a piezoelectric device causing their levitation phenomena under the influence of acoustic standing waves and cylinder modes of vibration is important in various fields of technology. The proposed method allows micro- or nanoparticle flows in the air to be controlled by a unique piezoelectric actuator mounted onto the cylindrical end of the container. The concept of the method is shown in the short cylinder experimentally and numerically.

3.4. Chapter Conclusions

1. The tools for the separation, handling and levitation of microparticles in the fluid and in the air by acoustic sonic frequency excitation waves were developed and manufactured. For the validation of the simulation results, the holographic interferometry setup PRISM was used for piezo transducer modal analysis without and with the fluid volume in it.
2. The tools for the separation of microparticles by acoustic ultrasonic frequency excitation waves were developed. For tube-shaped piezoceramic transducer modal analysis, a *Polytec* 3D scanning vibrometer was used, and a collector for microparticle gathering was manufactured.
3. The matching of the simulation (350 kHz) and the experimentally obtained (345 kHz) ultrasonic excitation frequencies as well as the coincidence of the diameters of microparticle concentration circles in both simulation and experimentat validates the mathematical model and suggests that it reproduces the real biological particle separation process.

4. DEVICE PROTOTYPES AND ORIGINAL SOLUTION

4.1 Separation of Microparticles by Using Sonic Frequency Acoustic Excitation

To carry out the experiment with a fluid, a plexiglass flask, a piezoceramic bimorph disc-shape transducer and a suspension of water and glycerin 50/50%, silicate mica with a particle size of 5–15 μm and a water-soluble pigment staining for contrasting results were used. A device was also developed that would allow the separation of concentrated accumulations of microparticles and fluids.

A schematic diagram of the device is shown in pic. 4.1, where 1 is a container of the fluid with microparticles; 2 is the inlet valve; 3 is a chamber of the acoustic separator with a fluid; 4 is a piezoelectric disc-shaped bimorph; 5 is the enriched phase of the fluid; 6 is the cleared phase of the fluid; 7 is the outlet valve of the enriched phase of the suspension; 8 is the outlet valve of the cleaned phase of the suspension; 9 is air. When the control valve is opened on container 1, through inlet valve 2, the suspension enters the chamber of the acoustic separator composed from conical vessel 3 and piezoelectric disc-shaped bimorph 4, where, under the action of the acoustic standing wave, microparticles drift in the volume of the fluid and accumulate in the nodal zones of the vessel wall standing wave. Then, the enriched phase of the suspension from the nodal circles through outlet valve 7 flows to container 5 and is cleaned from the microparticles phase of the suspension through outlet valve 8; it subsequently flows to container 6. Valve 9 serves for air escape.

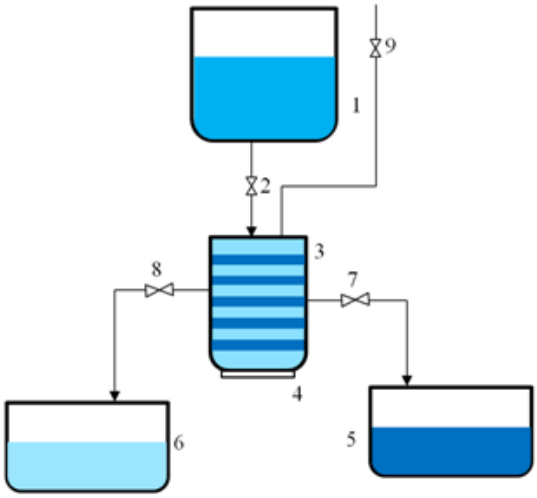

pic. 4.1. A schematic view of the microparticle separation system: 1 is a container of the fluid with microparticles; 2 is the inlet valve; 3 is a chamber of the acoustic separator with a fluid; 4 is a disc-shaped piezo transducer-bimorph; 5 is the enriched phase of the fluid; 6 is the cleaned phase of the fluid; 7 is the outlet valve of the enriched phase of the suspension; 8 is the outlet valve of the cleaned phase of the suspension; 9 is the air escape valve.

According to this scheme, a device was assembled, which is shown in pic. 4.2.

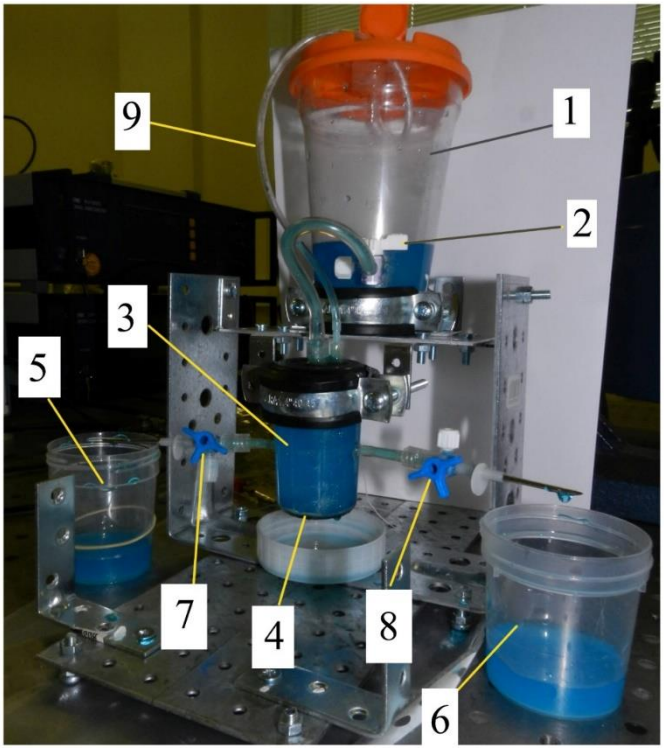

pic. 4.2. A device for microparticle separation. A prototype of the device: 1 is a container of the fluid with microparticles; 2 is the inlet valve; 3 is a conical container of the acoustic separator with a fluid; 4 is a disc-shaped piezo transducer-bimorph; 5 is the enriched phase of the fluid; 6 is the cleared phase of the fluid; 7 is the outlet valve of the enriched phase of the suspension; 8 is the outlet valve of the cleaned phase of the suspension; 9 is the air escape valve.

When examining the conical container of the acoustic separator after 12 seconds, it can be seen that microparticles have already accumulated on its wall (pic. 4.3).

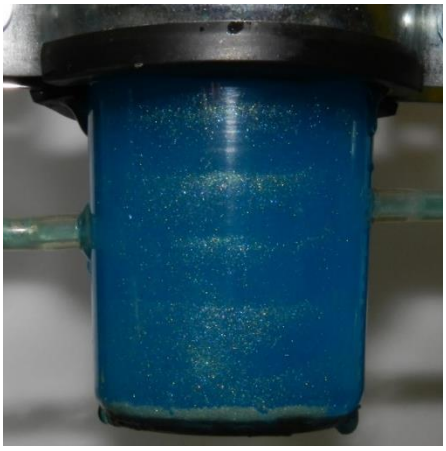

pic.4.3. The arrangement of concentrated zones with microparticles in a suspension under the influence of acoustic waves, at a frequency of 13.5 kHz.

Due to the fact that the disc-shaped piezo transducer-bimorph modes are different at different frequencies, the following effect occurs: in the first and second modes, the active mixing of the suspension due to large parasitic forces, such as the radiation pressure and the streaming takes place, and it is consequently not possible to obtain one or two stable circles of particle concentration on the inner surface of the container resonator. When switching to a higher mode, the number of the concentration circles increases, but the radiation pressure no longer maintains such a great relative value. The strength of the radiation pressure in the direction of the acoustic axis of the disc-shaped piezo transducer-bimorph is determined by the flux of the impulse through the surface of the object: to suppress the unnecessary action of these forces, an inactive disc-shaped piezo transducer-bimorph was used of a diameter of 6 mm less than the diameter of the conical container, which eliminated the possibility of touching the disc-shaped piezo transducer-bimorph against the wall of the container. As a result, a stable process of the distribution of microparticles in a suspension without mixing streaming, which prevented the formation of concentric zones, was obtained (pic. 4.4).

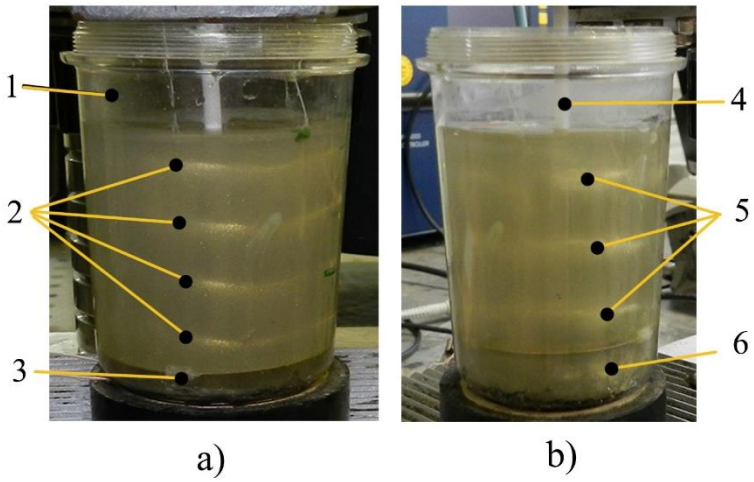

pic. 4.4. The use of a disc-shaped piezo transducer-bimorph for damping the streaming: 1 is the container with an active disc-shaped piezo transducer-bimorph radiator, 2 are the zones of concentration of microparticles in a suspension column, 3 is the membrane, 4 is an attachment of the disc-shaped piezo transducer-bimorph membrane support which is independent from the container, 5 is the zone of the active mixing of the suspension under the disc-shaped piezo transducer-bimorph membrane at different frequencies: a) at 13.5 kHz and b) at 17.5 kHz.

It is known from the classical theory of the propagation of acoustic waves that the wavelength of sound is found from the formula:

$$\lambda = v/f \tag{9}$$

where λ is the wavelength, v is the wave velocity, and f is the wave frequency. Based on this formula, it is possible to calculate that the wavelength in the fluid at v = 1430 m/s and f = 13500 Hz is 0.1059 m.

It turns out that the height of the container for obtaining at least one concentric circle of microparticles on the container's inside wall should be equal to or greater than 0.11 m. Our experimental data showed that the wavelength in the container with an active piezo transducer attached to the bottom was 0.02 m, which, according to the classical formula, should be obtained at a frequency $f = v/\lambda$ = 1430/0.02 = 71.50 kHz. To confirm the classical theory, a vibration single-component vibrator was used with a range of operating frequencies from 100 Hz to 80 kHz. The resonant frequency of this vibrator was at 70.5 kHz, the fluid in use was the same as for the previous experiments. The wavelength, in this case, was 0.021 m, which corresponds to the received data. Thus, with the help of a piezo transducer, it was possible with the sonic frequency and low power acoustic excitation to obtain the same results as for the ultrasonic frequency of powerful vibrators.

4.2 Separation of Microparticles by Using Ultrasonic Frequency Acoustic Excitation

For the extraction of microparticles from the biological suspension, a special collector was designed and manufactured (pic. 4.5). The distribution of channels of this collector is located in the circles whose diameters coincide with the diameters of the acoustic standing wave nodes circles or low-pressure areas in which solid microparticles precipitate (pic. 2.14 and pic. 3.18). After eight seconds of ultrasonic treatment in a tube-shaped piezo ceramic cylinder, the enriched by microparticles mixture was accumulated via the collector channels.

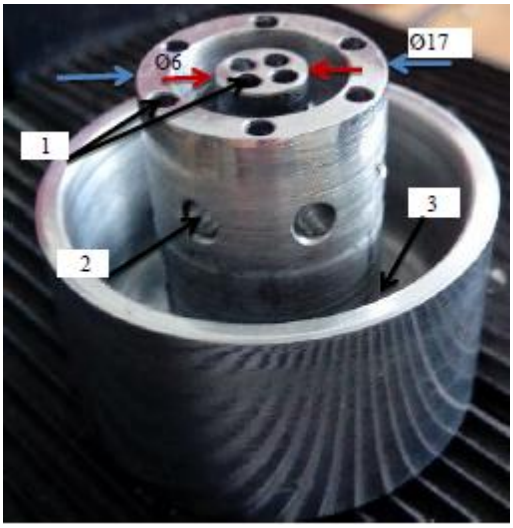

pic. 4.5. A photo of the fabricated collector: 1 – openings for the collection of the microparticles of the enriched phase; 2 – openings for the collection of the suspension phase; 3 – the volume of the suspension phase.

To determine the effectiveness of the microparticles separation in suspension, two separate samples were examined under a microscope. The results are shown in pic. 4.6. Image (a) depicts a sample of microparticles in the biological suspension before and (b) after the separation procedure.

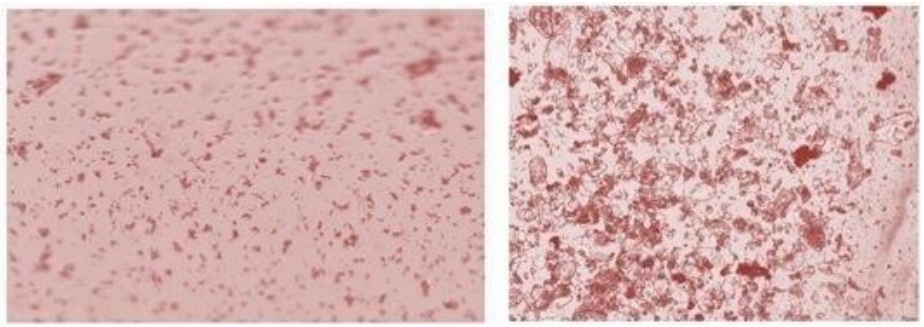

a) b)

pic. 4.6. A microscopic view of the biological suspension samples before a) and after b) the microparticle separation procedure

With these results, it can be concluded that even for suspensions with microparticles of a different shape and density, the separation in the suspension is possible.

As only the physical experiment with an elaborated purification device could confirm the appropriateness of the mathematical model, the experimental setup was assembled in order to ensure precise measurements. Two types of fluid suspension were considered: biological and water that included microparticles of the diameter of erythrocytes. We choose these types of suspensions to demonstrate the universality and validity of the proposed separation technologies with an experiment, which would otherwise be complicated due to the rapidly changing properties of erythrocytes in the blood. Standard guidelines for handling blood samples indicate that plasma or serum should be separated from the cells as soon as possible (20–30 minutes) after the clot formation is complete to avoid clot-induced changes in the serum concentrations of the analytic liquid caused by coagulation [45]. The agglutination of erythrocytes can occur within a few minutes after finding blood outside the body. Separately, the same red blood cell mass, when maintained at room temperature for more than 1 hour, is not to be used for transfusion; rather, it should be sent for recycling. For experimentation, artificial blood was taken to act as a substitute for erythrocytes [46]. While true blood serves many different functions, artificial blood is designed for the purpose of transporting oxygen and carbon dioxide throughout the body.

Two main parameters of the microparticles that form a nodal circle are related to the fluid acoustic excitation frequency and constructive dimensions of the piezo-actuator. Since the number of nodal circles or low-pressure areas in which the solid microparticles precipitate is increased by higher frequencies and was concentrated at a frequency of 345 kHz, the lower frequency of 202 kHz was abandoned in favor of stable and efficient acoustic forces produced at a frequency of 345 kHz. The diameters of microparticles concentration circles coincide in both cases – smulation and experimentation.

As it was shown experimentally and theoretically, the diameters of microparticle aggregation circles for both suspensions were identical, whereas the period of the circle formation differed twofold. This period (from 4 to 8 seconds) could be

considered as very short compared to other known methods of blood purification [47]. Keeping in mind the simplicity of the purified particle separation from biological suspensions, this method could be used in different emergency situations to keep spilled blood ready for further use. The results show that by increasing the amount of fluid and moving it away from the microarray, it is possible to get the same results as in the microflow [48]. Despite the fact that the biological fluid is very susceptible to the influence of the ultrasonic signals, our experience has shown that the frequency of 345 kHz is safe for cell membranes [49]. Whereas theory should make predictions, and good theoretical predictions should be supported by the results of experiments, the matching of our simulation (350 kHz) and the experimentally obtained (345 kHz) ultrasonic excitation frequencies as well as the coincidence of the diameters of microparticles concentration circles in both cases – simulation and experimentation – testifies that the mathematical model imitates the real blood purification process.

4.3 Research Approbation

Pic. 4.7 depicts a sectional diagram of an ultrasonic suspension separation device and an electrical control scheme, as well as a design of the device section A-A [78]. The structure and control system of the ultrasonic suspension separation device comprises: 1 – a tube for suspension feeding into the resonator chamber, 2 – a filtering chamber, 3 – a filtering element reducing the fluid flow turbulence, 4 – a piezoceramic cylinder-resonator which is activated by electrical signals from control unit 13. Inside it, acoustic standing waves are generated, in whose nodal circles microparticles 12 are concentrated, 5 – piezoceramic cylinder electrodes which are fed sequentially by electrical signals from excitation-control unit 13, 6 – a separation fraction distributor, 7 – a purified suspension chamber, 8 – microparticles separated from the suspension removal tubes, 9 – separation fraction distributor channels, 10 – the vibration damping spacer, 11 – the channel for cleaned-out microparticles, 12 – microparticles in the suspension generated by the deformation of the piezo-ceramic cylinder, 13 – the piezo-ceramic cylinder-resonator excitation control block.

By actuating a piezoceramic cylinder-resonator (4) when the resonance frequency electrical signal is applied to the electrodes (5), an acoustic standing wave inside the resonator (4) concentrates the microparticles in the suspension (12) in the nodal circles. According to the program, an electric signal with a consistently enlarged amplitude is sent from the excitation control unit (13) to the electrodes (5) of the piezoceramic cylinder (4), starting with the upper electrode, which results in a deformation of the corresponding points in the piezoceramic cylinder. The variable displacement of the generated mechanical vibrations at the excitation points of the piezoceramic cylinder (4) increases the temperature within the permissible limits from the top of the piezoceramic cylinder (4) to the bottom. Such a temperature regime changes the viscosity of the suspension, i.e., it reduces the resistance to the microparticles' deposition rate. In this way, solid microparticles are deposited and removed through the removal tubes (8) faster than in the usual equipment.

Compared to the nearest analog, this new ultrasonic suspension separator greatly simplifies the design of the separation devices and extends the functionality, i.e., it removes bundled microparticles from the fluid.

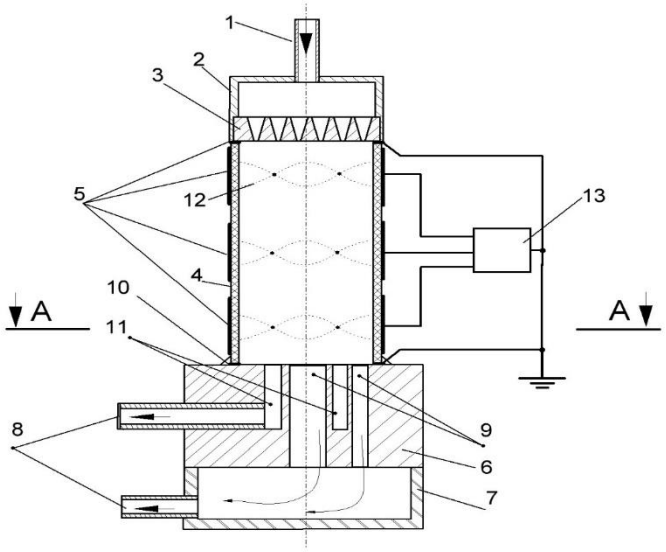

a)

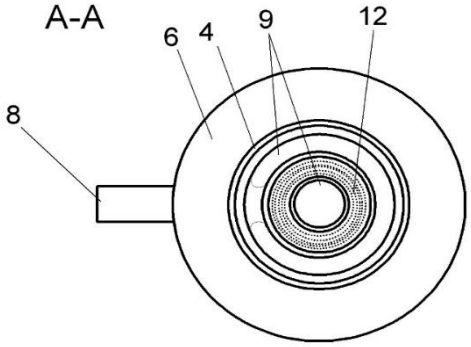

b)

pic. 4.7. A scheme of the device for microparticle separation in suspensions within a piezoceramic cylinder: a) a view with a vertical section; b) the horizontal cross-sectional view.

4.4 Chapter Conclusions.

1. A tool for the separation of microparticles in a suspension by acoustic sonic frequency excitation waves was developed and manufactured.
2. A tool for the separation of microparticles by acoustic ultrasonic frequency excitation waves was developed and manufactured. Samples of suspensions purified by microparticles were obtained.
3. The application for a patent for the separation of microparticles by acoustic ultrasonic waves was submitted.

GENERAL CONCLUSIONS

1. A review of the research works on the dissertation thematic area was carried out, and the aim and objectives of the research were formulated. The current methods of the separation of particles without vibration based on centrifugal sedimentation, magnetic, plasmapheresis or dialysis phenomena require expensive equipment and demonstrate limitations related to the requirements for the number of particles. The use of high frequency (ultrasonic) activation, when two mechanisms of the dominant particle manipulation are acoustic radiation forces (acting on a particle) and acoustic streaming (acting on the fluid, and thus on the drag on the particle) has so far been related to the single or several microparticles only.

2. Multilevel computing mathematical models of separation, processing, and levitation of microparticles by sound waves of acoustic excitation were developed. Vibrational regimes of the samples of purified microparticle suspensions were obtained. The third mode was chosen most efficiently, and the process of the separation of microparticles was modeled at the excitation frequency of 13.8 kHz. A conical, cylindrical, liquid-filled container with a lower mounted piezo transducer-bimorph works both for the container wall and for microparticles in the liquid and releases microparticles within 12 seconds.

3. A multi-physics mathematical model of the separation of microparticles by ultrasonic waves of acoustic excitation in a tubular piezoceramic converter was developed. The excitation frequency of 345 kHz was chosen as the most efficient. It was found that the rate of separation of microparticles depends on the viscosity of the suspension in which it is immersed. When the liquid is water, the microparticles fall into the field of low acoustic pressure after 4 seconds, whereas in the case of a biological suspension it takes twice as long, i.e., 8 seconds. The concentration areas of the biological suspension microparticles at the end of the process (i.e., when the liquid becomes stationary) are wider than those obtained by using water as a liquid. The third difference lies in the geometric mismatch between the low acoustic pressure regions of a small radius: in the case of a biological suspension, the radius of the region is less by 30% in comparison with the radius of water.

4. Computational models that combine both sonic and ultrasonic separation in different methods applicable for fluids were validated experimentally. The minor differences in simulation (350 kHz) and experimentally obtained (345 kHz) ultrasonic as well as respectively (13.5 kHz) and (13.8 kHz) sonic excitation frequencies, and the coincidence of the microparticle concentration in the low pressure Eigenmode zones in both cases – simulation and experimentation – testifies that the mathematical models imitate the real blood separation/purification process.

5. The tools for the microparticle sonic separation in fluid and their handling/levitation in the air were developed. For the validation of the simulation results, the holographic interferometry setup *PRISM* was used. During the experiment, the movement of microparticles was observed, which proves that the formation of the ribs is a result of the air vortex motion caused by acoustic stationary waves. The microparticles are aggregated in ribs at the pressure nodes of the acoustic wave in the waveguide. This results in a circular motion of the air on both sides of the

microparticles ribs. The vortex formation causes the regular levitating structures of microparticles.

6. A tool for the ultrasonic separation of microparticles was developed. For the piezo ceramic cylinder modal analysis, a *Polytec* 3D scanning vibrometer was used, and a collector for microparticle gathering was manufactured. Samples of enriched in microparticles and purified fluids were obtained.

7. A prototype device for the ultrasonic separation of microparticles in the fluid was proposed. The developed device can clean up to a liter of fluid per hour, which increases the volumes of separating microparticles from the liquid in comparison with other known prototypes. The small size of the device makes it possible to use it in many laboratories and organizations. External vibrations do not significantly influence the results of the proposed device operation due to the fact that the force of radiation and the acoustic pressure keeps the particles in the designated zones.

REFERENCES

1. LERCHE, D., SOBISCH, T. (2007). Consolidation of Concentrated Dispersions of Nano- and Microparticles Determined by Analytical Centrifugation. In: *Powder Techn*. 16 (2007), 46–49
2. MURRAY, C., PAO, E., TSENG, P., AFTAB, S., KULKARNI, R., RETTIG, M., DI CARLO, D. (2016). Quantitative Magnetic Separation of Particles and Cells Using Gradient Magnetic Ratcheting. In: *Small*. 2016, 12(14), 1891–1899
3. JUNG, Y., CHOI, Y., HAN, K.-H., FRAZIER, A.B. (2010). Six-Stage Cascade Paramagnetic Mode Magnetophoretic Separation System for Human Blood Samples. In: *Biomedical Microdevices*. August 2010, Volume 12, Issue 4, 637–645
4. DESITTER, I., GUERROUAHEN, B.S., BENALI-FORET, N., WECHSLER, J., JANNE, P.A., KUANG, Y., YANAGITA, M., WANG, L., BERKOWITZ, J.A., DISTEL, R.J., CAYRE, Y.E. (2011). A New Device for Rapid Isolation by Size and Characterization of Rare Circulating Tumor Cells. In: *Anticancer Research*. 2011, 31, 2, 427–441
5. HUANG, L.R., COX, E.C., AUSTIN, R.H., STURM, J.C. (2004). Continuous Particle Separation through Deterministic Lateral Displacement. In: *Science*. 14, 2004, 304, Issue 5673, 987–990
6. MAENAKA, H., YAMADA, M., YASUDA, M., SEKI, M. (2008). Continuous and Size-Dependent Sorting of Emulsion Droplets Using Hydrodynamics in Pinched Microchannels. In: *Langmuir*. 2008, 24 (8), 4405–4410
7. KI-HO HAN, BRUNO FRAZIER, A. (2008). Lateral-Driven Continuous Dielectrophoretic Microseparators for Blood Cells Suspended in a Highly Conductive Medium. In: *J. Lab on a Chip*. Issue 7, 2008, 1079-1086
8. BESKOK, A. (2010). AC Electrokinetic Flow. In: *Microfluidics Based Microsystems: Fundamentals and Applications*. 1st ed. (edited by Kaka, S., Kosoy, B., Li, D., Pramuanfaroenkij, A.). Berlin: Springer, 2010.
9. MIO, C., GONG, T., TERRAY, A., MARR, D.W.M. (2000). Design of a Scanning Laser Optical Trap for Multiparticle Manipulation. In: *Rev. Sci. Instrum*. 71(5), 2196
10. GOSSE, C., CROQUETTE, V. (2002). Magnetic Tweezers: Micromanipulation and Force Measurement at the Molecular Level. In: *Biophysical Journal*. Volume 82, June 2002, 3314–3329
11. CHE-HSIN LIN, CHENG-YAN LEE, CHIEN-HSIUNG TSAI, LUNG-MING FU. (2009). Novel Continuous Particle Sorting in Microfluidic Chip Utilizing Cascaded Squeeze Effect. In: *Microfluidics and Nanofluidics*. October 2009, 7:499
12. YAMADA., M., SEKI, M. (2005). Hydrodynamic Filtration for On-Chip Particle Concentration and Classification Utilizing Microfluidics. In: *Lab on a Chip*. Issue 11, 2005, 1233–1239
13. ZOUESHTIAGH, F., THOMAS, P.J., THOMY, V., MERLEN, A. (2008). Micrometric Granular Ripple Patterns in a Capillary Tube. In: *Phys. Rev. Lett*. 100, 054501 – published February 04, 2008

14. LUKASCHUK, S., DENISSENKO, P., FALKOVICH, G. (2007). Nodal Patterns of Floaters in Surface Waves. In: *Eur. Phys. J. Special Topics*. 145, 125–136
15. PETKOVIC-DURAN, K., MANASSEH, R., ZHU, Y., OOI, A. (2009). Chaotic Micromixing in Open Wells Using Audio-Frequency Acoustic Microstreaming. In: *BioTechniques*. 2009, 47(4) 827–834
16. WHITEHILL, J., NEILD, A., WAH NG, T., STOKES, M. (2010). Collection of Suspended Particles in a Drop Using Low Frequency Vibration. In: *Appl. Phys. Lett*. 96(5), 053501-3
17. VAINSHTEIN, P., SHAPIRO, M. (2008). Aerodynamic Focusing in a Channel with Oscillating Walls. In: *Aerosol Science*. 39, 929–939
18. OBERTI, S., NEILD, A., QUACH, R., DUAL, J. (2009). The Use of Acoustic Radiation Forces to Position Particles within Fluid Droplets. In: *Ultrasonics*. 49, 47–52
19. AGRAWAL, P., GANDHI, P.S., NEILD, A. (2013). The Mechanics of Microparticle Collection in an Open Fluid Volume Undergoing Low Frequency Horizontal Vibration. In: *Journal of Applied Physics*. 114, 114904
20. YOON, Y., KIM, S., LEE, J., CHOI, J., KIM, R.K., LEE, S-J., SUL, O., LEE, S.-B. (2016). Clogging-Free Microfluidics for Continuous Size-Based Separation Of Microparticles. In: *Scientific Reports*. 2016, 6, 26531
21. GORKOV, L.P. (1962). On the Forces Acting on a Small Particle in an Acoustical Field in an Ideal Fluid. In: *Sov Phys Dokl*. 1962; 6:773.
22. MULLER, P.B., BARNKOB, R., JENSEN, M.J.H., BRUUS, H. (2012). A Numerical Study of Microparticle Acoustophoresis Driven by Acoustic Radiation Forces and Streaming-Induced Drag Forces. In: *Lab on a Chip*. 2012, 22
23. TOWNSEND, R.J., HILL, M., HARRIS, N.R., WHITE, N.M. (2004). Modelling of Particle Paths Passing through an Ultrasonic Standing Wave. In: *Ultrasonics*. 42, 2004, 319–324
24. MANNEBERG, O., VANHERBERGHEN, B., SVENNEBRING, J., HERTZ, H.M., ÖNFELT, B., WIKLUND, M. (2008). A Three-Dimensional Ultrasonic Cage for Characterization of Individual Cells. In: *Appl. Phys. Lett*. 2008, 93
25. DING, X., LIN, S-C.S., KIRALY, B., YUE, H., LI, S., CHIANG, I.-K., SHI, J., BENKOVIC, S.J., HUANG, T.J. (2012). On-Chip Manipulation of Single Microparticles, Cells, and Organisms Using Surface Acoustic Waves. In: *Proc. Nat. Ac. Sc. of USA*. 109, 28, 2012, 11105–11109
26. COURTNEY, C.R.P.,DRINKWATER, B.W., DEMORE, C.E.M., COHRAN, S., GRINENKO, A. (2013). Dexterous Manipulation of Microparticles Using Bessel-Function Acoustic Pressure Fields. In: *Applied Physics Letters*. Vol. 102, 12
27. NAM, J., LEE, Y., SHIN, S. (2011). Size-Dependent Microparticles Separation Through Standing Surface Acoustic Waves. In: *Microfluidics and Nanofluidics*. 2011, Volume 11(3), 317–326
28. PETERSSON, F., NILSSON, A., HOLM, C., JÖNSSON, H., LAURELL, T. (2005). Continuous Separation of Lipid Particles from Erythrocytes by Means

of Laminar Flow and Acoustic Standing Wave Forces. In: *Lab on a Chip*. Issue 1, 2005

29. ROGERS, P., GRALINSKI, I., GALTRY, C., NEILD, A. (2013). Selective Particle and Cell Clustering at Air-Liquid Interfaces within Ultrasonic Microfluidic Systems. In: *Microfluidics and Nanofluidics*. 2013, 14(3–4), 469–477
30. KANAZAKI T., OKADA, T. (2012). Two-Dimensional Particle Separation in Coupled Acousti-Gravity-Flow Field Vertically by Composition and Laterally by Size. In: *Anal. Chem.* 2012**,** 84(24), 10750–10755
31. KOYAMA, D., ITO, Y., NAKAMURA, K. (2010). Noncontact Ultrasonic Particle Manipulation in a Circular Trajectory Using a Vibrating Disc. In: *Proceedings of 20th International Congress on Acoustics*. ICA, 2010 23–27 August 2010, Sydney, Australia
32. FORESTI, D., NABAVI, M., KLINGAUF, M., FERRARI, A., POULIKAKOS, D. (2013). Acoustophoretic Contactless Transport and Handling of Matter in Air. In: *Proc. Natl. Acad. Sci. U S A*. 2013 July 30; 110(31), 12549–12554
33. KOZUKA, T., YASUI, K., TUZIUTI, T., TOWATA, A., IIDA, Y. (2007). In*: Noncontact Acoustic Manipulation in Air. Japanese Journal of Applied Physics*. 46, 7B, 2007, 4948–4950
34. GLYNNE-JONES, P., DEMORE, C.E.M., YE, C; QIU, Y., COCHRAN, S., HILL, M. (2012). Array-Controlled Ultrasonic Manipulation of Particles in Planar Acoustic Resonator. In: *IEEE Transactions on Ultrasonics, Ferroelectrics, and Frequency Control*. 59(6), 2012**,** 1258–1266
35. MARZO, A., SEAH, S.A., DRINKWATER, B.W., SAHOO, D.R., LONG, B., SUBRAMANIAN, S. (2015). Holographic Acoustic Elements for Manipulation of Levitated Objects. In: *Nature Communications*. 2015, 6, 8661.
36. ZHENGHUI, Q., YAJI, H., NASO, V., WEI, D. (2017). Aerosol Manipulation through Modulated Multiple Acoustic Wave Packets with a Pair of Resonators. In: *Powder Technology*. 322, 2017, 24–31
37. CICEK, A., KOROZLU, N., ADEM KAYA, O., ULUG, B. (2017). Acoustophoretic Separation of Airborne Millimeter-Size Particles by a Fresnel Lens. In: *Pub. Med. Sci. Rep*. 2017; 7: 43374
38. WANG, S., ALLEN, J.S., ARDEKANI, A.M. (2017). Unsteady Particle Motion in an Acoustic Standing Wave Field. In: *European Journal of Computational Mechanics*. 2017, Vol. 26 (1–2): Fluid Flows With Interactive Boundaries, 115–130
39. JINGTAO WANG. (2012). Dual Theoretical and Numerical Calculation of the Acoustic Radiation Force Acting on a Circular Rigid Cylinder near a Flat Wall in a Standing Wave Excitation in an Ideal Fluid. In: *Ultrasonics*. Volume 52, Issue 2, February 2012, 325–332
40. SAADATMAND, M. (2012). *A Study on Vibration-Induced Particle Motion under Microgravity*. Doctor of Philosophy Thesis, University of Toronto. 259pp.
41. SETTNES, M., BRUUS, H. (2012). Forces Acting on a Small Particle in an Acoustical Field in a Viscous Fluid. In: *Phys. Rev. E*. 85, 016327, 1–12

42. MORGAN Advanced Materials. (2016). *High-Density, Defect-Free PZT Components from Morgan*. July 14, 2016
43. KARPUL, D., TAPSON, J., RAPSON, M., JONGENS, A., COHEN, G. (2010). Limiting Factors in Acoustic Separation of Carbon Particles in Air. In: *J. Acoust. Soc. Am.* 127, 2153–2158
44. TURCHIANO, M., NGUYEN, C., FIERMAN, A., LIFSHITZ, M., CONVIT, A. Impact of Blood Sample Collection and Processing Methods on Glucose Levels in Community Outreach Studies. In: *J. of Envir. and Pub. Health*. 2013(3), 256151, 1-4
45. OTTERSTEDT, J.E., BRANDRETH, D.A. (2013). *Small Particles Technology*. In: *Springer Sci. & Bus. Med*., 206–208
46. STEGMAYR, B.G. (2005). A Survey of Blood Purification Techniques. In: *Transf. Apher. Sci*. 2005, 32(2), 209–20
47. DEVENDRAN, C., GRALINSKI, I., NEILD, A. (2004). Separation of Particles Using Acoustic Streaming and Radiation Forces in an Open Microfluidic Channel. In: *Microfluid. Nanofluid*. 2004, 17, 879–890
48. WU, J., NYBORG, W.L. (2008). Ultrasound, Cavitation Bubbles and Their Interaction with Cells. In: *Adv. Drug. Deliv. Rev*. 2008, 60, 1103–1116
49. GOSSET, D.R., WEAVER, W.M., MACH, A.J., HUR, S.C., TSE, H.T., LEE, W., AMINI, H., DI CARLO, D. (2010). Label-Free Cell Separation and Sorting in Microfluidic Systems. In: *Analyt. Bioanalyt. Chem*. 2010, 397(8), 3249–3267
50. NOCE, A., FERRANNINI, M., FABRINI, R., BOCEDI, A., DESSI, M., GALLI, F., FEDERICI, G., PALUMBO, R., DI DANIELE, N., RICCI, G. (2012). Erythrocyte Glutathione Transferase: a New Biomarker for Hemodialysis Adequacy, Overcoming the Kt/Vurea Dogma? In: *Cell Death and Disease*. 2012, 3, e377
51. WLOCH, A., CZYZ, H., JASINSKI, T. (2015). Ultrasonic Methods of the Cells Separation in Human Blood. In: *Acta Physica Polonica A*. 2015, 128, 234–236
52. LEI, J., GLYNNE-JONES, P., HILL, M. (2013). Acoustic Streaming in the Transducer Plane in Ultrasonic Particle Manipulation Devices. In: *Lab. Chip*. 2013, 13(11), 2133–43
53. MOHAMED, M.A., FIKRY, N.M. MOHAMED, M.M. (2014). Experimental Investigation of Ultrasonic Trapping of Bioparticles Using Parallel Plane Cavity. In: *Int. J. of Biomed. Eng. and Sci. (IJBES)*. 2014, 1(3), 21–34
54. SETAYESHGAR, A., LIPSETT, M.G., KOCH, C.R., NOBES, D.S. (2013). Measurement of Particle Dynamics in a Coherent Acoustic Field. In: *10th Int. Symp. Part. Image Veloc*. PIV13 Delft, the Netherlands
55. WESTERWEEL, J. (1997). Fundamentals of Digital Particle Image Velocimetry. In: *Meas. Sci. Technol*. 1997, 8, 1379–1392
56. DEVENDRAN, C., GRALINSKI, I., NEILD, A. (2014). Separation of Particles Using Acoustic Streaming and Radiation Forces in an Open Microfluidic Channel. In: *Microfluid. Nanofluid*. 2014, 17, 879–890
57. HADDADI, B., FATHIPOUR, M. (2016). Numerical Analysis of 3D Model of the SSAW Separator System. In: *Int. J. of Comp. Appl*. In: 2016, 141(12), 7–12

58. KAPISHNIKOV, S., KANTSLER, V., STEINBERG, V. (2006). Continuous Particle Size Separation and Size Sorting Using Ultrasound in a Microchannel. In: *J. of Statist. Mech.: Theory and Exp*. 2006, 01, P01012
59. LAURELL, T., PETERSSON, F., NILSSON, A. (2007). Chip Integrated Strategies for Acoustic Separation and Manipulation of Cells and Particles. In: *Chem. Soc. Rev*. 2007, 36, 492–506
60. PETERSSON, F., NILSSON, A., HOLM, C., JONSSON, H., LAURELL, T. (2004). Separation of Lipids from Blood Utilizing Ultrasonic Standing Waves in Microfluidic Channels. In: *The Royal Soc. of Chem. J. Analyst*. 2004, 129, 938–943
61. BÖHM, H., BRIARTY, L.G., LOWE, K.C., POWER, J.B., BENES, E., DAVEY, M.R. (2002). Application of a Novel H-Shaped Ultrasonic Particle Separator under Microgravity Conditions. In: P*roc. Forum Acust. Sevilla Spain Spec. Sess. PHA-01: Acoust. Dispers. Part. Mat*.
62. SADIKOVA, D.G., PASHOVKIN, T.N. (2013). Cell Concentration and Separation in the Field of a Standing Ultrasonic Wave for Medicine and Biotechnology. In: *Open J. of Bioph*. 2013, 3(1A),70–75
63. GRÖSCH, M., BURGER, W., HANDL, B., DOBLHOFF-DIER, O., GAIDA, T., SCHMATZ, C. (1998). Ultrasonic Separation of Suspended Particles – Part III. In: *Applic. in Biotech. Acta Acust. United with Acust*. 1998, 84(5), 815–822
64. RIERA-FRANCO DE SARABIA, E., GALLEGO-JUAREZ, J.A., RODRIGUEZ-CORRAL, G., ELVIRA-SEGURA, L., GONZALEZ-GOMEZ, I. (2000). Application of High-Power Ultrasound to Enhance Fluid/Solid Particle Separation Processes. In: *Ultrasonics*. 38, 642–646
65. ANDRADE, M.A.B., BUIOCHI, F., ADAMOWSKI, J.C. (2010). Particle Manipulation by Ultrasonic Progressive Waves. In: *Phys. Proc*. 3 (2010), 283–288
66. RAHMAN, S., HAQUE, A. (2012). Mathematical Modeling of Blood Flow. In: *Inform. Electron. & Vision (ICIEV)*. 2012, 672–676
67. FONTAINE, I., SAVERY, D., CLOUTIER, G. (2002). Simulation of Ultrasound Backscattering by Red Cell Aggregates: Effect of Shear Rate and Anisotropy. In: *Bioph J*. 2002, 82, 1696–1710
68. LIU, Y., LIU, W.K. (2006). Rheology of Red Blood Cell Aggregation by Computer Simulation. In: *J. of Comp. Phys*. 2006, 220, 139–154
69. MASON, T.J., JOYCE, E., PHULL, S.S., LORIMER, J.P. (2003). Potential Uses of Ultrasound in the Biological Decontamination of Water. In: *Ultrason. Sonoch*. 2003, 10, 319–323
70. YIN, X., HAN, P., LU, X., WANG, Y. (2004). A Review on the Dewaterability of Bio-Sludge and Ultrasound Pretreatment. In: *Ultrason. Sonoch*. 2004, 11, 337–348
71. SAXENA, A., TRIPATHI, B.P., KUMAR, M., SHAHI, V.K. (2009). Membrane-Based Techniques for the Separation and Purification of Proteins: an Overview. In: *Advance. Coll. and Interf. Sci*. 2009, 145, 1–22
72. US patent. *US 6245207 B112 2001*

73. FORESTI, D., NABAVI, M., KLINGAUF, M., FERRARI, A., POULIKAKOS, D. (2013). Acoustophoretic Contactless Transport and Handling of Matter in Air. In: *Proc. Natl. Acad. Sci. USA*. Vol. 110(31), 12549–12554
74. KOZUKA, T., YASUI, K., TUZIUTI, T., TOWATA, A., IIDA, Y. (2007). Noncontact Acoustic Manipulation in Air. In: *Japanese Journal of Applied Physics*. Vol. 46(7B), 4948–4950
75. GLYNNE-JONES, P., DEMORE, C.E.M., YE, C., QIU, Y., COCHRAN, S., HILL, M. (2012). Array-Controlled Ultrasonic Manipulation of Particles in Planar Acoustic Resonator. In: *IEEE Transactions on Ultrasonics, Ferroelectrics, and Frequency Control*. Vol. 59 (6), 1258–1266
76. MARZO, A., SEAH, S.A., DRINKWATER, B.W., SAHOO, D.R., LONG, B., SUBRAMANIAN, S. (2015). Holographic Acoustic Elements for Manipulation of Levitated Objects. In: *Nature Communications*. 2015, 6, 8661
77. BUBULIS, A., GOLINKA, E., OSTASEVICIUS, V., JURENAS, V. (2017). *Ultrasonic Microparticles Separation Device:* 2017 507: 2017 04 28

List of Author's Publications

Articles in Journals Listed in Web of Science Database

1 Vytautas Ostasevicius, Vytautas Jurenas, **Ievgeniia Golinka**, Rimvydas Gaidys, Algiment Aleksa. (2018). **Separation of Microparticles from Suspension Utilizing Ultrasonic Standing Waves in a Piezoelectric Cylinder Actuator** // Actuators / MDPI, Basel, Switzerland / Actuators: EISSN 2076-0825. 2018, Vol 7(2), No. 14, pp. 1–12.

2. Ostaševičius, Vytautas; **Golinka, Evgenia**; Jūrėnas, Vytautas; Gaidys, Rimvydas. (2017). **High Frequency Separation of Suspended Micro/Nanoparticles** // Mechanika / Kauno technologijos universitetas, Lietuvos mokslų akademija, Vilniaus Gedimino technikos universitetas / Kaunas: KTU. ISSN 1392-1207. 2017, Vol. 23, No. 3, pp. 408–411. Impact Factor 0.382

3. Serhiy Horiashchenko, **Ievgeniia Golinka**, Algimantas Bubulis, Vytautas Jurenas. (2018). **Simulation and Research of the Nozzle with an Ultrasonic Resonator for Spraying Polymeric Materials Materials** // Mechanika / Kauno technologijos universitetas, Lietuvos mokslų akademija, Vilnias Gedimino technikos universitetas / Kaunas: KTU. ISSN 1392-1207. 2018, Vol. 24, No. 1, pp. 61–64. Impact Factor 0.382

Articles in ISI Proceedings

1. Vytautas Ostasevicius, Vytautas Jurenas, Rimvydas Gaidys, **Ievgeniia Golinka**. (2017). **Vibroacoustic Handling and Levitation of Microparticles in Air //** Journal of Vibroengineering / Vibromechanika. Lithuanian Academy of Sciences, Kaunas University of Technology, Vilnius Gediminas Technical University. Kaunas: Vibroengineering Procedia. ISSN 2345-0533. 2017, Vol No.15, pp. 100-104

2. Vytautas Ostasevicius, **Ievgeniia Golinka**, Vytautas Jurenas, Rimvydad Gaidys. (2017). **Fast Ultrasonic Micro/Nanoparticles Separation from Fluids,** 22nd International Scientific Conference Mechanika 2017

Articles in Conference Proceedings

- Mechanika 2015, Blood Purification Using Ultrasonic Erythrocytapheresis, April 23, 2015;
- Actual Problems of Computer Technology 2015. Simulation Process of Separation in Microfluidic Devices with the Use of Ultrasonic Standing Wave, May 21–23, 2015;
- Mechatronic Systems and Materials MSM 2015. Theoretical and Experimental Investigation to Improve Particles Separation in Liquid. July 07–09, 2015;
- International Conference of Young Scientists *Modern Technologies in Mechanics*. Analytical and Computer Modeling of the Impact of a Standing Ultrasonic Wave on Particles in a Liquid. April 21–23, 2016;
- 21st International Scientific Conference Mechanika 2016. Numerical Simulation for Particles Separation from Blood Flow. May 12–14, 2016;
- 22nd International Scientific Conference Mechanika 2017. Fast Ultrasonic Micro/Nanoparticles Separation from Fluids. May 19–20, 2017;

- VII Ukraińsko-Polskie naukowe dialogi. High-Frequency Separation of Suspended by Microparticles in Viscosity Liquid. October 18–21, 2017;
- 29th International Conference on Vibroengineering. Vibroacoustic Handling and Levitation of Microparticles in Air. December 01, 2017;
- Rapid Separation of Nanoparticles in Fluids by Sonic and Ultrasonic Acoustophoresis. 23rd International Scientific Conference Mechanika 2018. May 18, 2018

National Patent

A.Bubulis, E.Golinka, V.Jurenas, V. Ostaševičius, R.Gaidys **Ultragarsinis emulsijos separavimo įrenginys**

Application number: 2017 507.

Date of priority recorded: April 28, 2017.

SL344. 2018-05-30, 12 leidyb. apsk. l. Tiražas 12 egz. Užsakymas 191 .
Išleido Kauno technologijos universitetas, K. Donelaičio g. 73, 44249 Kaunas
Spausdino leidyklos „Technologija“ spaustuvė, Studentų g. 54, 51424 Kaunas